ANALYSIS OF INTERFERENCE TESTS WITH HORIZONTAL WELLS

by

Mohammed N. Al-Khamis

ProQuest LLC.
789 East Eisenhower Parkway
P.O. Box 1346
Ann Arbor, MI 48106 – 1346

A thesis submitted to the Faculty and Board of Trustees of the Colorado School of Mines in partial fulfillment of the requirements for the degree of Doctor of Philosophy (Petroleum Engineering).

Golden, Colorado

Date March 31, 2003

Signed: Mohammed N. Al-Khamis

Mohammed N. Al-Khamis

Approved: Erdal Ozkan

Dr. Erdal Ozkan

Thesis Advisor

Approved: Rajagopal Raghavan

Dr. Rajagopal Raghavan

Thesis Co-Advisor

Golden, Colorado

Date March 31, 2003

Craig W. Van Kirk

Dr. Craig W. Van Kirk

Professor and Head,

Department of Petroleum

Engineering

ABSTRACT

Interference tests between horizontal wells may provide more information about reservoir properties as compared to vertical wells because of the larger contact of the wells with the reservoir. However, unlike interference tests between vertical wells where the flow conversion is mainly radial, three-dimensional flow should be taken into consideration when analyzing interference tests between horizontal wells. In addition, when the interfering wells are horizontal, more than one flow regime may develop in the reservoir during the test period. Therefore, interference tests with horizontal wells introduce features and issues that are different from those for conventional wells. However, there has not been sufficient research on the special features of horizontal-well interference tests. The objective of this dissertation is to investigate the special features of interference tests between horizontal wells and present rigorous and approximate methods to analyze horizontal-well interference test data.

Because of the large reservoir area covered during an interference test between horizontal wells, the homogeneous reservoir assumption used in analytical models may be even less appropriate for some reservoirs. In these cases, numerical models need to be developed and carefully calibrated to capture the fine details of pressure interference between two horizontal wells. Therefore, a further objective of this study is to provide analytical models and tabulated data to calibrate the numerical simulators used in the analysis of horizontal-well interference tests.

To achieve the objectives of this work, two semi-analytical models have been developed where both active and observation wells are horizontal. The models consider three-dimensional reservoirs with two horizontal wells and incorporate the effect of wellbore-

hydraulics. Permeabilities in the three principal directions may be different, and the lengths, relative placements, and azimuth angles of the wells are completely arbitrary.

The analytical models developed in this study have been used to investigate the effects of horizontal and vertical separation between the wells, skin factors and distributions, permeability anisotropy, azimuth angles, and wellbore-hydraulics. The results have been compiled and generalized in the form of correlations. These results improve our understanding of the characteristics of horizontal-interference-well responses and help the analysis of horizontal-well interference tests.

The results of the study have shown that for most practical cases, the horizontal observation well responses display radial or pseudoradial flow characteristics. In these cases, the horizontal observation well responses may be matched by the responses generated at an optimum observation point by a single horizontal well or by the exponential integral solution. These approximations provide significant simplifications for the analysis of interference tests between horizontal wells but also indicate that only horizontal permeabilities may be determined from the analysis of these tests. Furthermore, it was found that the skin distributions on both active and observation wells have insignificant effect on the observation well pressure responses. This observation, however, is only limited to the case where wellbore storage is negligible. Finally, the results have also indicated that the effect of wellbore-hydraulics is not significant for the analysis of horizontal-well interference tests.

TABLE OF CONTENTS

LIST OF TABLES

LIST OF FIGURES

ACKNOWLEDGEMENTS

I would like to express my sincere appreciation to my advisor, Dr. Erdal Ozkan, for his continuous support, guidance and patience, which has contributed significantly in the completion of this work. His dedication and enthusiasm to explore new research frontiers have always given me the courage to move forward in the research. In addition, his excellent teaching skills have always inspired and motivated me to select him as a role model.

I am also thankful to Saudi Aramco Oil Company of Saudi Arabia for granting me a scholarship to complete this work and for their continuing financial support.

I would also like to express my deepest and most sincere gratitude to my wife Umm Ali, who made a lot of sacrifices in coming with me to the United States and has been an endless source of encouragement throughout the years I have known her. I am also indebted to my parents for their continual guidance, courage, and prayers.

This work is dedicated to my four children: Hawra, Fatimah, Hassan and Ali who have been always the inspiration and the illumination with which I look to see my future.

CHAPTER 1

INTRODUCTION

Since the early eighties, horizontal wells have become an integral part of field developments and many fields have been developed successfully by horizontal wells around the world. In addition, because of the improved productivity in applications such as IOR, thin formations, low-permeability reservoirs, formations with natural fractures, and reservoirs with severe gas/water coning problems, horizontal wells have gained additional advantages over conventional vertical and hydraulically fractured wells.

The increased reservoir coverage and complexity of flow convergence toward horizontal wells dictate the efforts to collect more detailed information about the reservoir characteristics. One of the means to obtain information about the reservoirs is to conduct interference tests between horizontal wells. These tests may provide information about the reservoir properties, such as the average transmissibility, storativity, and communication between wells. Because a larger volume is covered during the interference test between two horizontal wells, the information about the average properties may be more representative than that obtained from vertical-well interference tests. On the other hand, the analysis of horizontal well responses is considerably more complex than that of their vertical counterparts.[1,2,3]

In case of interference testing between two vertical wells, the observation well may be represented by a measurement point in the reservoir (the existence of the well at the observation point may be conveniently neglected). The geometry of a horizontal observation well, on the other hand, may disturb the flow lines and therefore may not be neglected. In

general, interference between two horizontal wells may create complex pressure transients that may not be correlated by interference between two vertical wells.[4] The complexity of the horizontal well interference responses significantly increases when the reservoir becomes more heterogeneous because the well has more exposure to the reservoir (considering the long reach of horizontal wells, homogeneous reservoir assumption may not be realistic for horizontal-well interference test analysis). In these cases, use of numerical simulation may be necessary to analyze horizontal-well interference tests. In addition, wellbore-hydraulics is known to influence the responses of high-rate, extended reach horizontal wells with relatively small wellbore radii. To fully understand and correctly interpret the interference tests between two horizontal wells, the special features of these tests noted above should be studied in detail. This constitutes the objective of this study.

This study consists of two sections. In the first section, a model is developed for cases where active and observation wells are parallel and aligned with one of the principal horizontal permeability directions. In the second section, another model is developed to simulate the interference between two horizontal wells that are not parallel and aligned with the principal permeability directions. Although the second model includes the first one, this approach is taken to verify the second model. Individual components of the first model, such as the single horizontal well algorithms, wellbore models, and computational procedures have been presented in the literature and provide the means for the verification of the first model. Once the first model is verified, it provides the results to verify the second, more general model.

Both models consist of the superposition of the responses of two horizontal wells. The wells may have finite conductivity; that is, the effect of wellbore pressure drop due to wellbore hydraulics is taken into account. Fluid withdrawal (production) from one of the horizontal wells is considered at a constant rate. The second horizontal well (observation well) is shut in at the heel (effect of wellbore storage is not considered in this work) but fluid may enter (production) and leave (injection) this well along its entire length with the total production

being equal to the total injection. Both producing and interference wells may have arbitrary skin distribution along their lengths. These models provide the pressure drawdown at the heel ends of the pulsing and observation wells as well as the flux and pressure distributions along both horizontal wells. Therefore, the models may be used not only to investigate the effect of interference at the pressure measurement points (the heels of the wells) but also to understand the local changes in and around the wells.

1.1 Objectives of the Study

The objective of this study is to enhance our understanding of the interference between two horizontal wells and improve our ability to analyze horizontal well observation tests. The specific objectives are the following:

i) Develop semi-analytical models that may be used to investigate the fundamental characteristics of horizontal interference-well responses.
ii) Develop and discuss the rigorous and approximate techniques to analyze interference tests between horizontal wells.
iii) Provide analytical models and tabulated data to calibrate numerical simulators.
iv) Document the information that may be obtained from horizontal well interference tests.

The effects of the following parameters are investigated in detail:

- Horizontal separation between the wells (Δx_w , Δy_w).
- Vertical separation between the wells (Δz_w).
- Permeability anisotropy.

- Azimuth angles of the wells.
- Skin factor and skin distribution.
- Wellbore conductivity.

In addition, the error that might be caused by ignoring the effect of the length of the horizontal interference well (that is, treating the observation well as if it were a point in the reservoir) is highlighted. Correlations relating horizontal observation well responses with the responses of an equivalent observation point are established. Horizontal-well interference test results are compared with those for vertical wells and the conditions to approximate horizontal-well interference responses with the exponential integral solution are documented. Finally, the results of this study are compared with similar results presented in the literature and differences in findings, if any, are highlighted.

1.2 Significance of the Study

Rigorous analytical models for interference testing between two horizontal wells have not been reported in the literature. These models are important to understand the details of horizontal-well interference tests and to develop rigorous and approximate techniques to interpret these tests. The analytical models are significantly more convenient for the regression techniques used in commercial well-test analysis software.

In many practical situations, horizontal-well interference tests may have to be evaluated by using numerical simulators. However, numerical modeling of transient flow toward horizontal wells is not a simple task especially when the details of flow in and around the horizontal observation well are important. In general, numerical models used for horizontal-well interference tests require sensitive calibration in order to produce accurate results. The

calibration of the numerical models is most conveniently accomplished by using rigorous analytical models like the ones developed in this study. Rigorous models are also essential to generate dimensionless pressure and derivative type curves for interference testing between horizontal wells.

1.3 Thesis Organization

This thesis is divided into nine chapters. A general introduction of the thesis is presented in Chapter 1. This chapter also includes the objectives and significance of the study, and a literature review.

Chapter 2 is devoted to the development of the first model, which deals with the cases when both horizontal wells are parallel and aligned with the principal horizontal permeability directions. Definitions of dimensionless variables used are presented in this chapter. In addition, Chapter 2 presents the details of the derivation of the coupled wellbore and reservoir model for both active and observation horizontal wells. The computational algorithm and the specific solution procedures are discussed in Chapter 3.

Chapter 4 discusses the general results obtained from the first model. Several examples are presented to illustrate the effect of various reservoir and well conditions on the responses of both wells.

In Chapter 5, two new correlations regarding the representation of the horizontal observation well by a point and the use of the exponential integral solution in the analysis of horizontal well interference tests are provided. Examples illustrating the use and limitations of these correlations are also presented.

Chapter 6 briefly introduces the second model where the wells have arbitrary azimuth angles. The details of the derivation of the analytical models for both wells are documented.

Chapter 7 discusses the effect of permeability anisotropy and well azimuth angles in the responses of both active and observation wells. Examples showing the effect of azimuth angles in the flux distribution and transient pressure responses are presented.

Finally, Chapter 8 summarizes the results of this work. The main conclusions derived from the results and the information that can be obtained from horizontal-well observation wells are documented. Suggestions for future investigations are also noted.

1.4 Literature Review

The advancement of horizontal well technology has increased the need to understand the fluid flow behavior of these wells. Over the last three decades, several researchers have studied the pressure behavior of horizontal wells under various reservoir and well conditions and presented analytical expressions. References 1-17 present some examples of such studies.

Although extensive research has been done on the drawdown and buildup behavior of horizontal wells, only few have considered interference between horizontal wells.[18,19] Some of these studies dealt also with the effect of reservoir permeability anisotropy on the performance of horizontal wells.[20-25] To our knowledge, the effect of permeability anisotropy on the interference responses of arbitrarily oriented horizontal wells has not been discussed in detail in the literature. The estimation of the directional permeabilities from vertical well interference tests, on the other hand, has been discussed in the literature.[26-28]

In 1991, Mukherjee and Economides[29] investigated the effects of permeability anisotropy, net pay thickness, and horizontal permeability on the productivity of horizontal wells. They also proposed guidelines to determine when horizontal wells are favorable over vertical wells. In addition, they compared the performance of fractured vertical and fractured horizontal wells. Furthermore, they established criteria using NPV to compare the optimum fracture size in a vertical well with the optimum number of fractures in a horizontal well.

In 1991, Malekzadeh and Tiab[18] studied interference testing of horizontal wells. They used an analytical model based on the method of source functions. This model assumes that the permeability in the horizontal plane is isotropic (permeability in the vertical direction may be different). In addition, it does not incorporate the effects of skin and wellbore hydraulics. More importantly, Malekzadeh and Tiab assumed that the observation well may be visualized as a vertical well. They presented dimensionless pressure and derivative type curves for interference testing of horizontal wells and equations to estimate transmissibility and storativity from interference test data. In 1992, Malekzadeh[19] presented additional work based on the model developed earlier.[18] Here, he presented a correlation between the observation well responses and the exponential integral solution (interference between vertical wells).

In 1996, Retnanto and Economides[30] studied the effect of multiple-laterals, permeability anisotropy, and well direction in the productivity index using numerical simulation. They concluded that multiple laterals in low-to moderate permeability reservoirs might provide high production rates. On the other hand, they found that in high-permeability reservoirs the incremental benefits from multiple-laterals are reduced.

In 1996, Retnanto *et al.*[31] studied the performance of several multi-lateral scenarios using a simulation model. They presented several examples illustrating how to identify optimum spacing, length and number of sidetracks for various reservoir conditions. In addition, they

stated that when the total horizontal-well length is the same, the productivity increases as the number of laterals and branches decreases. Moreover, they concluded that the length and number of branches (multilaterals) may be optimized by balancing incremental production against the costs of drilling and well completion.

In 1996, Economides *et al.*[21] investigated the effect of vertical-to-horizontal and horizontal-to-horizontal permeability anisotropies with respect to well azimuth angle in the performance of horizontal wells. They established a methodology to estimate the productivity index of these wells under anisotropic permeability based on a transformation of well and reservoir parameters and using horizontal plane shape factors.

In 1996, Zhang and Dusseault[22] presented graphical and numerical methods to estimate the permeability anisotropy from pressure transient tests in arbitrarily oriented horizontal wells. They established a semi-analytical model that assumes that the horizontal well is drilled at an angle from the k_x direction. They also found that the existence and duration of the early-time radial and intermediate-time linear flow periods depend on the orientation of the wells. Because of the dependence of anisotropic permeability on well orientation, two sets of well test data from two arbitrarily oriented horizontal wells are required in order to determine the permeability ellipse. The paper also presents a field example to demonstrate the application of the methods.

Similarly in 1997, Yildiz and Ozkan[23] developed an analytical solution in Laplace space to investigate the influence of well orientation and areal anisotropy on the transient pressure responses of a horizontal well whose axes are not aligned with one of the horizontal principal permeability directions. Their observations were in agreement with those of Zhang and Dusseault.[22] In addition, they found that small deviations of up to 20° from the minimum areal permeability direction do not significantly increase the pressure drop. However, for greater azimuth angles the pressure drop increases substantially. Moreover,

their analysis showed that the principal permeabilities predicted by using the conventional straight line methods are erroneous but the geometric mean of the areal and 3-D equivalent system permeability estimates are reasonable. Finally, they indicated that well orientation significantly influences the early-time well productivity.

In 1998, Retnanto and Economides[32] presented dimensionless IPR curves for horizontal and multilateral wells in solution-gas-drive reservoir. The results obtained were based on numerical simulation. The data presented encompasses a wide range of reservoir data, PVT properties and relative permeability characteristics. They found that the bubble-point pressure and reservoir depletion have a significant effect on the curves. In addition, they developed an empirical equation that relates dimensionless flow rate to dimensionless pressure.

In 1999, Alkhonifer and Ershaghi[33] established a method to detect channel sands and vertical shale continuity using interference responses of parallel horizontal wells. Their method is based on integrating the responses at multiple isolated probing points along a horizontal observation well path, and mapping the permeability profiles from the application of a hybrid method that consists of deterministic and stochastic models.

In 1999, Hatzignatiou[34] developed a numerical model to simulate gas flow in naturally fractured reservoirs. The model considers a stochastically generated natural fracture network. Simulation of horizontal-well responses in naturally fractured gas reservoirs indicate that well location, degree of clustering, fracture density, fracture aperture distribution, and degree of fracture interconnectedness are the significant factors influencing gas production rates, gas recovery, and reservoir drainage effectiveness.

In 1999, Spivey and Lee[24] presented a method for finding the equivalent isotropic system for a horizontal well or a hydraulically fractured well at an arbitrary azimuth angle in an

anisotropic reservoir. Their method therefore enables calculating the pressure response of an anisotropic system using a transformed isotropic system. They also matched and confirmed some of the observations of Yildiz and Ozkan.[23]

In 2000, Chen *et al.*[28] established a method to determine the magnitude and orientation of permeability anisotropy by using interference tests between conventional wells. Four reservoir cases were studied: homogeneous isotropic, homogeneous anisotropic, heterogeneous isotropic, and heterogeneous anisotropic. They concluded that a log-log plot of the pressure change versus time/(distance)^2, provides a reliable diagnostic tool to establish the existence of flow/permeability anisotropy. In addition, the method may be used to identify the well-pattern quadrant in which the orientation of flow/permeability anisotropy is within a range of 45°. Moreover, the degree/contrast of anisotropy can also be described qualitatively.

In 2001, Cline and Tiab[25] investigated the vertical and horizontal well flow behavior in cases of permeability anisotropy. They demonstrated, through various simulation experiments, that for vertical wells, the geometric mean is a good estimate of effective horizontal permeability regardless of the contrast in k_x and k_y. However, they found that the geometric mean horizontal permeability is not a good approximation for horizontal wells. Also, they demonstrated that as the contrast in k_x and k_y increases while keeping the geometric mean constant, the simulation results diverge increasingly from one another. This is a result that is not predicated by most horizontal well analytical equations that utilize the geometric mean of horizontal permeability. Moreover, they found that the difference between the responses of horizontal wells in isotropic and anisotropic reservoirs increase as the well length increases for a given reservoir thickness and dimension and when the contrast in k_x and k_y increases.

In 2001, Al-Khamis *et al.*[35] developed a semi-analytical model for interference tests of parallel horizontal wells. The model was used to investigate the general characteristics of interference

test responses of horizontal wells. Their results indicated that the vertical interference well assumption is not always valid for interference testing between two horizontal wells. In addition, they recommended that interference tests between two horizontal wells should be analyzed by semi-analytical models like the one presented in the study or by reservoir simulators.

In 2002, Erwin *et al.*[36] presented information on a multi-well interference test conducted in Colville River Filed which is located in the north slope of Alaska. In this field, every development well is a horizontal openhole completion. The primary objectives of conducting the test were to enhance understanding of field scale reservoir continuity, evaluate and determine directional permeability trends, confirm the presence and impact of existing faults on waterflood patterns, and feasibility of water injection. The data obtained were also used to validate and calibrate a numerical simulation model, which was used to predict reservoir performance.

Another related area of work in the literature is on the modeling of finite-conductivity effect in horizontal wells. In this dissertation, interference testing between finite-conductivity horizontal wells is investigated. In the literature, several finite-conductivity horizontal well models have been proposed.[37-43] The models developed here are based on the finite-conductivity horizontal well model discussed in Refs. 38,39 and 41.

CHAPTER 2

MODEL FOR WELLS ALIGNED WITH THE PRINCIPAL PERMEABILITY DIRECTIONS

As mentioned in the Introduction, one of the objectives of this study is to develop semi-analytical models. These models serve as a main tool to investigate the fundamental features of interference testing between two horizontal wells. The models should also be useful to calibrate numerical simulators and develop horizontal well interference type curves.

In this chapter, we discuss the general physical model and present the development of the first semi-analytical model. Here, we restrict our attention to the cases where the horizontal wells are aligned with one of the principal horizontal permeability directions. Later, in Chapter 6, we will discuss a more general model where the azimuth angles of the wells with respect to the directions of the principal horizontal permeabilities are arbitrary. The reason for presenting two models (although the second model includes the first) is the necessity to verify the computational algorithms and discuss the relatively simpler cases first for ease of understanding. Most of the computational algorithms used in the first model have been used in the previous studies[38,39,41] and tested. Therefore, the results of the first model provide the asymptotic cases to be used for verifying the second more general and more complex model. Also, because a relatively simple well-permeability orientation is considered, this model leads to some correlations to be used in the analysis of horizontal-well interference tests.

2.1 Physical Model

To develop the semi-analytical model, we assume an anisotropic but homogeneous reservoir of thickness, h. The flow is single phase and isothermal. We consider a fluid of constant compressibility, c, and viscosity, μ. Although the derivations presented here are for liquid flow, they can be readily extended to single phase gas flow by the pseudopressure concept.[41,44] The reservoir pressure is uniform initially and equal to p_i.

Figure 2-1 shows a sketch of the system considered here. The two horizontal wells are parallel and aligned with the permeability in x-direction. We use the convention that Well 1 is the pulsing well and Well 2 is the observation well. The lengths of the pulsing and observation wells are L_{h1} and L_{h2}, respectively. In this study, however, the lengths of both wells are assumed to be equal. The coordinates of the heel ends of the wells are denoted by x_{wi}, y_{wi}, z_{wi} for i= 1 or 2.

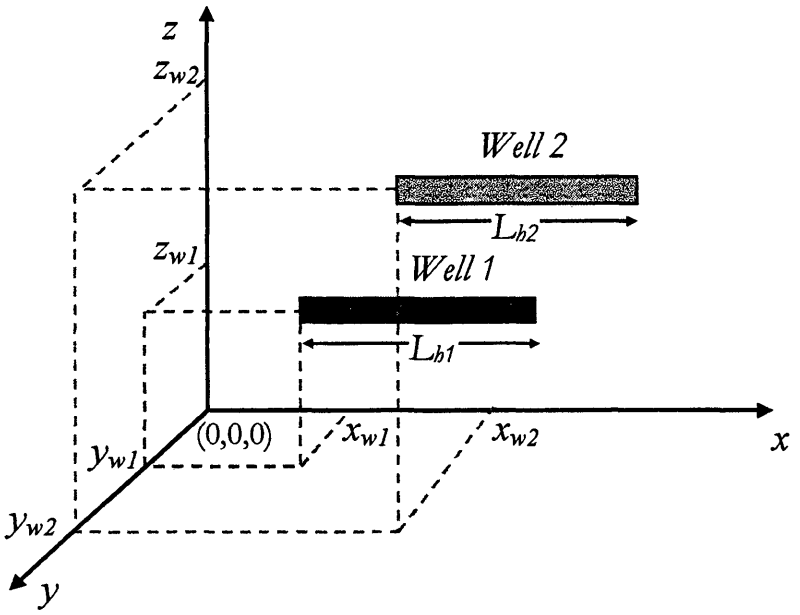

Figure 2-1. Horizontal well configuration for the first model, 3-D view.

Fluid can enter and leave both wells along their entire length. At a point x, the flow rate in Well i, q_{hci}, is given by the following relation:

$$q_{hci}(x,t) = \int_{x}^{L_{hi}+x_{wi}} q_{hi}(x',t)dx' \tag{2-1}$$

where $q_{hi}(x,t)$ is the flux entering or leaving well i at point x and time t (rate per unit length). A positive value for flux, q_{hi}, indicates influx (production) whereas a negative value corresponds to outflux (fluid leaving the well or injection). Note that the flux distribution along a well is a function of time. At the heel of the pulsing well (x_{wJ}), we set $q_{hc1}(x_{w1},t) = q$ where q is the constant production rate. Because there is no production from the observation well and we assume that the wells are produced or shut-in at the sandface (we do not consider the effect of wellbore storage in this study), we impose the condition at the heel of the observation well that $q_{hc2}(x_{w2},t) = 0$. The toes of both wells ($x = L_{hi} + x_{wi}$) are sealed.

Note that because there is no production from the observation well, flux distribution along this well should be induced by the pressure gradients due to the production of the active well. Specifically, if there is pressure gradient along the sandface of the observation well, the fluid will enter the wellbore at the higher pressure points and travel toward the lower pressure points (because the wellbore has higher conductivity than the reservoir) where it will exit the wellbore. By the requirement that the cumulative flux along the observation well must be zero, the influx will be equal to the outflux along the observation well. Therefore, until the radius of investigation for the pulsing well reaches the observation well, the flux distribution along the observation well should be uniform and zero. After the radius of investigation of the pulsing well reaches the observation well, the far end of the observation well should start producing fluid and the near end should inject the fluid back into the

reservoir. This indicates that the observation well serves as a high conductivity path for the production from the pulsing well. Because in practice, the observation well will not be very close to the active well, the contribution of the high conductivity flow path provided by the observation well may not be noticeable at the active well (the contribution of the observation well should be in the form of a reduction in the drawdown). The pressure responses measured at the heel of the observation well, however, may be significantly affected by the fluid flow in the observation well. This is the underlying physical phenomenon of the semi-analytical model. Before presenting the semi-analytical model, however, we introduce the dimensionless variables.

2.2 Dimensionless Variables

For convenience and generality, we use dimensionless variables in this study. We define the dimensionless pressure and time by the following expressions, respectively:

$$p_D(t_D) = \frac{kh}{141.2\,qB\mu}[p_i - p(x_D, y_D, z_D, t_D)], \tag{2-2}$$

and

$$t_D = \frac{6.328\times10^{-3}\,k}{\phi c_t\,\mu l^2}t, \tag{2-3}$$

for t in days. The term l in Eq. 2-3 is a characteristic length in the system that we choose as the half-length of the horizontal well in this study; that is, $l = L_h/2$. The permeability k is

the geometric average of the permeabilities in the x, y, and z directions ($k = \sqrt[3]{k_x k_y k_z}$). The dimensionless distances in x, y, and z directions are defined, respectively, by

$$x_D = \frac{x}{l}\sqrt{\frac{k}{k_x}}, \tag{2-4}$$

$$y_D = \frac{y}{l}\sqrt{\frac{k}{k_y}}, \tag{2-5}$$

and

$$z_D = \frac{z}{h}. \tag{2-6}$$

We also define the dimensionless formation thickness, dimensionless horizontal well length, and dimensionless wellbore radius by the following expressions, respectively:

$$h_D = \frac{h}{l}\sqrt{\frac{k}{k_z}}, \tag{2-7}$$

$$L_D = \frac{L_h}{2h}\sqrt{\frac{k_z}{k}}, \tag{2-8}$$

and

$$r_{wD} = \frac{r_{we}}{h}, \tag{2-9}$$

where r_{we} is the equivalent wellbore radius for an anisotropic reservoir[45] given by

$$r_{we} = \frac{r_w}{2}\left[\left(\frac{\sqrt{k_x k_y}}{k_z}\right)^{0.25} + \left(\frac{k_z}{\sqrt{k_x k_y}}\right)^{0.25}\right]. \tag{2-10}$$

Finally, the dimensionless flux is defined by

$$q_{hD} = \frac{2q_h l}{qB}\sqrt{\frac{k_x}{k}}. \tag{2-11}$$

In our derivations, we use two dimensionless groups to correlate the effect of wellbore hydraulics when the frictional pressure drop in the wellbore is significant.[41] These are the Reynolds number and dimensionless conductivity defined, respectively, by the following relations:

$$N_{\mathrm{Re}c}(x) = 6.157\times10^{-2}\,\frac{\rho q_{hc}(x)}{\mu r_w}, \tag{2-12}$$

and

$$C_{hD} = 7.395\times10^{13}\,\frac{r_w^4}{k\,h\,L_h}. \tag{2-13}$$

The dimensionless roughness factor is given by

$$\varepsilon_D = \frac{\varepsilon}{2r_w}. \tag{2-14}$$

Note that the above definitions are used for both active and observation wells. We use the subscripts 1 and 2 with the above definitions to indicate the property related to the active and observation wells, respectively.

2.3 Semi-Analytical Model

The semi-analytical model is based on the superposition of two finite-conductivity horizontal well solutions for the physical conditions discussed above. The development of the finite-conductivity horizontal well solution has been discussed in Refs. 38 and 41 and involves coupling of the wellbore and reservoir flow equations. The reservoir flow equation [dimensionless pressure at a point (x_D, y_D, z_D)] for a single horizontal well of length, L_h, located at (x_{wD}, y_{wD}, z_{wD}) in an infinite slab reservoir of thickness, h, is obtained by using the method of sources and sinks[2,45] and is given by:

$$\Delta p = \frac{1}{\phi c_t}\int_0^t\int_0^{L_h} q_h(x',\tau)\frac{1}{2\sqrt{\pi\eta_x(t-\tau)}}\exp\left[-\frac{(x-x_w-x')^2}{4\eta_x(t-\tau)}\right]dx'\frac{1}{2\sqrt{\pi\eta_y(t-\tau)}}$$
$$\exp\left[-\frac{(y-y_w)^2}{4\eta_y(t-\tau)}\right]\frac{1}{h}\left\{1+2\sum_{n=1}^{\infty}\exp\left[-\frac{n^2\pi^2\eta_z(t-\tau)}{h^2}\right]\cos n\pi\frac{z_w}{h}\cos n\pi\frac{z}{h}\right\}d\tau \quad , \qquad (2\text{-}15)$$

here

$$\eta_i = \frac{6.328x10^{-3}k_i}{\phi c_t \mu}, \qquad i = x, y \text{ or } z. \qquad (2\text{-}16)$$

Using the definitions of dimensionless variables (Eqs. 2-2 – 2-14), Eq. 2-15 may be written as follows:

$$\Delta p = \frac{1}{4\pi h\phi c_t}\int_0^t\int_0^{L_h} q_h(x',\tau)\exp\left[-\frac{(x_D - x_{wD} - x_D')^2 l^2 \frac{k_x}{k}}{4\eta_x(t-\tau)}\right]dx' \frac{1}{\sqrt{\eta_x\eta_y}(t-\tau)}$$

$$\exp\left[-\frac{(y_D - y_{wD})^2 l^2 \frac{k_y}{k}}{4\eta_y(t-\tau)}\right]\left\{1+2\sum_{n=1}^{\infty}\exp\left[-\frac{n^2\pi^2\eta_z(t-\tau)}{h^2}\right]\cos n\pi z_D \cos n\pi z_{wD}\right\}d\tau$$

$$= \frac{\eta}{4\pi h l^2\phi c_t\sqrt{\eta_x\eta_y}}\int_0^t\int_0^{L_h} q_h(x',\tau)\exp\left[-\frac{\left(x_D - x_{wD} - \frac{x'}{l}\sqrt{\frac{k}{k_x}}\right)^2}{4(t_D-\tau)}\right]dx' \frac{1}{(t_D-\tau)}$$

$$\exp\left[-\frac{(y_D - y_{wD})^2}{4(t_D-\tau)}\right]\left\{1+2\sum_{n=1}^{\infty}\exp\left[-\frac{n^2\pi^2 l^2\eta_z\eta(t-\tau)}{h^2\eta l^2}\right]\cos n\pi z_D \cos n\pi z_{wD}\right\}d\tau. \quad (2\text{-}17)$$

Now, if we let

$$\alpha = \frac{x'}{l}\sqrt{\frac{k}{k_x}}, \quad (2\text{-}18)$$

Eq. 2-17, may be simplified to

$$\Delta p = \frac{\eta}{4\pi h l^2\phi c_t\sqrt{\eta_x\eta_y}}\int_0^t l\sqrt{\frac{k_x}{k}}\int_0^{\frac{L_h}{l}\sqrt{\frac{k}{k_x}}} q_h(\alpha,\tau)\exp\left[-\frac{(x_D - x_{wD} - \alpha)^2}{4(t_D-\tau)}\right]d\alpha$$

$$\exp\left[-\frac{(y_D - y_{wD})^2}{4(t_D-\tau)}\right]\left\{1+2\sum_{n=1}^{\infty}\exp\left[-\frac{n^2\pi^2(t_D-\tau)}{h_D^{\,2}}\right]\cos n\pi z_D \cos n\pi z_{wD}\right\}\frac{d\tau}{(t_D-\tau)} \quad (2\text{-}19)$$

Finally, after rearranging and substituting the definitions of dimensionless pressure (Eq. 2-2) and time (Eq. 2-3), Eq. 2-19 may be written as

$$p_D(x_D,y_D,z_D,t_D)=\frac{1}{4}\sqrt{\frac{k^2}{k_x k_y}}\int_0^{t_D}\int_0^{2L_D h_D\sqrt{\frac{k}{k_x}}} q_{hD}(\alpha,\tau)\exp\left[-\frac{(x_D-x_{wD}-\alpha)^2}{4(t_D-\tau)}\right]d\alpha$$
$$\exp\left[-\frac{(y_D-y_{wD})^2}{4(t_D-\tau)}\right]\left\{1+2\sum_{n=1}^{\infty}\exp\left[-\frac{n^2\pi^2(t_D-\tau)}{h_D{}^2}\right]\cos n\pi z_D\cos n\pi z_{wD}\right\}\frac{d\tau}{(t_D-\tau)}. \tag{2-20}$$

In order to obtain the dimensionless pressure at a point x_D,y_D,z_D in the reservoir because of two horizontal wells, we use the superposition theorem with Eq. 2-20 as follows

$$p_D(x_D,y_D,z_D,t_D)=p_{D1}(x_D,y_D,z_D;x_{wD1},y_{wD1},z_{wD1},t_D)$$
$$+p_{D2}(x_D,y_D,z_D;x_{wD2},y_{wD2},z_{wD2},t_D). \tag{2-21}$$

Where p_{Dk} is written from Eq. 2-20 as follows

$$p_{Dk}(x_D,y_D,z_D;x_{wDk},y_{wDk},z_{wDk},t_D)=\frac{1}{4}\sqrt{\frac{k^2}{k_x k_y}}\int_0^{t_D}\int_0^{2L_{Dk}h_D\sqrt{\frac{k}{k_x}}} q_{hDk}(\alpha,\tau)$$
$$\exp\left[-\frac{(x_D-x_{wDk}-\alpha)^2}{4(t_D-\tau)}\right]d\alpha\ \ \exp\left[-\frac{(y_D-y_{wDk})^2}{4(t_D-\tau)}\right] \tag{2-22}$$
$$\left\{1+2\sum_{n=1}^{\infty}\exp\left[-\frac{n^2\pi^2(t_D-\tau)}{h_D{}^2}\right]\cos n\pi z_D\cos n\pi z_{wDk}\right\}\frac{d\tau}{(t_D-\tau)}$$

In this case p_{Di} indicates the contribution of Well i (i = 1 or 2) to the dimensionless pressure at point (x_D, y_D, z_D). So far, only reservoir pressure drop has been considered. Because of high production rates and long lengths, wellbore hydraulics in horizontal wells may be significant. To develop a finite conductivity model we now need to incorporate wellbore hydraulics into our model (Eq. 2-21) for both the active and observation wells.

2.3.1 Coupled Wellbore-Reservoir Model for Active Well

Following Ozkan, *et al.*[38,39] we may write the following equations for Well 1 (active well). The steady-state momentum equation for single-phase isothermal flow in a horizontal wellbore is given by (in this case, the elevation term equals to zero and kinetic energy term is neglected since it is small):

$$\frac{dp_{h1}}{dx} = Efq_{hc}^2. \tag{2-23}$$

Here p_{h1} stands for the pressure at some point in horizontal Well 1, f is the fanning friction factor and

$$E = 9.117x10^{-13}\frac{\rho}{\pi^2 r_w^5}. \tag{2-24}$$

Differentiating Eq. 2-23 with respect to x, we obtain

$$\frac{d^2 p_{h1}}{dx^2} = E\left(q_{hc1}^2 \frac{df_1}{dx} - 2 f_1 q_{hc1} q_{h1} \right), \tag{2-25}$$

here q_{hc1} is the flow rate in Well 1 (at some point x) and q_{h1} is the flux entering Well 1 (at point x). Note that in Eq. 2-25, we have used the following relation between q_{hc1} and q_{h1}:

$$\left(\frac{\partial q_{hc1}}{\partial x} \right)_{(x,t)} = -q_{h1}(x,t). \tag{2-26}$$

We now integrate Eq. 2-25 and use the following boundary condition

$$\left(\frac{dp_{h1}}{dx} \right)_{x=x_{w1}} = E f_{t1} q^2 B^2 \tag{2-27}$$

to obtain

$$\frac{dp_{h1}}{dx} = E f_{t1} q^2 B^2 + E \int_{x_{w1}}^{x} \left(q_{hc1}^2 \frac{df_1}{dx'} - 2 f_1 q_{hc1} q_{h1} \right) dx', \tag{2-28}$$

where q is the surface production rate of Well 1 and f_{t1} is the friction factor at the heel of Well 1. Integrating Eq. 2-28 once more gives

$$p_{h1}(x,t) - p_{wf1}(t) = E f_{t1} q^2 B^2 (x - x_{w1}) + E \int_{x_{w1}}^{x} \int_{x_{w1}}^{x'} \left(q_{hc1}^2 \frac{df_1}{dx''} - 2 f_1 q_{hc1} q_{h1} \right) dx'' dx'. \tag{2-29}$$

Equation 2-29 represents the pressure drop in the wellbore at a particular time. In terms of dimensionless variables, Eq. 2-29 may be written as:

$$p_{wD1}(t_D) - p_{hD1}(x_D, t_D) = \frac{N_{Ret1} f_{t1}}{16} \frac{\pi}{C_{hD1}}$$

$$\left[\frac{2(x_D - x_{wD1})}{L_{D1} h_D \sqrt{\frac{k}{k_x}}} - \frac{1}{L_{D1} h_D \sqrt{\frac{k}{k_x}}} \int_{x_{wD1}}^{x_D} \int_{x_{wD1}}^{x'_D} \left(\frac{D_1}{N_{Ret1} f_{t1}} q_{hD1} \right) dx''_D dx'_D \right]. \quad (2\text{-}30)$$

In Eq. 2-30, we have used:

$$\frac{N_{Re1}}{N_{Ret1} f_1} \left(\frac{df_1}{dx_D} \right) - q_{hD1} = -\frac{1}{2} \left(\frac{N_{Re1}}{f_1} \frac{df}{dN_{Re1}} + 2 \right) q_{hD1}, \quad (2\text{-}31)$$

where N_{Ret} is the Reynolds number at the heel of the well (x=0) which is known [$q_{hc}(x=0) = q$]. Along the horizontal section, however, the flux will vary and therefore $N_{Re}(x)$ will be a correlating group for the friction factor, f, which will also determine the flow regime. Detailed derivation of Eq. 2-31 is shown in Appendix A. In Eq. 2-30, D_1 is defined by

$$D_1 = (N_{Re1})^2 \left(\frac{df_1}{dN_{Re1}} \right) + 2 N_{Re1} f_1 . \quad (2\text{-}32)$$

Note that the terms p_{wD1} and $p_{hD1}(x_D, t_D)$ in Eq. 2-30 are the dimensionless wellbore pressures measured at the heel of the active well (x_D=0) and at some point x_D, respectively. Note that by the continuity of pressure, $p_{hD1}(x_D, t_D)$ is equal to the sandface pressure given by Eq. 2-21 except that the skin factor for Well 1 should be included. Incorporating the skin factor in Eq. 2-21 gives the following dimensionless pressure along the sandface of Well 1:

$$p_{hD1}(x_D,t_D)=p_{D1}(x_D,y_{wD1},z_{wD1}+r_{wD1};x_{wD1},y_{wD1},z_{wD1},t_D)+q_{hD1}(x_D,t_D)S_1(x_D) \\ +p_{D2}(x_D,y_{wD1},z_{wD1}+r_{wD1};x_{wD2},y_{wD2},z_{wD2},t_D) \quad (2\text{-}33)$$

Here $S_1(x_D)$ is the mechanical skin factor around Well 1 at point x_D and p_{Di} is given by Eq. 2-22. Again by the continuity of flux along the surface of the well, q_{hDi} terms (i = 1) in Eqs. 2-30 and 2-33 are the same. Therefore, Eqs. 2-30 and 2-33 represent the coupled wellbore-reservoir flow model for the active well.

As shown in Ref. 39, the coupled flow equation may be discretized along the horizontal well and solved for the wellbore pressure, p_{wD1}, and the dimensionless flux, q_{hD1}. Note, however, that in this two-well problem, the computation of the p_{D2} term in Eq. 2-33 requires the flux distribution for Well 2. Therefore, to be able to evaluate the coupled flow equation for the active well, we need to know the flux distribution for the observation well. This can be accomplished by developing the coupled flow equation for the observation well.

2.3.1.0 Definition of Skin Term

Ozkan and Raghavan[47] have defined the horizontal well skin factor as follows:

$$S_{hm}=\frac{P_h(r_w,x,t)-P_s(r_w+\Delta r_{ws},x,t)}{\frac{Lk_{\tilde{r}}}{hk}\left(\tilde{r}\frac{\partial P}{\partial \tilde{r}}\right)_{\tilde{r}=r_w,x}}=\frac{\frac{kh}{141.2qB\mu}\Delta P_s}{\tilde{q}_{hD}}, \quad (2\text{-}34)$$

here the subscript s indicates the skin zone property, $\tilde{r}$ is the radial coordinate in the y-z plane (centered at the well axis); that is,

$$\tilde{r} = \sqrt{y^2 + z^2}\,, \tag{2-35}$$

$k_{\tilde{r}}$ is the equivalent isotropic permeability in the y-z plane ($k_{\tilde{r}} = \sqrt{k_y k_z}$), and

$$\tilde{q}_{hD} = \frac{q_h(x,t)L}{qB} = \frac{Lk_{\tilde{r}}}{141.2qB\mu}\left(\tilde{r}\frac{\partial P}{\partial \tilde{r}}\right)_{\tilde{r}=r_w,x}. \tag{2-36}$$

Using the definition of q_{hD} given by Eq. 2-11, Eq. 2-36 may be written as

$$\tilde{q}_{hD} = q_{hD}L_D h_D\sqrt{\frac{k}{k_x}}, \tag{2-37}$$

and Eq. 2-34 may be rearranged to yield

$$\frac{kh}{141.2qB\mu}\Delta P_s = q_{hD}L_D h_D S_{hm}\sqrt{\frac{k}{k_x}}. \tag{2-38}$$

In dimensionless form, Eq. 2-38 becomes

$$p_{Ds} = q_{hD}L_D h_D S_{hm}\sqrt{\frac{k}{k_x}}. \tag{2-39}$$

Eq. 2-39 is the dimensionless pressure drop due to skin. The term $L_D h_D S_{hm}\sqrt{\frac{k}{k_x}}$ in Eq. 2-39, is equivalent to the term $S_1(x_D)$ in Eq. 2-33 which is in analogous to the skin factor of a vertical well.

2.3.2 Coupled Wellbore-Reservoir Model for Observation Well

Development of the coupled flow equation for the observation well follows the same lines as above except, because Well 2 is shut in, Eq. 2-27 is replaced by:

$$\left(\frac{dp_{h2}}{dx}\right)_{x=x_{w2}} = 0. \tag{2-40}$$

Then, the counter part of Eq. 2-29 for Well 2 (observation well) may be written as:

$$p_{h2}(x,t) - p_{wf2} = E\int_{x_{w2}}^{x}\int_{x_{w2}}^{x'}\left(q_{hc2}^2\frac{df_2}{dx''} - 2f_2 q_{hc2} q_{h2}\right)dx''dx', \tag{2-41}$$

or in dimensionless form,

$$p_{wD2}(t_D) - p_{hD2}(x_D,t_D) = -\frac{\pi}{16C_{hD2}}\frac{1}{L_{D2}h_D\sqrt{\frac{k}{k_x}}}\int_{x_{wD2}}^{x_D}\int_{x_{wD2}}^{x_D'} D_2 q_{hD2}dx_D''dx_D', \tag{2-42}$$

where D_2 is given by

$$D_2 = (N_{\mathrm{Re}2})^2\left(\frac{df_2}{dN_{\mathrm{Re}2}}\right) + 2N_{\mathrm{Re}2}f_2. \tag{2-43}$$

Therefore, similar to Eq. 2-33 for Well 1, the dimensionless pressure for Well 2 is given by

$$\begin{aligned} p_{hD2}(x_D,t_D) = {} & p_{D1}(x_D, y_{wD2}, z_{wD2} + r_{wD2}; x_{wD1}, y_{wD1}, z_{wD1}, t_D) \\ & + p_{D2}(x_D, y_{wD2}, z_{wD2} + r_{wD2}; x_{wD2}, y_{wD2}, z_{wD2}, t_D) + q_{hD2}(x_D,t_D)S_2(x_D) \end{aligned}. \tag{2-44}$$

In this case, $S_2(x_D)$ is the skin distribution along Well 2 given by

$$S_2(x_D) = \frac{\frac{kh}{141.2qB\mu}\Delta p_{2skin}(x,t)}{q_{hD2}(x_D,t_D)}. \tag{2-45}$$

Eqs. 2-30 and 2-42 constitute the coupled flow equations for finite-conductivity active and observation wells. Note that, we do not normally expect considerable frictional pressure drop in the observation well because the flow rates along the horizontal section in this well should be small. However, because one of the objectives of this study is to investigate the validity of our common expectations and assumptions, here we have modeled the finite-conductivity effects in the observation well.

The objective now is to compute the pressure distribution in the reservoir by using Eq. 2-21. To be able to use Eq. 2-21, the flux distributions, q_{hD1} and q_{hD2} along the horizontal sections of the active and interference wells, respectively, need to be known. To estimate the flux distributions, a semi-analytical algorithm needs to be developed.

2.3.3 Flux Distribution Estimation

Let us first consider Eq. 2-30 for Well 1 and for convenience, assume that the center of the coordinate axis in x-y plane is at the heel of Well 1; that is, $x_{w1}=y_{w1}=0$. In this case Eq. 2-30 simplifies to:

$$p_{wD1}(t_D) - p_{hD1}(x_D,t_D) = \frac{N_{Re1}f_{t1}}{16}\frac{\pi}{C_{hD1}L_{D1}h_D\sqrt{\frac{k}{k_x}}}\left[2x_D - \int_{x_{wD1}}^{x_D}\int_{x_{wD1}}^{x_D'}\left(\frac{D_1}{N_{Re1}f_{t1}}q_{hD1}\right)dx_D''dx_D'\right] \tag{2-46}$$

Here $p_{hD1}(x_D,t_D)$ may also be written from Eq. 2-33 at $x_{w1}=y_{w1}=0$ as

$$p_{hD1}(x_D,t_D)=p_{D1}(x_D,0,z_{wD1}+r_{wD1};0,0,z_{wD1},t_D)+q_{hD1}(x_D,t_D)S_1(x_D) + p_{D2}(x_D,0,z_{wD1}+r_{wD1};x_{wD2},y_{wD2},z_{wD2},t_D) \tag{2-47}$$

If Well 1 is divided into M segments, and the center of a segment is denoted by x_{Dj}, then the double integral in Eq. 2-46 may be written as:

$$\int_{x_{wD1}}^{x_{Dj}}\int_{x_{wD1}}^{x_D'} D_1 q_{hD1}\,dx_D''dx_D' = \sum_{i=1}^{j-1}\left(x_{Dj}-i\Delta x_{D1}+\frac{\Delta x_{D1}}{2}\right)\Delta x_{D1}D_{1i}q_{hD1i}+\frac{(\Delta x_{D1})^2}{8}D_{1j}q_{hD1j}. \tag{2-48}$$

Here, D_{1i} and q_{hD1i} are evaluated at the center of the i^{th} interval. Similarly, Eq. 2-47 will need to be discretized. Let us assume that the flux, q_{hD}, is constant in each segment, divide each well into M equal segments, and define the following relation:

$$G_{ki}(x_D,y_D,z_D;x_{wDk},y_{wDk},z_{wDk},t_D)=\frac{\sqrt{\pi}}{4}\sqrt{\frac{k^2}{k_xk_y}}\exp\left[-\frac{(y_D-y_{wDk})^2}{4t_D}\right] \left[erf\left(\frac{x_D-x_{wDk}-\frac{i-1}{M}\tilde{L}_{Dk}}{2\sqrt{t_D}}\right)-erf\left(\frac{x_D-x_{wDk}-\frac{i}{M}\tilde{L}_{Dk}}{2\sqrt{t_D}}\right)\right], \tag{2-49}$$
$$\left\{1+2\sum_{n=1}^{\infty}\exp\left[-\frac{n^2\pi^2t_D}{h_D^{\,2}}\right]\cos n\pi z_D\cos n\pi z_{wDk}\right\}\frac{1}{\sqrt{t_D}}$$

where

$$\tilde{L}_{Dk}=L_{Dk}h_D\sqrt{\frac{k}{k_x}}. \tag{2-50}$$

Using Eq. 2-49, we can write p_{Dk} in Eq. 2-47 as follows:

$$p_{Dk}\left(x_{Dj}, y_D, z_D; x_{wDk}, y_{wDk}, z_{wDk}, t_D\right) = \int_0^{t_D} \sum_{i=1}^{M} q_{hDki}(\tau) G_{ki}\left(x_{Dj}, y_D, z_D; x_{wDk}, y_{wDk}, z_{wDk}, t_D - \tau\right) d\tau \quad (2\text{-}51)$$

Eq. 2-51 may also be discretized in time as follows:

$$p_{Dk}\left(x_{Dj}, y_D, z_D; x_{wDk}, y_{wDk}, z_{wDk}, t_D\right) = \sum_{l=1}^{N} \int_{t_{Dl-1}}^{t_{Dl}} \sum_{i=1}^{M} q_{hDki}(\tau) G_{ki}\left(x_{Dj}, y_D, z_D; x_{wDk}, y_{wDk}, z_{wDk}, t_D - \tau\right) d\tau \quad (2\text{-}52)$$

Assuming q_{hDki} is constant in each time interval (t_{Dl}-t_{Dl-1}), Eq. 2-52 can be written as

$$p_{Dk}\left(x_{Dj}, y_D, z_D; x_{wDk}, y_{wDk}, z_{wDk}, t_D\right) = \tilde{p}_{Dk}\left(x_{Dj}, y_D, z_D; x_{wDk}, y_{wDk}, z_{wDk}, t_D\right) + \sum_{i=1}^{M} q_{hDki}\left(t_{DN}\right) \int_0^{t_{DN}-t_{DN-1}} G_{ki}\left(x_{Dj}, y_D, z_D; x_{wDk}, y_{wDk}, z_{wDk}, \tau\right) d\tau \quad (2\text{-}53)$$

In Eq. 2-53,

$$\tilde{p}_{Dk}\left(x_{Dj}, y_D, z_D; x_{wDk}, y_{wDk}, z_{wDk}, t_D\right) = \sum_{l=1}^{N-1} \sum_{i=1}^{M} q_{hDki}\left(t_{Dl}\right) \left[\int_0^{t_{DN}-t_{Dl-1}} G_{ki}\left(x_{Dj}, y_D, z_D; x_{wDk}, y_{wDk}, z_{wDk}, \tau\right) d\tau - \int_0^{t_{DN}-t_{Dl}} G_{ki}\left(x_{Dj}, y_D, z_D; x_{wDk}, y_{wDk}, z_{wDk}, \tau\right) d\tau \right] \quad (2\text{-}54)$$

Substituting Eqs. 2-47, 2-48, 2-53 and 2-54 into Eq. 2-46, we obtain:

$$
\begin{aligned}
&p_{wD1}(t_{DN}) - \tilde{p}_{D1}\left(x_{D1j},0,z_{wD1}+r_{wD1};0,0,z_{wD1},t_D\right) \\
&-\sum_{i=1}^{M} q_{hD1i}(t_{DN}) \int_0^{t_{DN}-t_{DN-1}} G_{1i}\left(x_{D1j},0,z_D;0,0,z_{wDk},\tau\right)d\tau \\
&-q_{hD1j}S_{1j} - \tilde{p}_{D2}\left(x_{D1j},0,z_{wD1}+r_{wD1};x_{wD2j},y_{wD2j},z_{wD2},t_D\right) \\
&-\sum_{i=1}^{M} q_{hD2i}(t_{DN}) \int_0^{t_{DN}-t_{DN-1}} G_{2i}\left(x_{D1j},0,z_{wD1}+r_{wD1};x_{wD2j},y_{wD2j},z_{wD2},\tau\right)d\tau = \\
&\frac{\pi N_{Re1} f_{t1}}{8C_{hD1}} \frac{1}{L_{D1}h_D\sqrt{\frac{k}{k_x}}} x_{D1j} \\
&-\frac{\pi}{16C_{hD1}} \frac{1}{L_{D1}h_D\sqrt{\frac{k}{k_x}}} \left[\sum_{i=1}^{j-1}\left(x_{D1j}-i\Delta x_{D1}+\frac{\Delta x_{D1}}{2}\right)\Delta x_{D1}D_{1i}q_{hD1i} + \frac{(\Delta x_{D1})^2}{8}D_{1j}q_{hD1j}\right]
\end{aligned}
\tag{2-55}
$$

Here the reference point is at the heel of Well 1 and

$$
S_{1j} = S_1(x_{D1j}). \tag{2-56}
$$

By similar lines, we derive the following counterpart of Eq. 2-55 for Well 2:

$$
\begin{aligned}
&p_{wD2}(t_{DN}) - \tilde{p}_{D1}\left(x_{D2j},0,z_{wD2}+r_{wD2};x_{wD1},y_{wD1},z_{wD1},t_D\right) - \\
&\sum_{i=1}^{M} q_{hD1i}(t_{DN}) \int_0^{t_{DN}-t_{DN-1}} G_{1i}\left(x_{D2j},0,z_{wD2}+r_{wD2};x_{wD1},y_{wD1},z_{wD1},\tau\right)d\tau \\
&-\tilde{p}_{D2}\left(x_{D2j},0,z_{wD2}+r_{wD2};0,0,z_{wD2},t_D\right) \\
&-\sum_{i=1}^{M} q_{hD2i}(t_{DN}) \int_0^{t_{DN}-t_{DN-1}} G_{1i}\left(x_{D2j},0,z_{wD2}+r_{wD2};0,0,z_{wD2},\tau\right)d\tau - q_{hD2j}S_{2j} = \\
&\frac{\pi}{16C_{hD2}} \frac{1}{L_{D2}h_D\sqrt{\frac{k}{k_x}}} \left[\sum_{i=1}^{j-1}\left(x_{D2j}-i\Delta x_{D2}+\frac{\Delta x_{D2}}{2}\right)\Delta x_{D2}D_{2i}q_{hD2i} + \frac{(\Delta x_{D2})^2}{8}D_{2j}q_{hD2j}\right]
\end{aligned}
\tag{2-57}
$$

In this case, the reference point is at the heel of Well 2. x_{wD} and y_{wD} in Eqs. 2-55 and 2-57 are simply the distances between the heels of Well 1 and 2 for the first model where both wells are parallel.

To solve Eqs. 2-55 and 2-57, we discretize both horizontal wells into M segments and evaluate Eqs. 2-55 and 2-57 at the center of each segment i (x_{Dki}). The discretization of the flow equations follow the same lines as in Ref. 39 and will not be discussed here. The discretized flow equations yield $2M$ expressions in $2M+2$ unknowns; p_{wD1}, p_{wD2}, q_{hD1i}, and q_{hD2i} (i= 1, M). Two additional expressions may be obtained from the condition that the sum of the fluxes along the active well must be equal to the total production rate and the sum of the fluxes along the observation well must be zero. These conditions may be expressed, respectively, as follows:

$$\sum_{i=1}^{M} q_{hD1i} = \frac{M}{L_{D1} h_D \sqrt{\frac{k}{k_x}}}, \tag{2-58}$$

and

$$\sum_{i=1}^{M} q_{hD2i} = 0, \tag{2-59}$$

where q_{hDki} is the flux of Well k at the center of the i^{th} segment (x_{Dki}). The discretized forms of Eqs. 2-55 and 2-57 with Eqs. 2-58 and 2-59 provide $2M+2$ equations in $2M+2$ unknowns. This system of equations needs to be solved by an iteration process because Eqs. 2-55 and 2-57 are non-linear (D_1 and D_2 are functions of q_{hD1} and q_{hD2}, respectively).

CHAPTER 3

MODEL SOLUTION

The model developed in the previous chapter requires special procedures in order to solve the resulted system of equations. Before solving these equations however, it is essential to simplify some of the terms involved in order to put the system of equations in a simple matrix form. This chapter is divided into two sections. The first section discusses the solution algorithm which focuses on simplifying and organizing the system of equations while the second section discusses the solution procedures used to solve them.

3.1 Solution Algorithm

The solution algorithm discussed here is similar to that discussed in Refs. 38 and 39. Our objective is to solve the discretized forms of Eqs. 2-55 and 2-57 with Eqs. 2-58 and 2-59 which provide $2M+2$ equations. First we note the following relations that result from discretizing the well into M segments:

$$x_{kDj} = \tilde{L}_{Dk} \frac{2j-1}{2M}, \tag{3-1}$$

$$\Delta x_{kD} = \tilde{L}_{Dk} \frac{1}{M}, \tag{3-2}$$

and

$$\widetilde{L}_{Dk} = 2L_{Dk}h_D\sqrt{\frac{k}{k_x}}. \tag{3-3}$$

We also note that the tips of the i^{th} segment are located, respectively at $\widetilde{L}_{Dk}\dfrac{i-1}{M}$ and $\widetilde{L}_{Dk}\dfrac{i}{M}$. For convenience, let us make the following definitions:

$$\widetilde{p}_{Dkkj} = \widetilde{p}_{Dk}\left(\frac{2j-1}{2M}\widetilde{L}_{Dk},0,z_{wDk}+r_{wDk};0,0,z_{wDk};t_D\right), \tag{3-4}$$

$$\widetilde{p}_{Dklj} = \widetilde{p}_{Dk}\left(\frac{2j-1}{2M}\widetilde{L}_{Dl},0,z_{wDl}+r_{wDl};x_{wDk},y_{wDk},z_{wDk};t_D\right);\quad k\neq l, \tag{3-5}$$

$$\widetilde{S}_{kkij} = \int_0^{t_{DN}-t_{DN-1}} G_{ki}\left(x_{Dkj},0,z_{wDk}+r_{wDk};0,0,z_{wDk};\tau\right)d\tau, \tag{3-6}$$

and

$$\widetilde{S}_{klij} = \int_0^{t_{DN}-t_{DN-1}} G_{ki}\left(x_{Dlj},0,z_{wDl}+r_{wDl};x_{wDk},y_{wDk},z_{wDk};\tau\right)d\tau. \tag{3-7}$$

In Eqs. 3-6 and 3-7, we have defined

$$G_{ki}\left(x_D,y_D,z_D;x_{wDk},y_{wDk},z_{wDk},t_D\right) = \frac{\sqrt{\pi}}{4}\sqrt{\frac{k^2}{k_xk_y}}\exp\left[-\frac{(y_D-y_{wDk})^2}{4t_D}\right]$$
$$\left[erf\left(\frac{x_D-x_{wDk}-\dfrac{i-1}{M}\widetilde{L}_{Dk}}{2\sqrt{t_D}}\right)-erf\left(\frac{x_D-x_{wDk}-\dfrac{i}{M}\widetilde{L}_{Dk}}{2\sqrt{t_D}}\right)\right] \tag{3-8}$$
$$\left\{1+2\sum_{n=1}^{\infty}\exp\left[-\frac{n^2\pi^2t_D}{h_D{}^2}\right]\cos n\pi z_D\cos n\pi z_{wDk}\right\}\frac{1}{\sqrt{t_D}}$$

Using the above definitions, we can write Eq. 2-55 for Well 1 as follows:

$$P_{wD1}(t_{DN})-\sum_{i=1}^{M}q_{hD1i}(t_{DN})\tilde{S}_{11ij}-\sum_{i=1}^{M}q_{hD2i}(t_{DN})\tilde{S}_{21ij}-q_{hD1j}(t_{DN})S_{1j}$$
$$+\frac{2\pi\tilde{L}_{D1}}{16C_{hD1}}\left[\sum_{i=1}^{j-1}\left(\frac{j-i}{M^2}\right)D_{1i}q_{hD1i}+\frac{1}{8M^2}D_{1j}q_{hD1j}\right] \qquad (3\text{-}9)$$
$$-\frac{\pi N_{Re\,t1}f_{t1}}{8C_{hD1}}\frac{(2j-1)}{2M}-\tilde{P}_{D11j}-\tilde{P}_{D21j}=0$$

which upon rearranging yields

$$P_{wD1}(t_{DN})-\sum_{i=1}^{j-1}\left[\tilde{S}_{11ij}-\frac{\pi\tilde{L}_{D1}}{8C_{hD1}}\left(\frac{j-i}{M^2}\right)D_{1i}\right]q_{hD1i}$$
$$-\left[\tilde{S}_{11jj}-\frac{\pi\tilde{L}_{D1}}{8C_{hD1}}\left(\frac{1}{M^2}\right)D_{1j}+S_{1j}\right]q_{hD1j} \qquad (3\text{-}10)$$
$$-\sum_{i=j+1}^{M}\tilde{S}_{11ij}q_{hD1i}-\sum_{i=1}^{M}\tilde{S}_{21ij}q_{hD2i}-\frac{\pi N_{Re\,t1}f_{t1}}{8C_{hD1}}\frac{(2j-1)}{2M}-\tilde{P}_{D11j}-\tilde{P}_{D21j}=0$$

Similarly, we can write Eq. 2-57 for Well 2 as follows:

$$P_{wD2}(t_{DN})-\sum_{i=1}^{M}\tilde{S}_{12ij}q_{hD1i}-\sum_{i=1}^{j-1}\left[\tilde{S}_{22ij}-\frac{\pi\tilde{L}_{D1}}{8C_{hD1}}\left(\frac{j-i}{M^2}\right)D_{2i}\right]q_{hD2i}$$
$$-\left[\tilde{S}_{22jj}-\frac{\pi\tilde{L}_{D1}}{8C_{hD1}}\left(\frac{1}{8M^2}\right)D_{2j}+S_{2j}\right]q_{hD2j}-\sum_{i=j+1}^{M}\tilde{S}_{22ij}q_{hD2i}-\tilde{P}_{D12j}-\tilde{P}_{D22j}=0 \qquad (3\text{-}11)$$

From Eqs. 2-58 and 2-59, we also have the following relations respectively:

$$\sum_{i=1}^{M}q_{hD1i}=\frac{2M}{\tilde{L}_{D1}}, \qquad (3\text{-}12)$$

and

$$\sum_{i=1}^{M} q_{hD2i} = 0 . \tag{3-13}$$

Let us now define the following terms:

$$\widetilde{S}_{ji} = \begin{Bmatrix} \widetilde{S}_{11ij} & for & j \le M & i \le M \\ \widetilde{S}_{21(i-M)j} & for & j \le M & i > M \\ \widetilde{S}_{12i(j-M)} & for & j > M & i \le M \\ \widetilde{S}_{22(i-M)(j-M)} & for & j > M & i > M \end{Bmatrix} for \begin{matrix} 1 \le i \le 2M \\ 1 \le j \le 2M \end{matrix}, \tag{3-14}$$

$$H_{ji} = \begin{Bmatrix} \frac{\pi \widetilde{L}_{D1}}{8C_{hD1}} \left(\frac{j-i}{M^2} \right) D_{1i} & for & j \le M & i \le j-1 \\ \frac{\pi \widetilde{L}_{D1}}{8C_{hD1}} \left(\frac{1}{8M^2} \right) D_{1i} & for & j \le M & i = j \\ 0 & for & j \le M & i > j \\ 0 & for & j > M & i \le j \\ \frac{\pi \widetilde{L}_{D1}}{8C_{hD1}} \left(\frac{(j-M)-(i-M)}{M^2} \right) D_{2(i-M)} & for & j > M & M < i \le j-1 \\ \frac{\pi \widetilde{L}_{D1}}{8C_{hD1}} \left(\frac{1}{8M^2} \right) D_{2(i-M)} & for & j > M & i = j \\ 0 & for & j > M & i > j \end{Bmatrix} for \begin{matrix} 1 \le i \le 2M \\ 1 \le j \le 2M \end{matrix}, \tag{3-15}$$

$$R_{ji} = \widetilde{S}_{ji} - H_{ji} \quad for \begin{matrix} 1 \le i \le 2M \\ 1 \le j \le 2M \end{matrix}, \tag{3-16}$$

$$B_j = \begin{Bmatrix} \frac{\pi N_{Ref1} f_{t1}}{8C_{hD1}} \frac{(2j-1)}{2M} + \widetilde{P}_{D11j} + \widetilde{P}_{D21j} & for & j \le M \\ \widetilde{P}_{D12j} + \widetilde{P}_{D22j} & for & M < j \le 2M \\ \frac{2M}{\widetilde{L}_{D1}} & for & j = 2M+1 \\ 0 & for & j = 2M+2 \end{Bmatrix} for\ 1 \le j \le 2M+2, \tag{3-17}$$

and

$$Q_i = \begin{Bmatrix} P_{wD1} & for & i=1 \\ P_{wD2} & for & i=2 \\ q_{hD1(i-2)} & for & 3 \le i \le M+2 \\ q_{hD2(i-M-2)} & for & i \ge M+3 \end{Bmatrix} \qquad for\ 1 \le i \le 2M+2. \tag{3-18}$$

Using the definitions given in Eqs. 3-14 to 3-18, we can write Eqs. 3-10 and 3-11 in the following general form:

$$\sum_{i=1}^{2M+2} G_{ji} Q_i - B_j = 0 \qquad for \qquad 1 \le j \le 2M+2, \tag{3-19}$$

where

$$G_{ji} = \begin{Bmatrix} 1 & for & j \le M & i=1 \\ 0 & for & j \le M & i=2 \\ 0 & for & M < j \le 2M & i=1 \\ 1 & for & M < j \le 2M & i=2 \\ -R_{j(i-2)} & for & j \le 2M & i>2 \\ 0 & for & j > 2M & i \le 2 \\ 1 & for & j = 2M+1 & 2 < i \le M+2 \\ 0 & for & j = 2M+1 & i > M+2 \\ 0 & for & j = 2M+2 & 2 < i \le M+2 \\ 1 & for & j = 2M+2 & i > M+2 \end{Bmatrix} \quad for \begin{matrix} 1 \le i \le 2M+2 \\ 1 \le j \le 2M+2 \end{matrix}. \tag{3-20}$$

Eq. 3-19 defines our (2*M*+2) x (2*M*+2) matrix problem to be solved for Q_i for $1 \le i \le 2M+2$. Because this problem is nonlinear, we use Newton-Raphson iteration method in the solution described below.

Let us define:

$$f_j(\underline{Q}) = \sum_{i=1}^{2M+2} G_{ji} Q_i - B_j = 0, \tag{3-21}$$

and assume $\hat{\underline{Q}}$ is the solution vector. If $\underline{Q}$ is close to $\hat{\underline{Q}}$, we must have

$$f_j(\hat{\underline{Q}}) = f_j(\underline{Q}) + \sum_{i=1}^{2M+2} (\hat{Q}_i - Q_i) \frac{df_j(\underline{Q})}{dQ_i} \qquad for \quad 1 \le j \le 2M+2. \tag{3-22}$$

Because $f_j(\hat{\underline{Q}}) = 0$, we can write Eq. 3-22 as

$$\sum_{i=1}^{2M+2} (\hat{Q}_i - Q_i) \frac{df_j(\underline{Q})}{dQ_i} = -f_j(\underline{Q}) \qquad for \quad 1 \le j \le 2M+2. \tag{3-23}$$

Eq. 3-23 suggests the following iterative scheme:

$$\sum_{i=1}^{2M+2} (Q_i^{k+1} - Q_i^k) \frac{df_j(\underline{Q}^k)}{dQ_i} = -f_j(\underline{Q}^k) \qquad for \quad 1 \le j \le 2M+2. \tag{3-24}$$

Now let

$$\delta_i^{k+1} = Q_i^{k+1} - Q_i^k \qquad for \quad 1 \le i \le 2M+2. \tag{3-25}$$

Then we can write Eq. 3-24 as follows:

$$J(\underline{Q}^k)\underline{\delta}^{k+1} = -f_j(\underline{Q}^k), \tag{3-26}$$

where

$$J(\underline{Q}^k)=\left[\begin{array}{cccc} \frac{\partial f_1}{\partial Q_1} & \frac{\partial f_1}{\partial Q_2} & \cdots & \frac{\partial f_1}{\partial Q_{2M+2}} \\ \frac{\partial f_2}{\partial Q_1} & \frac{\partial f_2}{\partial Q_2} & \cdots & \frac{\partial f_2}{\partial Q_{2M+2}} \\ \vdots & & & \\ \frac{\partial f_{2M+2}}{\partial Q_1} & \frac{\partial f_{2M+2}}{\partial Q_2} & \cdots & \frac{\partial f_{2M+2}}{\partial Q_{2M+2}} \end{array}\right]_{\underline{Q}^k}, \tag{3-27}$$

$$\underline{\delta}^{k+1}=\left[\begin{array}{c} \delta_1^{k+1} \\ \delta_2^{k+1} \\ \vdots \\ \delta_{2M+2}^{k+1} \end{array}\right], \tag{3-28}$$

and

$$f\,(\underline{Q}^k)=\left[\begin{array}{c} f_1(\underline{Q}^k) \\ f_2(\underline{Q}^k) \\ \vdots \\ f_{2M+2}(\underline{Q}^k) \end{array}\right]. \tag{3-29}$$

3.2 Solution Procedure

The Newton-Raphson iteration method discussed above suggests the following solution scheme:

1. Initial guess: $\underline{Q}^0=\left(Q_1^0,Q_2^0,\cdots,Q_{M+1}^0\right)$ where $\underline{Q}^0$ is define by Eq. 3-18.

2. Solve $J(\underline{Q}^k)\underline{\delta}^{k+1} = -f_j(\underline{Q}^k)$ (Eq. 3-26) for $\underline{\delta}^{k+1}$ and compute $Q_i^{k+1} = Q_i^k + \delta_i^{k+1}$ (Eq. 3-25) for k=0,1,....(number of iterations).
3. Iteration is stopped when the following convergence criteria is satisfied:

$$\left|\frac{Q_i^{k+1} - Q_i^k}{Q_i^{k+1}}\right| \le \varepsilon \quad for \quad 1 \le i \le 2M+2$$, here ε is a preset tolerance.

Let us now write Eq. 3-27 as follows:

$$J(\underline{Q}^k) = \begin{bmatrix} A_{11} & A_{12} & \cdots & A_{1(2M+2)} \\ A_{21} & A_{22} & \cdots & A_{2(2M+2)} \\ \vdots & & & \\ A_{j1} & A_{j2} & \cdots & A_{j(2M+2)} \\ \vdots & & & \\ A_{(2M+2)1} & A_{(2M+2)2} & \cdots & A_{(2M+2)(2M+2)} \end{bmatrix}_{\underline{Q}^k}, \tag{3-30}$$

where

$$A_{ji} = \frac{\partial f_j}{\partial Q_i} = \sum_{l=1}^{2M+2}\left\{\frac{\partial G_{jl}}{\partial Q_i}Q_l + G_{jl}\frac{\partial Q_l}{\partial Q_i}\right\} \qquad for \begin{matrix} 1 \le i \le 2M+2 \\ 1 \le l \le 2M+2 \end{matrix}. \tag{3-31}$$

In Eq. 3-31, we have

$$\frac{\partial G_{jl}}{\partial Q_i} = \begin{cases} 0 & for \begin{cases} l \le 2 & 1 \le i \le 2M+2 \\ i \le 2 & 1 \le j \le 2M+2 \end{cases} \\ -\dfrac{\partial R_{j(l-2)}}{\partial Q_i} & Otherwise \end{cases}, \tag{3-32}$$

$$-\frac{\partial R_{j(l-2)}}{\partial Q_i}=\frac{\partial H_{j(l-2)}}{\partial Q_i}=$$

$$\begin{Bmatrix}
\frac{\pi\tilde{L}_{D1}}{8C_{hD1}}\left(\frac{j-l+2}{M^2}\right)\frac{\partial D_{1(l-2)}}{\partial Q_i} & for \quad j\le M \quad l\text{-}2\le j-1\\
\frac{\pi\tilde{L}_{D1}}{8C_{hD1}}\left(\frac{1}{8M^2}\right)\frac{\partial D_{1(l-2)}}{\partial Q_i} & for \quad j\le M \quad l\text{-}2=j\\
0 & for \quad j\le M \quad l\text{-}2>j\\
0 & for \quad j>M \quad l\text{-}2\le j\\
\frac{\pi\tilde{L}_{D1}}{8C_{hD1}}\left(\frac{(j-M)-(l-2-M)}{M^2}\right)\frac{\partial D_{2(l-2-M)}}{\partial Q_i} & for \quad j>M \quad M<l-2\le j-1\\
\frac{\pi\tilde{L}_{D1}}{8C_{hD1}}\left(\frac{1}{8M^2}\right)\frac{\partial D_{2(l-2-M)}}{\partial Q_i} & for \quad j>M \quad l\text{-}2=j\\
0 & for \quad j>M \quad l\text{-}2>j
\end{Bmatrix}$$

$$for \quad \begin{matrix} i\neq 2 & 1\le i\le 2M+2\\ l\neq 2 & 1\le l\le 2M+2\end{matrix} \qquad , (3\text{-}33)$$

and

$$\frac{\partial Q_l}{\partial Q_i}=\begin{Bmatrix}0 & \text{for} \quad l\neq 1\\ 1 & \text{for} \quad l=i\end{Bmatrix} \quad for \quad \begin{matrix}1\le i\le 2M+2\\ 1\le j\le 2M+2\end{matrix}. \qquad (3\text{-}34)$$

In Eq. 3-33, $\frac{\partial D_{k(l-2)}}{\partial Q_i}$ terms are given by:

$$\frac{\partial D_{k(l-2)}}{\partial Q_i}=\frac{\partial}{\partial Q_i}\left[\left(N_{\mathrm{Re}ck(l-2)}\right)^2\left(\frac{df_{ck}}{dN_{\mathrm{Re}ck}}\right)_{(l-2)}+2N_{\mathrm{Re}ck(l-2)}f_{ck(l-2)}\right]$$

$$=\frac{\partial\left(N_{\mathrm{Re}ck(l-2)}\right)^2}{\partial Q_i}\left(\frac{df_{ck}}{dN_{\mathrm{Re}ck}}\right)_{(l-2)}+\left(N_{\mathrm{Re}ck(l-2)}\right)^2\frac{\partial}{\partial Q_i}\left(\frac{df_{ck}}{dN_{\mathrm{Re}ck}}\right)_{(l-2)}. \qquad (3\text{-}35)$$

$$+2\frac{\partial N_{\mathrm{Re}ck(l-2)}}{\partial Q_i}f_{ck(l-2)}+2N_{\mathrm{Re}ck(l-2)}\frac{\partial f_{ck(l-2)}}{\partial Q_i}$$

In Eq. 3-35, we have:

$$\frac{\partial\left(N_{\mathrm{Re}ck(l-2)}\right)^2}{\partial Q_i}=\frac{\partial\left(N_{\mathrm{Re}ck(l-2)}\right)^2}{\partial N_{\mathrm{Re}ck(l-2)}}\frac{\partial N_{\mathrm{Re}ck(l-2)}}{\partial Q_i}=2N_{\mathrm{Re}ck(l-2)}\frac{\partial N_{\mathrm{Re}ck(l-2)}}{\partial Q_i}, \tag{3-36}$$

$$\frac{\partial}{\partial Q_i}=\left(\frac{\partial}{\partial N_{\mathrm{Re}ck}}\right)_{(l-2)}\frac{\partial N_{\mathrm{Re}ck(l-2)}}{\partial Q_i}, \tag{3-37}$$

$$\frac{\partial}{\partial Q_i}\left(\frac{df_{ck}}{dN_{\mathrm{Re}ck}}\right)_{(l-2)}=\left(\frac{d^2f_{ck}}{dN^2_{\mathrm{Re}ck}}\right)_{(l-2)}\frac{\partial N_{\mathrm{Re}ck(l-2)}}{\partial Q_i}, \tag{3-38}$$

and

$$\frac{df_{ck(l-2)}}{dN_{\mathrm{Re}ck}}=\frac{df_{ck(l-1)}}{dN_{\mathrm{Re}ck(l-1)}}\frac{\partial N_{\mathrm{Re}ck(l-1)}}{\partial Q_i}. \tag{3-39}$$

Substituting Eqs. 3-36 to 3-39 into Eq. 3-35, we obtain

$$\frac{\partial D_{k(l-2)}}{\partial Q_i}=\frac{\partial N_{\mathrm{Re}ck(l-2)}}{\partial Q_i}\left[4N_{\mathrm{Re}ck(l-2)}\left(\frac{df_{ck}}{dN_{\mathrm{Re}ck}}\right)_{(l-2)}+2f_{ck(l-2)}+\left(N_{\mathrm{Re}ck(l-2)}\right)^2\left(\frac{d^2f_{ck}}{dN^2_{\mathrm{Re}ck}}\right)_{(l-2)}\right]. \tag{3-40}$$

Let us consider the $\frac{\partial N_{\mathrm{Re}ck(l-2)}}{\partial Q_i}$ term in Eq. 3-40. We can note the following relation:

$$q_{hck(l-2)}=\sum_{n=l}^{M}q_{hkn}\Delta x_k=\sum_{n=l}^{M}q_{hkn}\frac{L_{hk}}{M}. \tag{3-41}$$

Using the definitions of dimensionless variables and groups, we can write Eq. 3-41 as follows:

$$N_{\mathrm{Re}ck(l-2)} = \tilde{L}_{hDk} \frac{r_{wl}}{r_{wk}} \frac{N_{\mathrm{Re}fl}}{2M} \sum_{n=l-2}^{M} q_{hDkn} \,. \tag{3-42}$$

Then, we have

$$\frac{\partial N_{\mathrm{Re}ck(l-2)}}{\partial Q_i} = \begin{cases} 0 & for \quad i < l\text{-}2 \\ \tilde{L}_{hDk} \dfrac{r_{wl}}{r_{wk}} \dfrac{N_{\mathrm{Re}fl}}{2M} & for \quad i \geq l \end{cases} \tag{3-43}$$

and thus, substituting Eq. 3-43 into Eq. 3-40, we obtain

$$\frac{\partial D_{k(l-2)}}{\partial Q_i} =$$

$$\begin{cases} 0 & for \quad i < l\text{-}2 \\ \tilde{L}_{hDk} \dfrac{r_{wl}}{r_{wk}} \dfrac{N_{\mathrm{Re}fl}}{2M} \left[4N_{\mathrm{Re}ck(l-2)} \left(\dfrac{df_{ck}}{dN_{\mathrm{Re}ck}} \right)_{(l-2)} + 2f_{ck(l-2)} + \left(N_{\mathrm{Re}ck(l-2)}\right)^2 \left(\dfrac{d^2 f_{ck}}{dN^2_{\mathrm{Re}ck}} \right)_{(l-2)} \right] & for \; i \geq l \end{cases} \tag{3-44}$$

Eq. 3-44, implies that any analytical expression for the friction-factor and any flow regime indicator may be used in this model. Ref. 48 lists some of the most commonly used analytical expressions for friction-factor estimation.

In general, there are three distinctive flow regimes in fluid flow through conduits: laminar, transition and turbulent. In the laminar flow region, friction factor is inversely proportional to Reynolds Number and the relation used to estimate the friction factor is rather simple. On

the other hand, in the turbulent flow region, friction factor is sensitive to characteristics of the pipe wall. Therefore, generally these correlations are merely designed to estimate the friction factor at the turbulent flow region. For simplicity, in this study however we have used Blasius[49] equation. In addition, it was assumed that the turbulent flow region covers the transitional flow region, $2300 < N_{Re} < 4000$, since there is no commonly used friction factor correlation is available in this region and the use of turbulent flow assumption yields reasonable estimates of the friction factor.

CHAPTER 4

RESULTS AND DISCUSSION

In this study a through investigation will be carried out to study the effect of several parameters on the interference responses between two horizontal wells using the model developed in the previous chapters. Transient pressure plots are generated to show the general characteristics of the active and observation well responses for the parameter investigated.

This chapter is divided into the following sections where examples and discussion of results are presented. Correlation between the results obtained with similar ones presented in the literature will be discussed where applicable.

- Flux Distribution.
- Transient Pressure Responses
- Effect of:
    - Horizontal Separation (Δx_w, Δy_w).
    - Vertical Separation (Δz_w).
    - Skin Factor and Skin Distribution.
    - Wellbore Conductivity.

In Chapter 7, effect of permeability anisotropy and well azimuth angles will be investigated using the results obtained from the second model.

4.1 Flux Distribution

Flux distribution along horizontal wells is a complex phenomenon due to the interaction of several factors, such as well interference, skin and perforation distribution, wellbore hydraulics, well location and well orientation. This complexity is clearly displayed by the results of logs run in horizontal wells.[50-53] The models presented in this study and the results on flux distribution discussed here may be useful in the interpretation of production logs as well as in the physical understanding of flow convergence toward horizontal wells.

In order to discuss the convergence of flow toward the active and observation horizontal wells, several cases will be investigated here. Figures 4-1 to 4-4 show the flux distributions along the active (Well 1) and observation (Well 2) wells for cases given in Table 4-1. The first case is considered as the base case in this study. In this case, the distance between the heels of both wells in the x direction is Δx_w = 1000 ft and in the normal direction is Δy_w = 3000 ft . In the vertical direction, both wells are located in the middle of the payzone. Case 2 is similar to Case 1 but with a larger separation between the two wells in the x direction (Δx_w = 3000 ft). Case 3 represents stacked dual laterals where both wells are equally spaced from the top and bottom boundaries and to each other. Finally, Case 4 represents dual opposed horizontal laterals where now the distance between the tips of the wells is 1000 ft. In all cases, both wells are set to have equal lengths. For the discussion here, the wells are assumed to have infinite conductivity except where we discuss the effect of wellbore conductivity.

As expected from results of earlier studies[21,38,39,41,54,55], Figure 4-1 shows that the flux distribution is uniform at early times and has a U-shape at late times for the active well. This is the characteristic behavior for infinite-conductivity horizontal wells. The flux distribution along the observation well, on the other hand, is zero at early times because the radius of influence of the active well does not cover the observation well at these times. When the effect of production is felt at the observation well (at late times), however, a different flux

profile develops. Approximately half of the horizontal observation well length (Segments 6-10) have positive flux (production) and the other half (Segments 1-5) have negative flux (injection). This means that portions of the observation well far away from the active well produce fluid from the reservoir and then transfers it to sections closer to the active well where fluid exits the observation well to converge toward the active well. This indicates that the observation well acts like a flow conduit which eases the flow toward the active well. Similar trend is also observed in Figure 4-2 for Case 2 where the x-direction separation between the wells is larger. It should be noted, however, that the magnitude of the flux along the observation well is always relatively small as compared to the one along the active well which is consistent with our physical expectations discussed earlier.

Table 4-1. Data for flux distribution cases.

Parameter	Case 1	Case 2	Case 3	Case 4
q, STBD	2000	2000	2000	2000
L_h, ft	2000	2000	2000	2000
h, ft	100	100	100	100
k_x, md	50	50	50	50
k_y, md	100	100	100	100
k_z, md	25	25	25	25
r_w, ft	0.165	0.165	0.165	0.165
Δx_w, ft	1000	3000	0	3000
Δy_w, ft	3000	3000	0	0
z_{w1}, ft	50	50	33.3	50
z_{w2}, ft	50	50	66.6	50

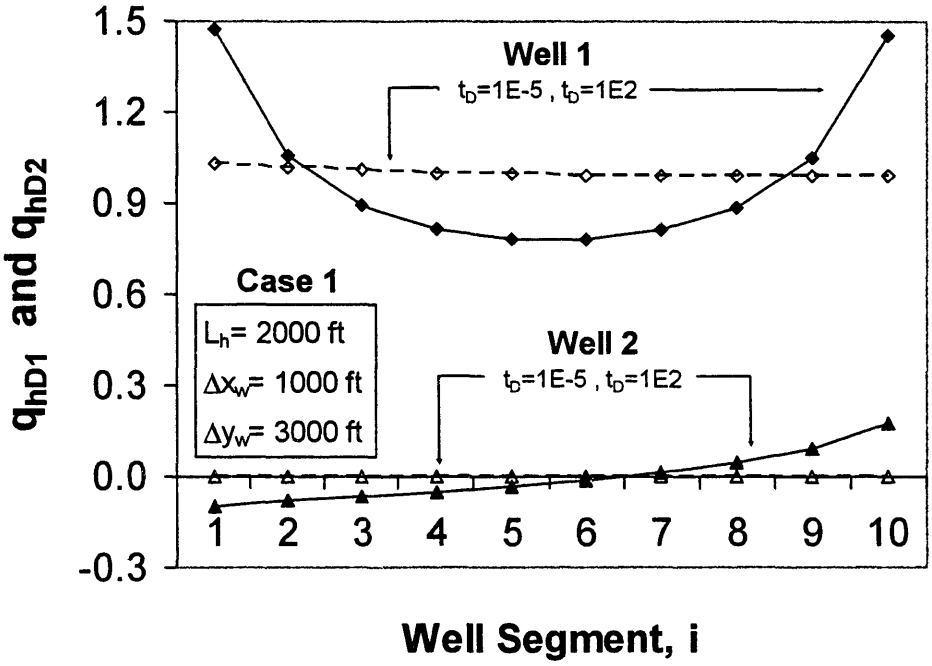

Figure 4-1. Flux distributions along the active and observation wells, Case 1.

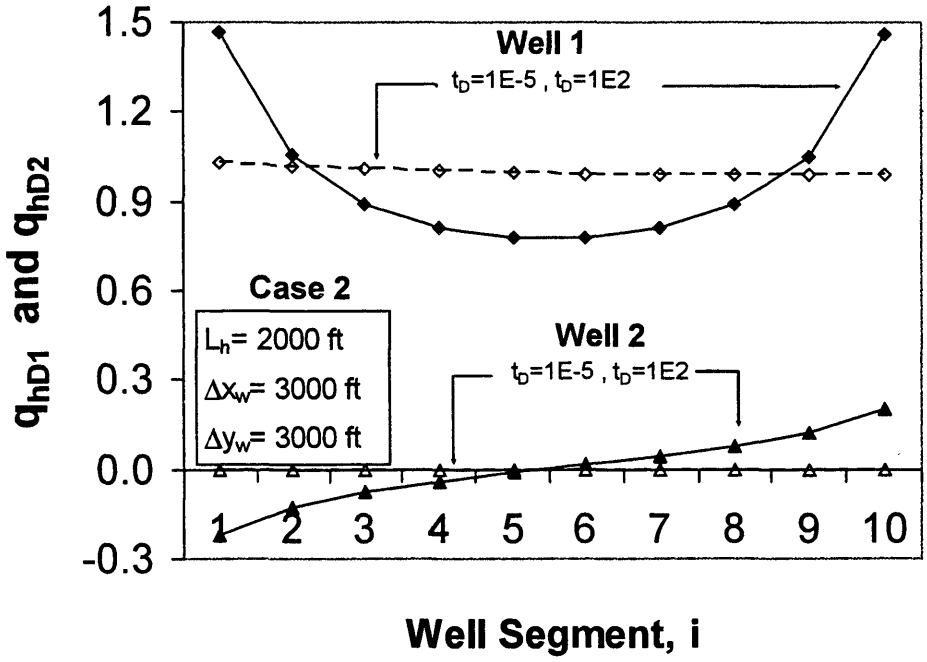

Figure 4-2. Flux distributions along the active and observation wells, Case 2.

For the case of vertically stacked dual laterals (Case 3), the flux distribution of the observation well is similar in shape to the one for the active well with the middle segments having negative flux while segments at both ends of the well having positive flux (Figure 4-3). Interesting to note here is that in spite of the fact that the maximum withdrawal in the active well is at its both ends, the corresponding ends of the observation well are also producing (fluid is entering the well)

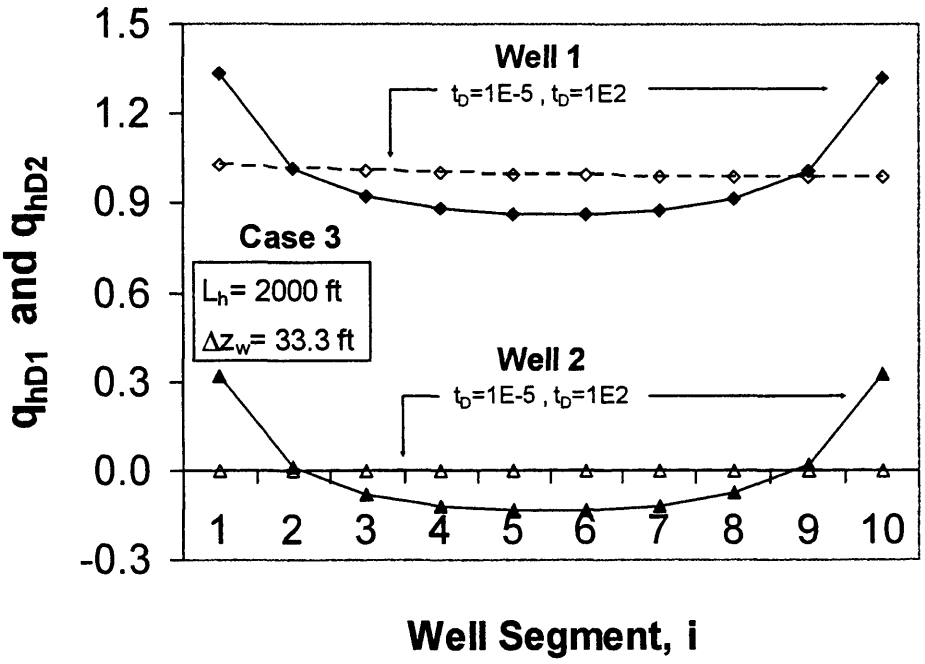

Figure 4-3. Flux distributions along the active and observation wells, Case 3.

Finally, Figure 4-4 shows flux distribution for the dual opposed horizontal laterals with the active well being in the right. As observed in the previous examples, the closer segments to the active well have negative flux while the ones farther a way have positive flux.

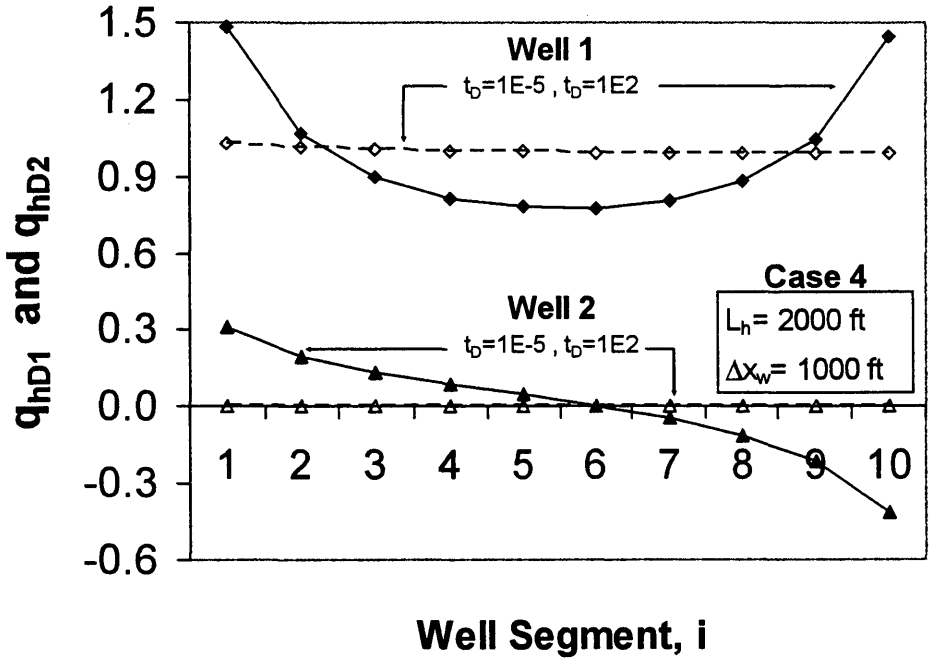

Figure 4-4. Flux distributions along the active and observation wells, Case 4.

Although the characteristics of flux distributions are important to understand the flow behaviors of horizontal wells, pressure transient characteristics are more commonly analyzed to determine flow regimes and estimate the properties of the reservoir. The next section discusses the transient pressure responses of the active and observation horizontal wells.

4.2 Transient Pressure Responses

In this section, transient pressure and derivative responses for the cases presented in Table 4-1 will be considered in order to discuss the general flow characteristics of the active and observation wells. The results discussed here will also be compared to the results presented in literature.[18,19]

Dariush Malekzadeh[19] has discussed that the early time radial and linear flow periods may not be detected in the horizontal observation well responses. He stated that the early-radial flow period is not displayed in observation well tests due to the fact that the pressure transients created by the active horizontal well have already reached the upper and lower boundaries before they reach the observation well. The results of this study verify the observations of Malekzadeh when the active and observation well are far apart. When the distance between the two wells is relatively short, as in the case of vertically stacked horizontal laterals, however, a linear flow period may be displayed by the observation well responses.

Transient pressure and derivative responses for the base case (Case 1) in Table 4-1 is shown in Figure 4-5. The data for Figure 4-5 are also tabulated in Appendix B for those who may wish to compare their results with this study. As expected, the active well pressure responses are not significantly affected by the existence of a horizontal interference well when both wells are relatively far apart. This observation is supported by the classical derivative responses of the active well which clearly display the characteristic flow regimes (early-time radial flow, intermediate-time linear flow, and late-time pseudoradial flow) of horizontal wells. In addition, although in this case small amount of influx (production) and outflux (injection) takes place along the horizontal section of the observation well, as shown in Figure 4-1, Figure 4-5 indicates that the pressure responses measured at the observation well display characteristics which are similar to radial or pseudoradial flow regime. This is clearly

evident from the derivative responses which match the active well derivative responses during pseudoradial flow. This trend is similar to the flow characteristics of a vertical observation well which suggests the possibility of representing the horizontal observation well by a single pressure measurement point. In Chapter 5, we will explore this idea in detail and develop a correlation to determine when the flow disturbance caused by the horizontal observation well may be ignored. Under these conditions, horizontal observation well responses may be closely approximated by the pressure drop at an equivalent point in the reservoir created by a single horizontal well. This idea presents great potential to simplify the analysis of horizontal well interference tests.

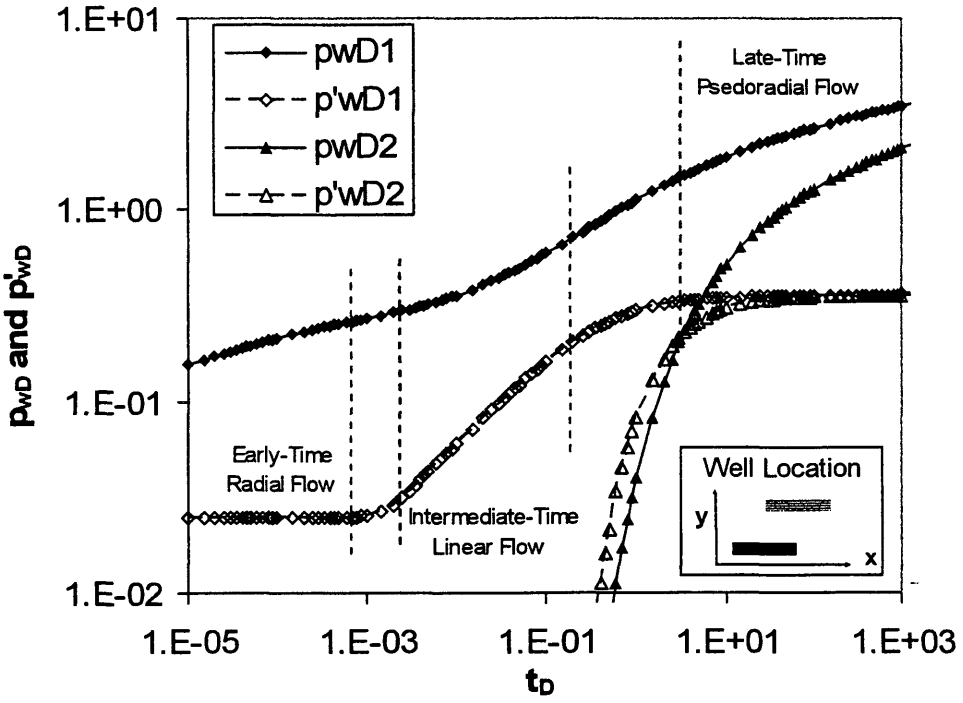

Figure 4-5. Dimensionless pressure and derivative responses, Case 1.

The case presented in Figure 4-6 is the same as that in Figure 4-5 except the x-direction distance between the wells is larger (Case 2 in Table 4-1). For this case the observation well responses are delayed because of the larger distance between the two wells.

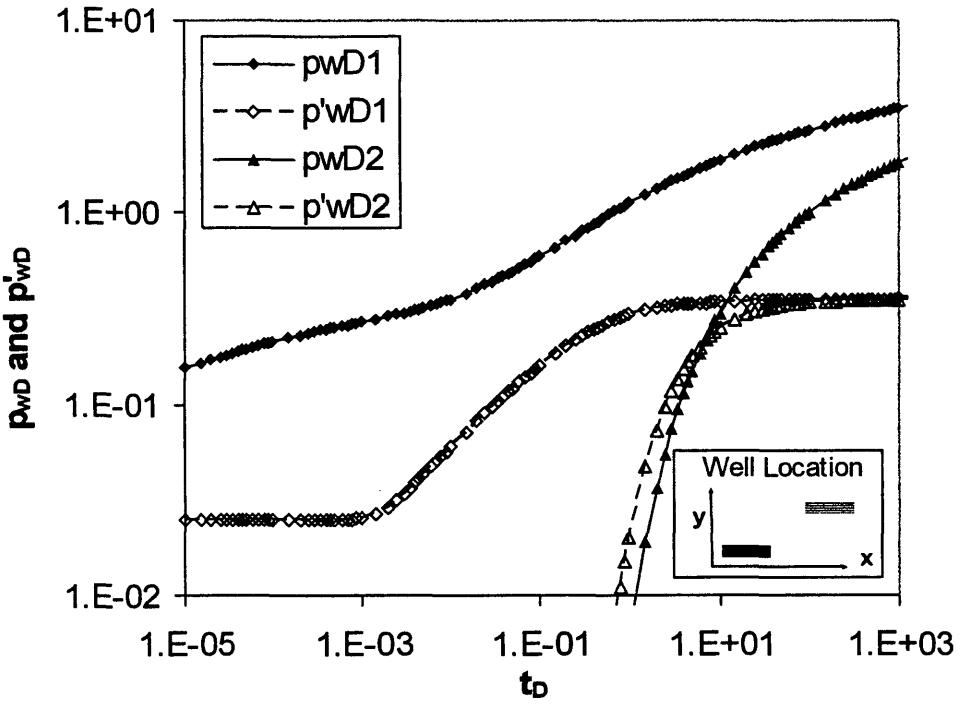

Figure 4-6. Dimensionless pressure and derivative responses, Case 2.

Figure 4-7 shows the transient pressure and derivative plot for Case 3 in Table 4-1 (vertically stacked laterals where the vertical distance between the wells is 33.3 ft). Similar to the other cases, the active well responses do not display any influence of interference as the same flow regimes are observed without any distortion. The observation well responses, however, become noticeable much sooner as compared to the other cases. More importantly, in this case the derivative responses of the observation well display an almost linear flow regime (the intermediate-time data follow an approximate one-half slope straight line). The same observation has also been noticed when the horizontal separation between the two wells is relatively small (results not shown here). This observation contradict Malekzadeh's[19] conclusion which states that linear flow period does not exist in the observation well responses in horizontal well interference tests.

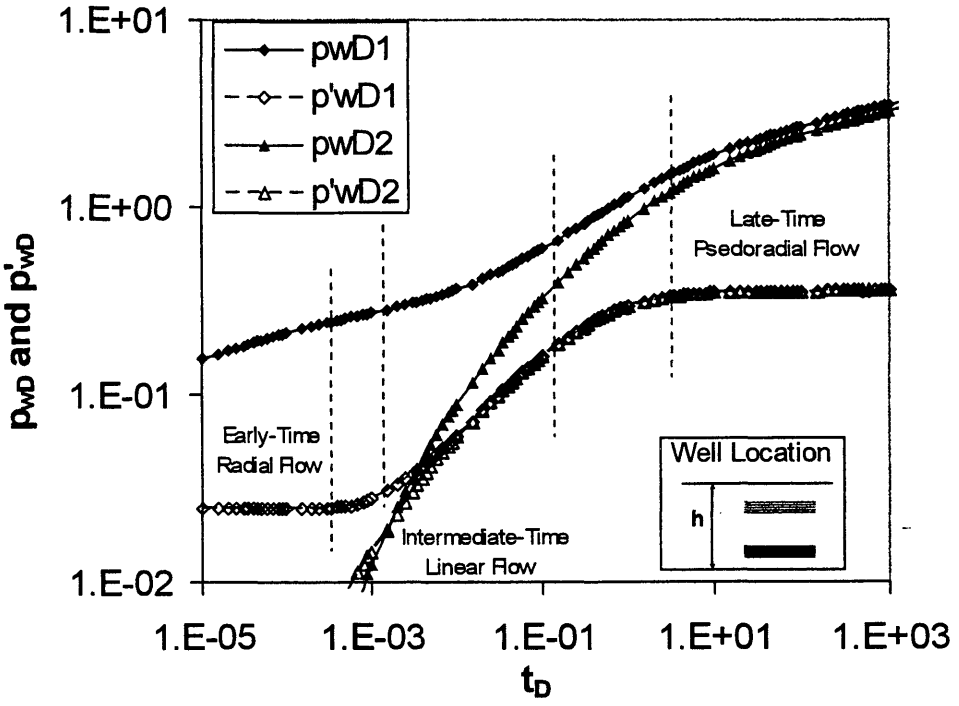

Figure 4-7. Dimensionless pressure and derivative responses, Case 3.

Finally, Figure 4-8 shows the transient pressure and derivative responses for Case 4 in Table 4-1 (the dual opposed horizontal laterals). The general characteristics of the pressure and derivative responses in this case are the same as those in Cases 1 and 2. The effect of horizontal and vertical separation of the wells, skin distribution and wellbore conductivity are discussed in the following sections in detail.

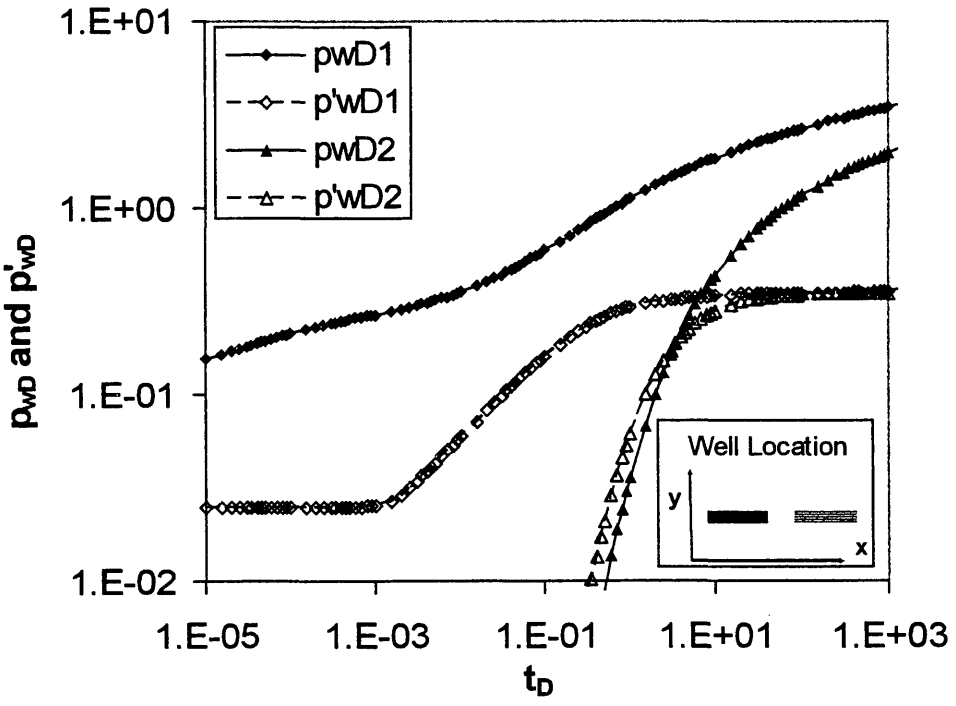

Figure 4-8. Dimensionless pressure and derivative responses, Case 4.

4.3 Effect of Horizontal Separation

In this section, the effect of horizontal separation between the two wells on pressure responses will be investigated. As expected, for early times the results not shown here have

indicated that the horizontal separation between the active and observation wells has no effect in their responses. This is attributed to the fact that the effect of the active well has not yet reached the observation well and therefore neither well is influenced by the presence of the other. Once the active well response reaches the observation well, however, the responses of both wells may be influenced. Figure 4-9 shows an example of the effect of horizontal separation between the active and observation wells at t = 128 days. The base case properties given in Table 4-1 have been used for the reservoir and well in Figure 4-9.

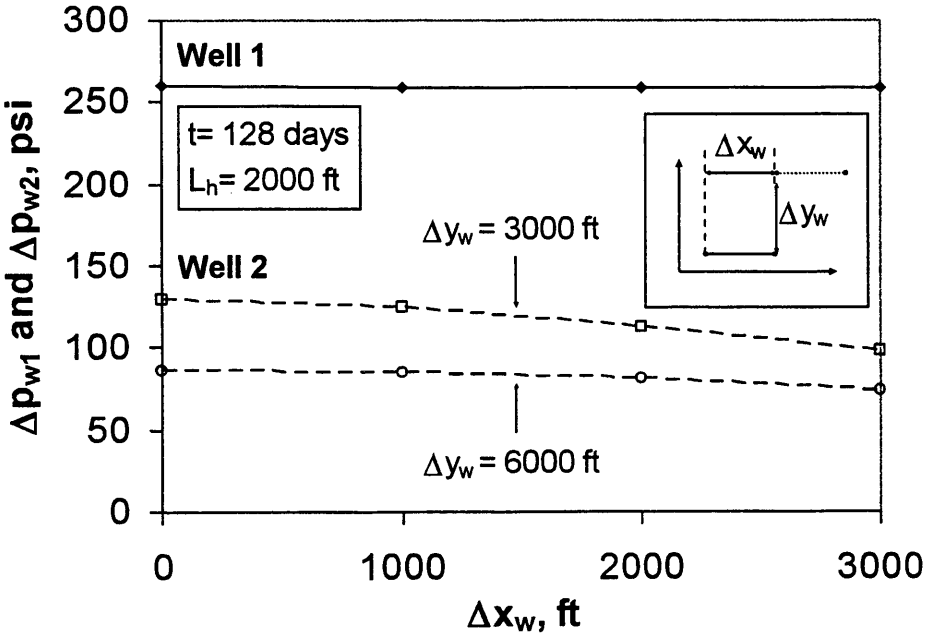

Figure 4-9. The effect of horizontal separation on the pressure drop of the active and observation wells at t=128 days.

It can be concluded from Figure 4-9 that the horizontal separation between the two wells has practically no effect on the active well responses. For the conditions used in Figure 4-9, a small effect is noticed on the observation well pressure responses at late times. In this case, the separation in the normal direction (Δy_w) has more significant influence on the observation well pressure responses than the separation in the axial direction (Δx_w). This result should be attributed to the fact that the y-direction permeability is twice as large as the x-direction permeability in this example.

4.4 Effect of Vertical Separation

Because the effect of vertical separation between stacked dual laterals should be the most severe case and this effect should diminish as the horizontal separation of the wells increases, here we consider an example of vertically stacked laterals. Figure 4-10 shows the effect of vertical distance (Δz) at late times (at t = 128 days) for the case where both active and observation horizontal wells are aligned in the vertical plane. The reservoir and well data used in this example are the ones for the base case (Table 4-1), except that the formation length in this case is set to 200 ft. In addition, the location of the active well in all cases is set at 70 ft from the bottom of the reservoir.

The figure shows that in this case too, the observation well pressures are slightly affected by the distance between the two wells while the active well pressure responses are practically unaffected. This observation is similar to the effect of horizontal separation between the two wells. The results presented in Figure 4-10 shows that even when the distance between the two wells is relatively short, the active well practically does not receive any benefit from the existence of a nearby high conductivity flow path provided by the wellbore of the observation horizontal well.

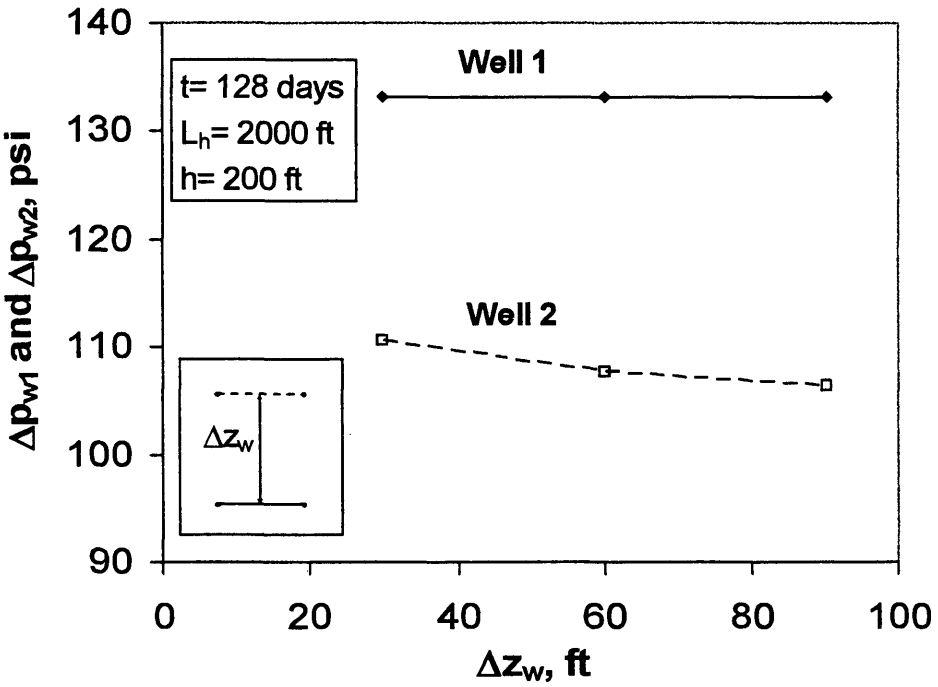

Figure 4-10. The effect of vertical separation on the pressure drop of the active and observation wells at t=128 days.

4.5 Effect of Skin Factor and Skin Distribution

In this section, the effect of skin factor and skin distribution in active and observation wells will be investigated. The effect of skin on horizontal well responses has been well discussed in the literature.[14,44,57] Figure 4-11 shows the effect of three skin cases on the pressure responses of a producing horizontal well (the active well in this work). The first case (diamonds) is an undamaged horizontal well (S=0). Case 2 (triangles) considers the effect of a uniform skin distribution for S=0.5 and Case 3 (solid and dashed lines without data points) examines the effect of a conical skin distribution where the skin factor decreases from 0.5 at

the heel to 0.05 at the toe of the well. As noted in Ref. 47, the pressure responses in Fig 4-1 indicate that the magnitude of the skin factor affects the pressure drop of the horizontal well but the derivative responses indicate that the flow regime characteristics are not influenced by uniform skin (diamonds and triangles). Conical skin distribution (dashed line), however, distorts the early and intermediate times flow regime characteristics as indicated by the change in the derivative behavior.

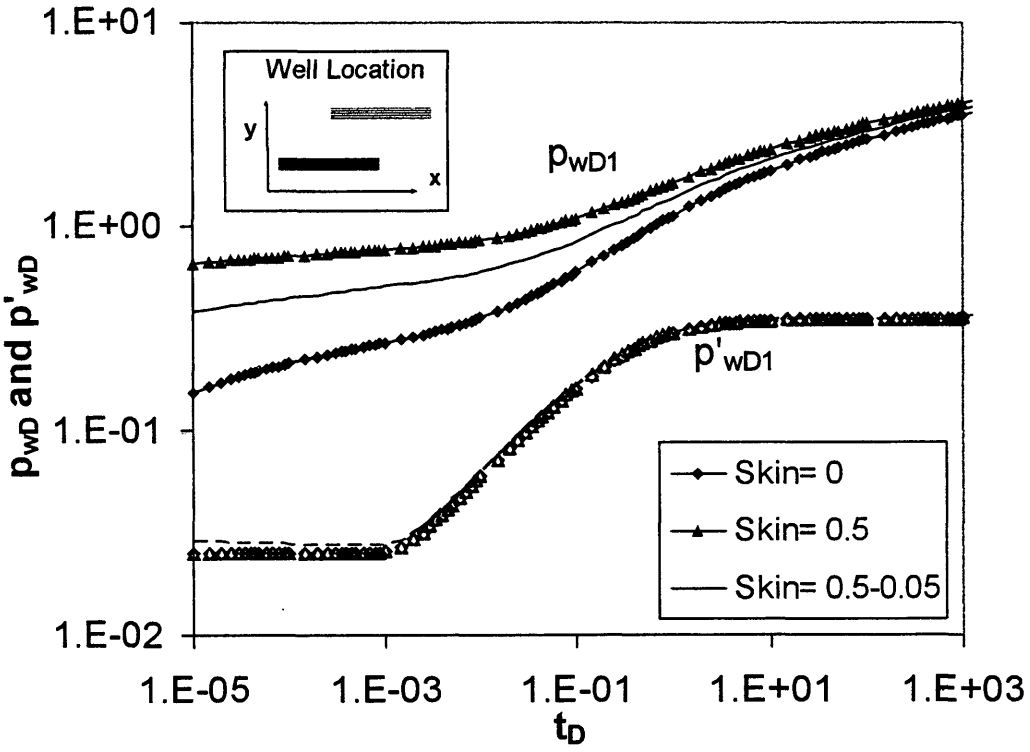

Figure 4-11. Skin effect on active well responses for the base case.

The emphasis of this work is on the effect of skin on interference responses. If both active and observation wells are vertical, it has been shown in the literature[56,57] that the observation well responses are not influenced by the effect of skin factor unless wellbore storage is significant in either or both of the wells. In general for a horizontal well, even when the total flow rate is fixed, the distribution of flux along the well is influenced by the skin distribution. For horizontal observation wells, although the total flow rate is zero, the influx and outflux are influenced by the magnitude and distribution of skin along these wells (for example, if there is very high skin damage along the observation well, influx and outflux would be essentially zero). Therefore, we may expect to see some effect of skin damage on the interference responses between two horizontal wells even when wellbore storage is neglected.

In order to discuss the effect of the magnitude and distribution of the active- and observation-well skin factors, we consider the interference between two horizontal wells for the base case in Table 4-1. Four different skin cases are investigated in Figures 4-12 and 4-13. The first case (diamonds) corresponds to a conical skin distribution where S= 0.5 at the heel and 0.05 at the toe of the active well and there is no skin at the observation well. In Case 2 (squares), both wells have the same conical skin distribution ($0.5 \geq S \geq 0.05$) and in Case 3 (triangles), both wells are undamaged (S= 0). Finally, Case 4 represents the uniform skin distribution (S= 0.5) on both wells.

Figure 4-12 indicates that the active-well skin affects its flux distribution (diamonds and triangles) but the observation well skin has no discernable effect on the active well flux distribution (diamonds and squares). Figure 4-12, on the other hand indicates that the flux distribution along the observation well is not only a function of the observation well skin, but is also influenced by the skin along the active well. Moreover, the observation well flux distribution is affected by both the magnitude (triangles and circles) and distribution (squares and circles) of the active and observation well skin factors.

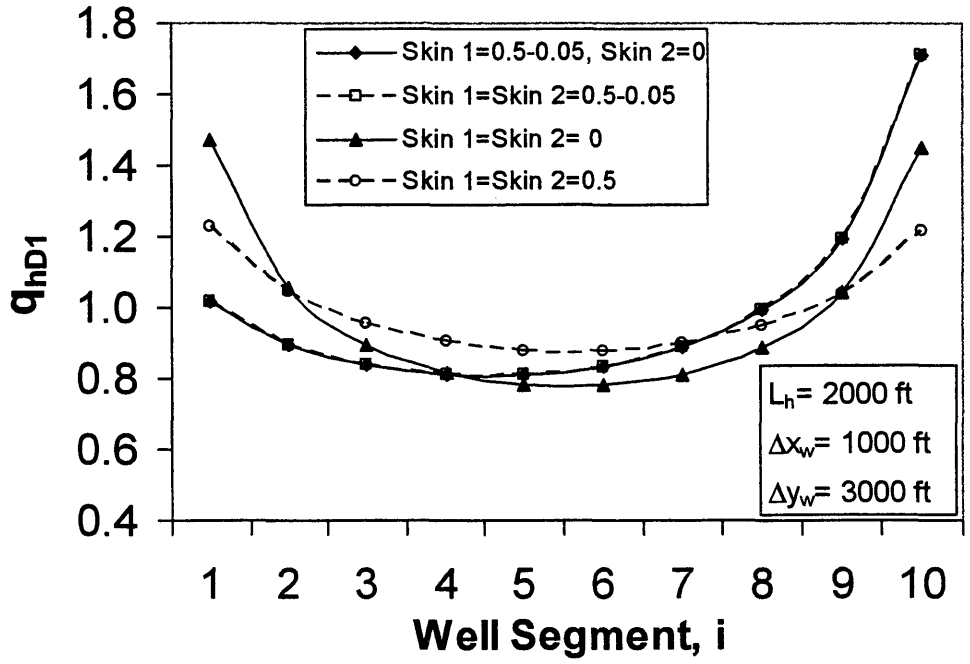

Figure 4-12. Skin effect on the flux distribution along the active well at t_D=100.

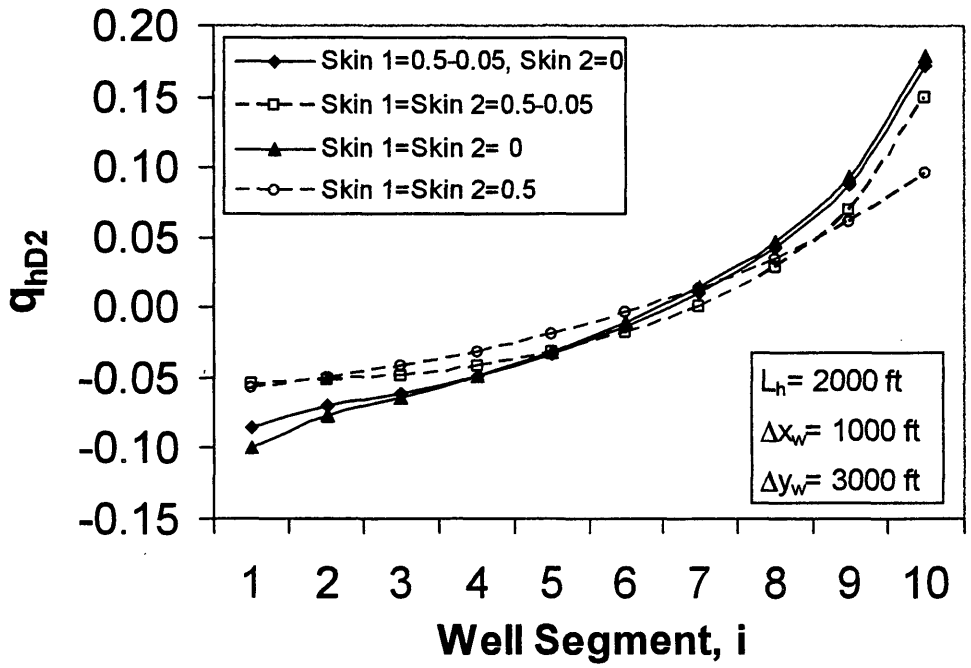

Figure 4-13. Skin effect on the flux distribution along the observation well at t_D=100.

The observations noted above from Figures 4-12 and 4-13 support our physical intuition on the relation between the skin effects and flux distributions. Despite the effect of the skin factor on the flux distributions, the results not shown here indicate that the pressure responses of horizontal observation wells are not considerably affected by the skin factors on both the active and observation wells. Therefore, we can conclude that similar to vertical wells, the interference responses between two horizontal wells are not influenced by the skin factor on either or both of the wells. This result, however, has been derived in the absence of wellbore storage effects and based our knowledge on interference between vertical wells; we can expect wellbore storage to change this conclusion. Although this is an important issue, the investigation of wellbore storage effects is not within the scope of this dissertation.

4.6 Effect of Wellbore Conductivity

As stated earlier, one of the objectives of this study is to investigate the effect of wellbore hydraulics on the interference responses. Effect of wellbore hydraulics may be a crucial factor influencing the performance of extended reach horizontal wells especially with high rates and small wellbore radius. The coupled reservoir-wellbore model developed in this work can be used to study the effect of wellbore hydraulics -finite wellbore conductivity- on both the active and the observation well responses. The dimensionless conductivity defined by Eq. 2-13 implies that wellbore conductivity is a function of both wellbore parameters (conductivity of the wellbore) and formation parameters (conductivity of the formation). Therefore in order to study the effect of wellbore conductivity, one has to consider the overall effect of the two groups of parameters. In general, based on the results of Ref. 41 and the definition of dimensionless conductivity given by Eq. 2-13, we can expect that the effect of wellbore conductivity becomes an issue in high permeability reservoirs and at high flow rates.

In this study, several cases covering a wide range of wellbore and formation parameters have been investigated. Figure 4-14 shows an example of a transient pressure plot for the base case (Case 1 in Table 4-1) along with the case when the permeabilities are increased to k_x= 2000 md, k_y= 4000 md and k_z= 1000 md. We note that the dimensionless conductivity for the base case is C_{hD}= 5470 and it decreases to C_{hD}= 137 when the permeability is increased. The results show that the observation well responses are not affected while a noticeable change is observed in the active well responses when the conductivity of the wells is decreased (Note that Figure 4-14 shows higher dimensionless pressure for the higher permeability case. This result, contradicting our physical expectation, is simply because of the existence of permeability as a scaling parameter in the definition of dimensionless pressure given by Eq. 2-2 and may be corrected by rescaling the dimensionless pressure by permeability as in Figure 4-15).

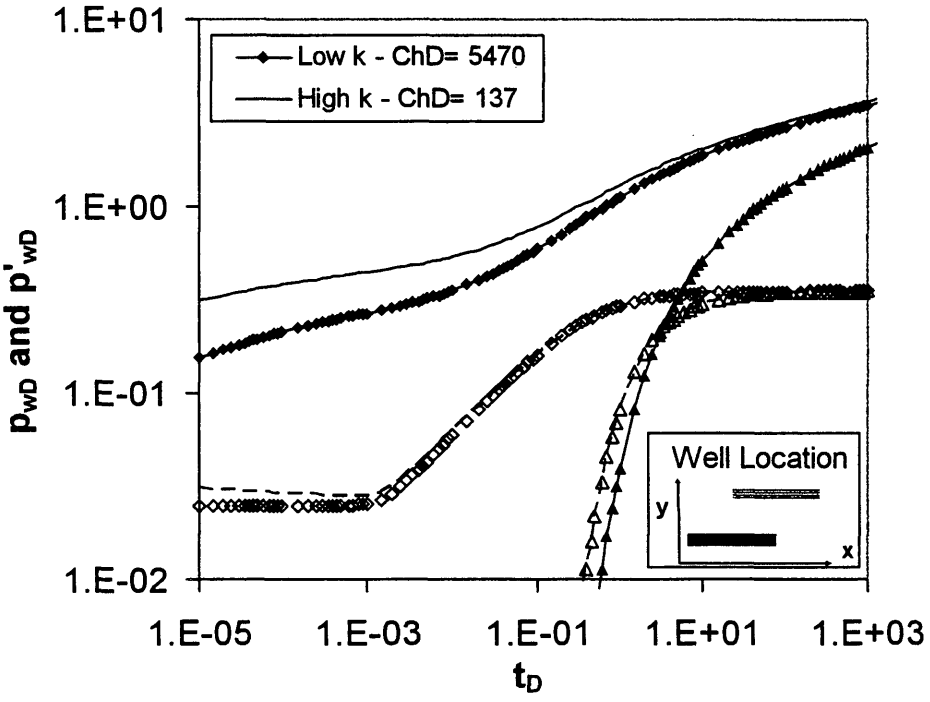

Figure 4-14. Effect of wellbore conductivity on active and observation well responses; high permeability case.

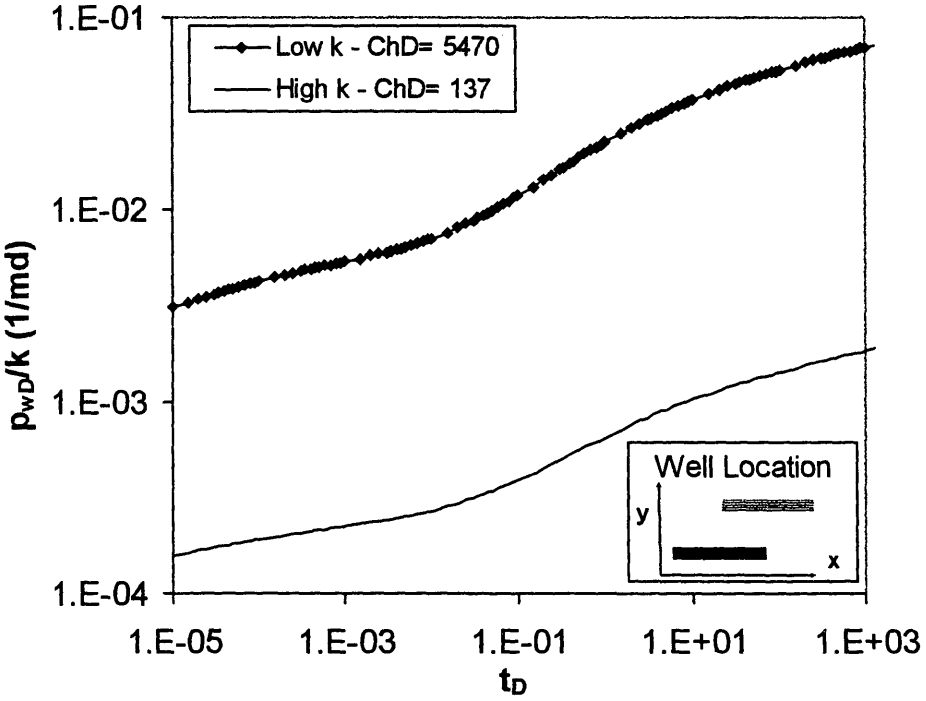

Figure 4-15. Effect of wellbore conductivity on active and observation well responses; normalized high permeability case.

Similarly, Figure 4-16 shows the same cases presented in Figure 4-14 but now in the second case the rate is further increased to 8000 bbl/d (the Reynolds number for the base case is R_{et}= 23890 and it increases to R_{et} = 95560). As can be seen, the increase in rate (or R_{et}) creates similar changes to those observed in Figure 4-15. Finally, Figure 4-17 shows a comparison between two vertically stacked lateral cases. In both cases the permeabilities are k_x= 2000 md, k_y= 4000 md and k_z= 1000 md, horizontal well length is equal to 2500 ft and well rate is 3000 bbl/d. The well inside diameter is equal to 3.958 in in the first case and 6.366 in in the second case. Because decreasing the wellbore diameter while keeping everything constant decreases wellbore conductivity, the pressure drop in the active well

increases. Similar to the previous cases, however, no discernable effect of wellbore pressure drop is observed on the observation well responses.

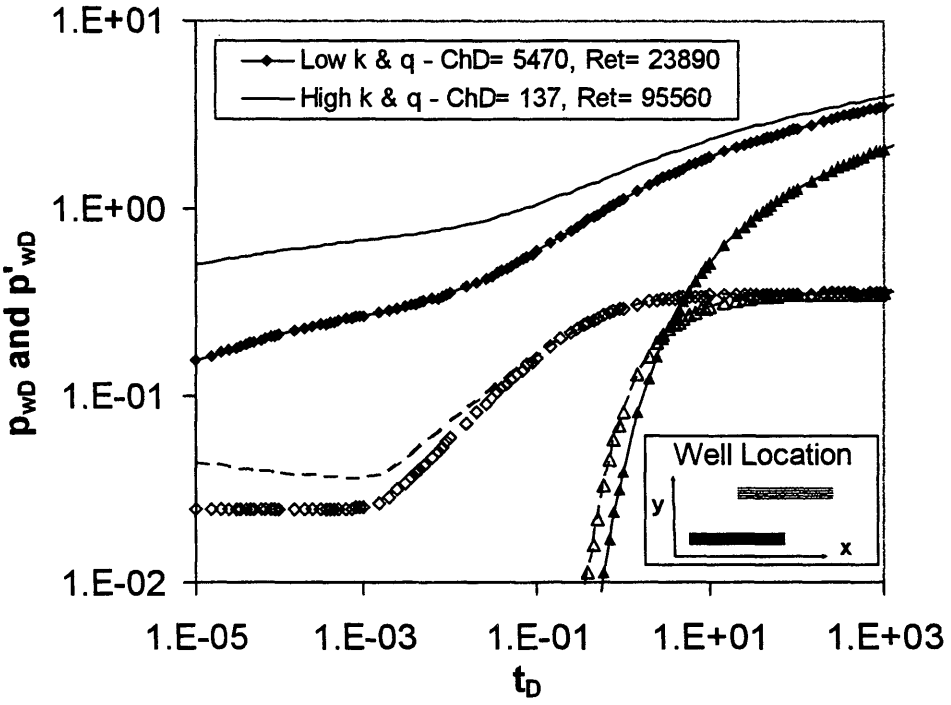

Figure 4-16. Effect of wellbore conductivity on active and observation well responses; high permeability and rate case.

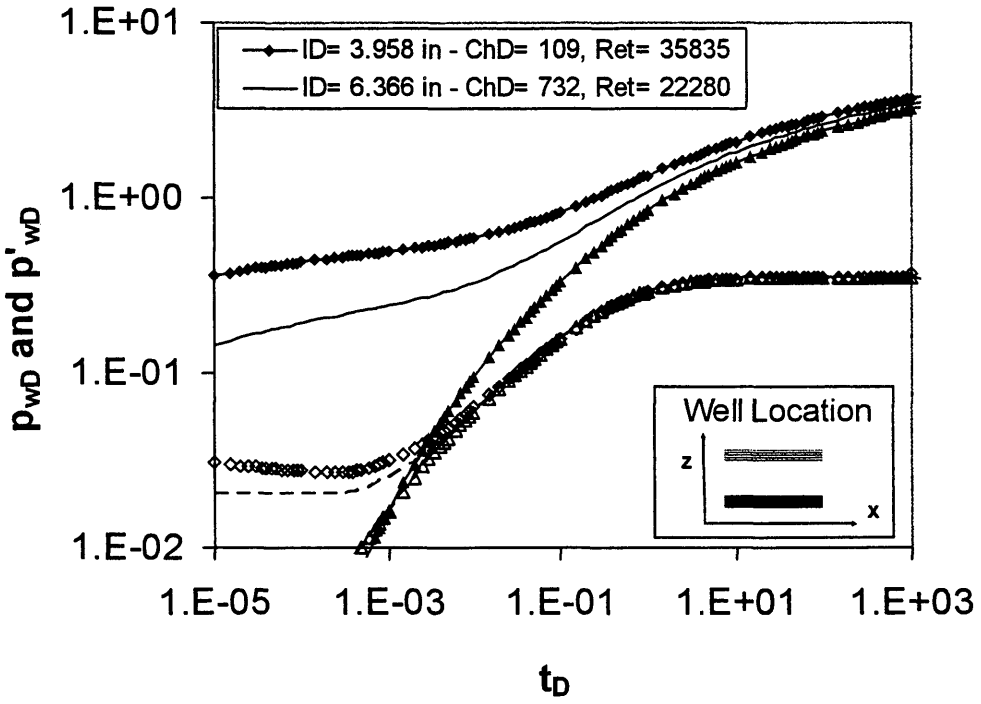

Figure 4-17. Effect of wellbore conductivity on active and observation well responses for two tubing sizes.

In conclusion, in all the cases examined, it was found that the effect of finite-conductivity was only noticeable in the active well responses. In general, no noticeable effect was observed in the pressure responses of the observation well even when the two laterals were reasonably close as in the case presented in Figure 4-17. This may be attributed to the fact that for the low flow rates in the observation well, the frictional pressure drop should be normally negligible.

Before completing our discussion of the effect of wellbore conductivity, we briefly comment on the flux distribution for completeness. Figure 4-18 shows the flux distributions for the cases presented in Figure 4-17. It is clear that as the wellbore hydraulics becomes significant,

the flux distributions along the horizontal sections of the wells are influenced. In this case, areas close to the heel of the active well have higher flux than the areas close to the toe. Consequently, the outflux close to the heel of the observation well increases to compensate for the increase in flux in the same place at the active well while the influx closer to the toe also increases to balance the outflux (net flow must be zero along the observation well).

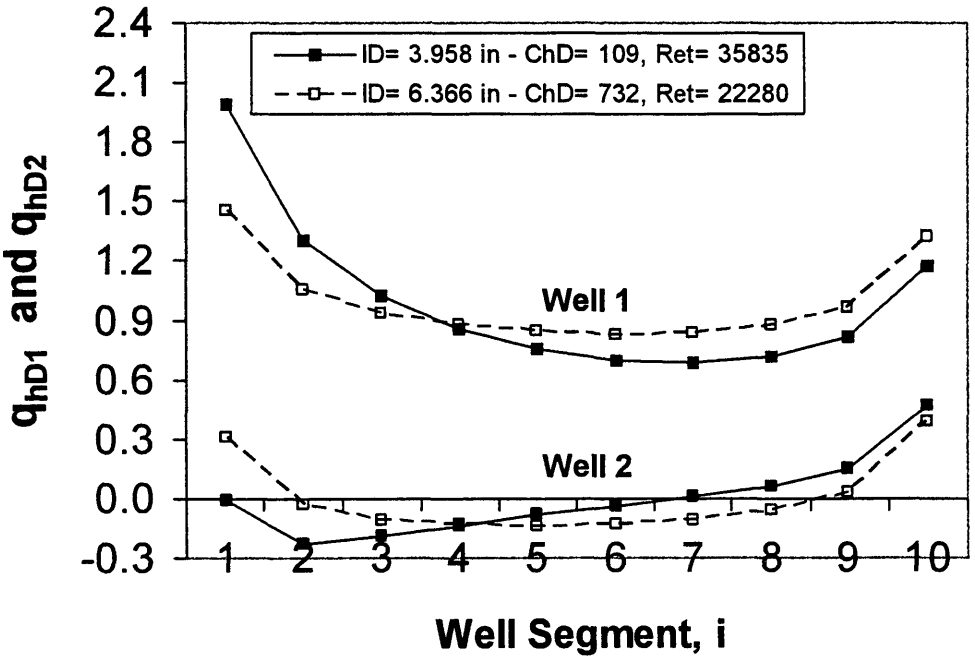

Figure 4-18. Flux distributions for stacked laterals at t_D=1000.

CHAPTER 5

ANALYSIS OF INTERFERENCE TESTS BETWEEN TWO HORIZONTAL WELLS

The results presented in Chapter 4 indicate that when the distance between two horizontal wells is relatively large, the observation well responses show characteristics of a radial or pseudoradial flow regime. Under these conditions, the horizontal observation well responses may be closely approximated by the pressure drop at an equivalent point in the reservoir created by a horizontal or even a vertical well (flow disturbance caused by the observation horizontal well may be ignored). This idea presents great potential to simplify the analysis of horizontal well interference tests as the models to calculate the pressure drop at a point in the reservoir are much simpler than the rigorous model discussed in the previous Chapters. The representation of a horizontal interference well by a point in the reservoir and matching the horizontal observation well responses by the exponential integral solution for vertical-vertical interference tests are the common ideas used in the literature.[58,59] Because we have a rigorous model, in this chapter we explore these ideas and delineate the conditions under which they are applicable.

This chapter is divided into three sections. In the first section, a correlation is presented to find the equivalent interference point to approximate the horizontal observation well pressure responses. In the second section, another correlation is presented to determine when the horizontal observation well responses may be approximated by the exponential integral solution. A formula to calculate the equivalent radial distance between the two horizontal wells is also given in this section. In the third section, several examples are

discussed to show how and when these correlations can be applied. In addition, the intent here is to give a quantitative measure of the errors to be expected from the application of the approximate analysis techniques.

5.1 Approximation by the Optimum Observation Point

In this section, the possibility of interpreting the observation well responses as if the well was an observation point in the reservoir will be investigated. Previous researchers[18,19] used this idea without rigorous justification. An important gap in the previous studies is in the choice of the location of the observation point. It was usually assumed that a "good" location for the equivalent observation point would be the heel of the actual horizontal observation well.[18,19] This choice of the observation point location may not be correct because a horizontal observation well distorts the equipotential lines. Therefore, one of our objectives here is to find the location of the optimum observation point along the actual horizontal observation well. Figure 5-1, shows a 3-D schematic of the active and observation horizontal wells and the optimum observation point.

Representing the horizontal observation well by an observation point could be of significant benefit since the models are simpler and the computations involved are not as extensive. In general, once the optimum location of the observation point is determined, a single horizontal well solution may be used to determine the responses at this point. The single-horizontal-well solutions are more convenient to implement in the regression algorithms used by computerized well test analysis software and the speed of the calculations is greatly enhanced as compared to the rigorous, two-well models (the increase in the speed of the calculations is usually more than six folds).

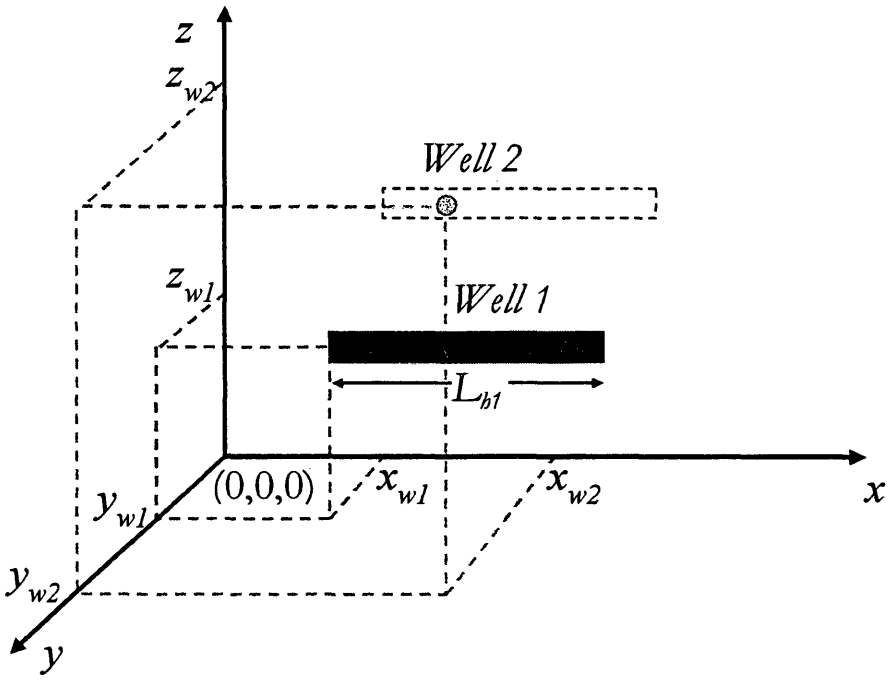

Figure 5-1. 3-D view showing the location of the optimum observation point.

The first step in developing a procedure to represent a horizontal observation well by an equivalent observation point is to find when this approximation will be valid. Numerous cases have been investigated in this study covering a variety of well locations and wide ranges of reservoir and well properties. (Although, only parallel orientation of the horizontal wells was considered in all cases, the distances between the wells in all three directions were allowed to vary.) For each horizontal active and observation well configuration, several locations of the equivalent observation point along the actual horizontal observation well were tested. Responses were then evaluated by using the average absolute error (E_a) and maximum error (E_m) for p_{wD} values greater or equal to $1x10^{-2}$ and t_D less than $1x10^5$ which should cover a reasonable practical range. The average absolute error and maximum error are defined, respectively, by the following expressions:

$$E_a = \frac{\sum_{i=1}^{n} \frac{\left|(p_{wDh2}(i) - p_{OOPD}(i))\right|}{p_{wDh2}(i)} * 100}{n} \tag{5-1}$$

and

$$E_m = Max\left[\sum_{i=1}^{n} \frac{\left|(p_{wDh2}(i) - p_{OOPD}(i))\right|}{p_{wDh2}(i)} * 100\right]. \tag{5-2}$$

Table 5-1, shows the reservoir and well data for the examples that will be discussed in this section. Figure 5-2 shows the average error trend for the case when both horizontal wells are aligned in the horizontal plane (Case 1 of Table 5-2). In this case, the error resulting from representing the horizontal observation well by an observation point is estimated at various observation point locations along the actual horizontal observation well. Interesting observation to note here is that there are two locations where the average error decreases to a minimum, at a distance (fraction of the horizontal well length) of about 0.19 and 0.81 units measured from the heel of the well. This relation was also found to be valid for any separation in the y-direction, however, the estimated average and maximum errors where found to decrease as the distance between the two wells increases. Figure 5-3 shows a comparison between the dimensionless pressure responses of the actual horizontal observation well and of the observation point locations around the second minimum. As can be seen here, for this well configuration, the single horizontal well responses computed at the optimum observation point match the actual horizontal well responses very well.

Table 5-1. Test data for optimum observation point examples.

Parameter	Case 1	Case 2	Case 3	Case 4
q, B/D	2000	2000	2000	2000
L_h, ft	2000	2000	2000	2000
h, ft	100	100	100	100
k_x, md	50	50	100	100
k_y, md	100	100	100	100
k_z, md	25	25	25	25
r_w, ft	0.165	0.165	0.165	0.165
Δx_w, ft	0	500	1000	8000
Δy_w, ft	1000	1000	2000	2000

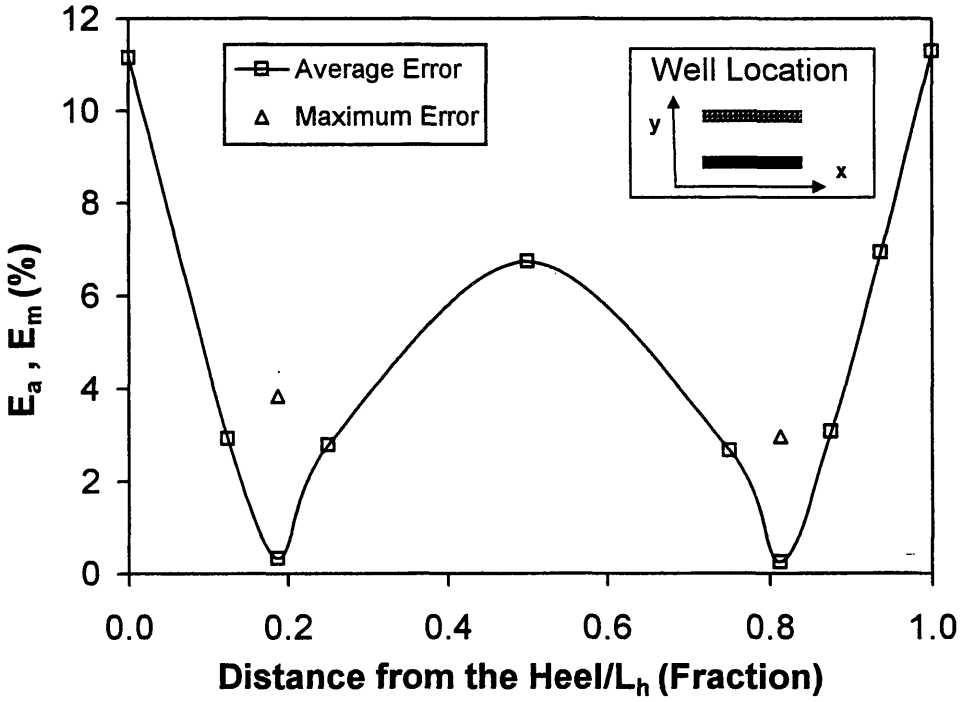

Figure 5-2. Average and maximum error trends for Case 1 of Table 5-1.

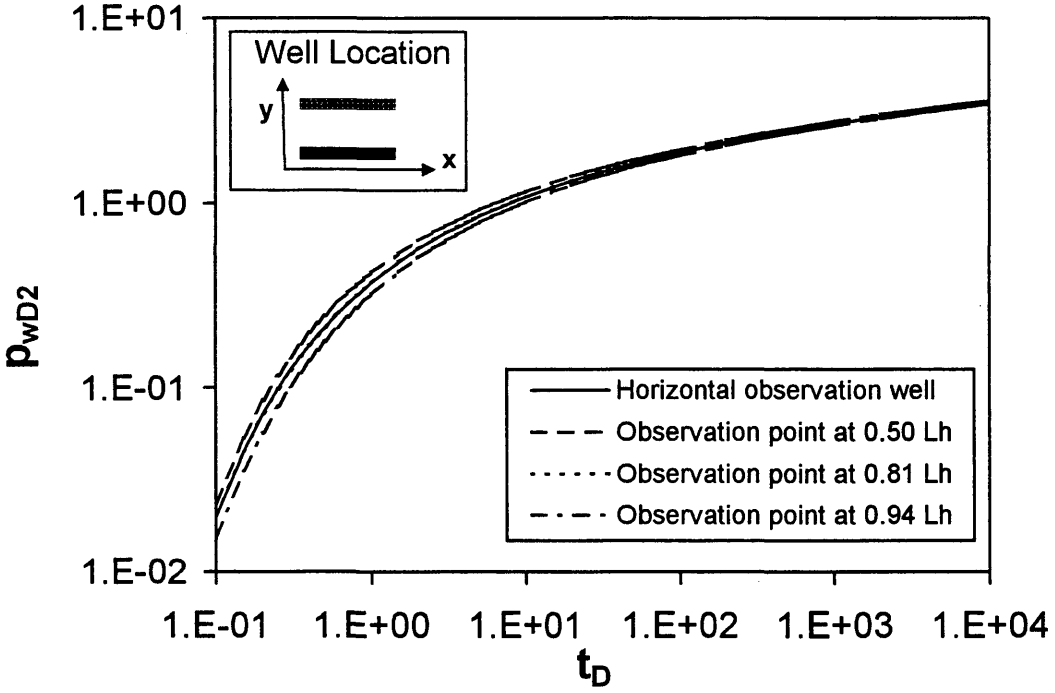

Figure 5-3. Comparison of the dimensionless pressure computed at observation points to actual horizontal observation well responses; Case 1, Table 5-1.

Similarly, Figures 5-4 and 5-5 show the error and pressure response comparisons, respectively, for Case 2 of Table 5-1. Because in this case, the observation well is slightly shifted to the right with respect to the active horizontal well location, the optimum location (second minimum) now starts to shift toward the center of the actual horizontal observation well. Moreover, the first minimum observed in Case 1, where the wells were horizontally aligned, now shifts farther to the left and fall outside the actual horizontal observation well (first minimum vanishes). It has been found that continuing to shift the observation well location to the right in the x-direction, as in Cases 3 and 4 of Table 5-1, causes the optimum location of the observation point to be closer to the middle of the actual horizontal observation well. Figures 5-6 to 5-9 show the error and pressure response comparisons for

Cases 3 and 4, respectively. One observation to highlight here is that as the location of the horizontal observation well gets farther away from the active well in both x and y directions, the match between the horizontal and optimum observation point pressure responses improves. This observation is consistent with our expectations because the geometry of horizontal well becomes less significant as the distance between the wells becomes relatively large.

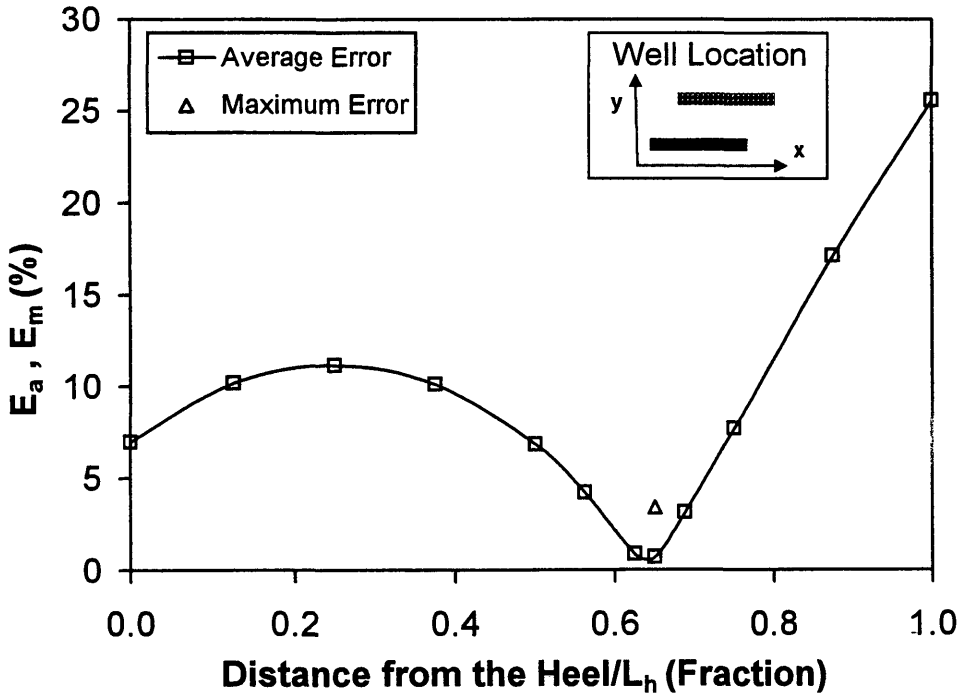

Figure 5-4. Average and maximum error trends for Case 2 of Table 5-1.

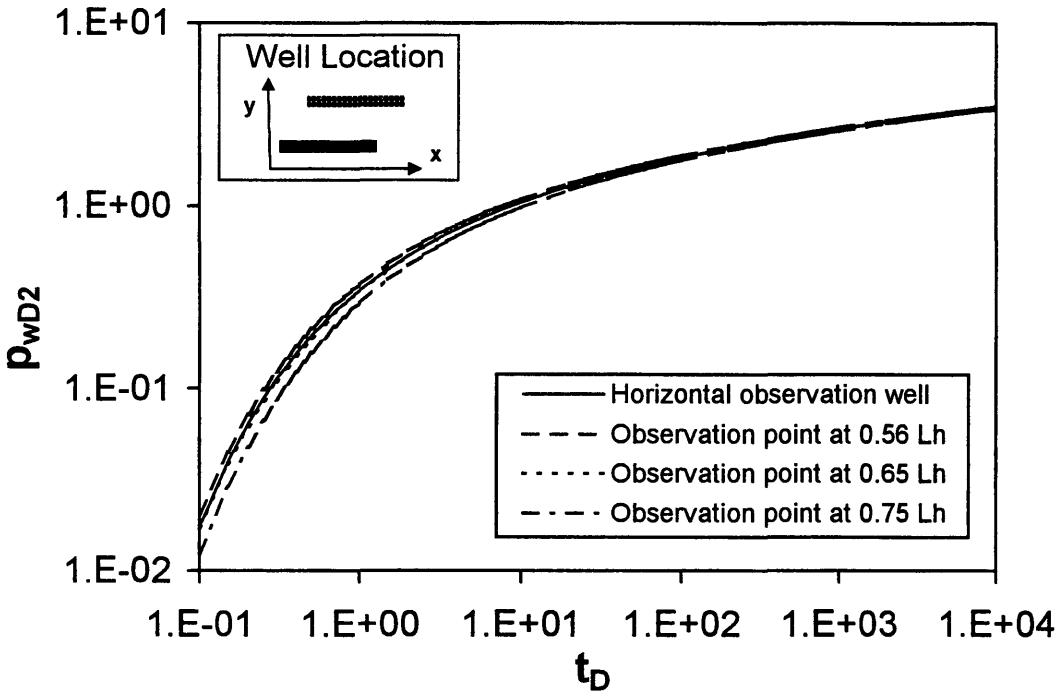

Figure 5-5. Comparison of the dimensionless pressure computed at observation points to actual horizontal observation well responses; Case 2, Table 5-1.

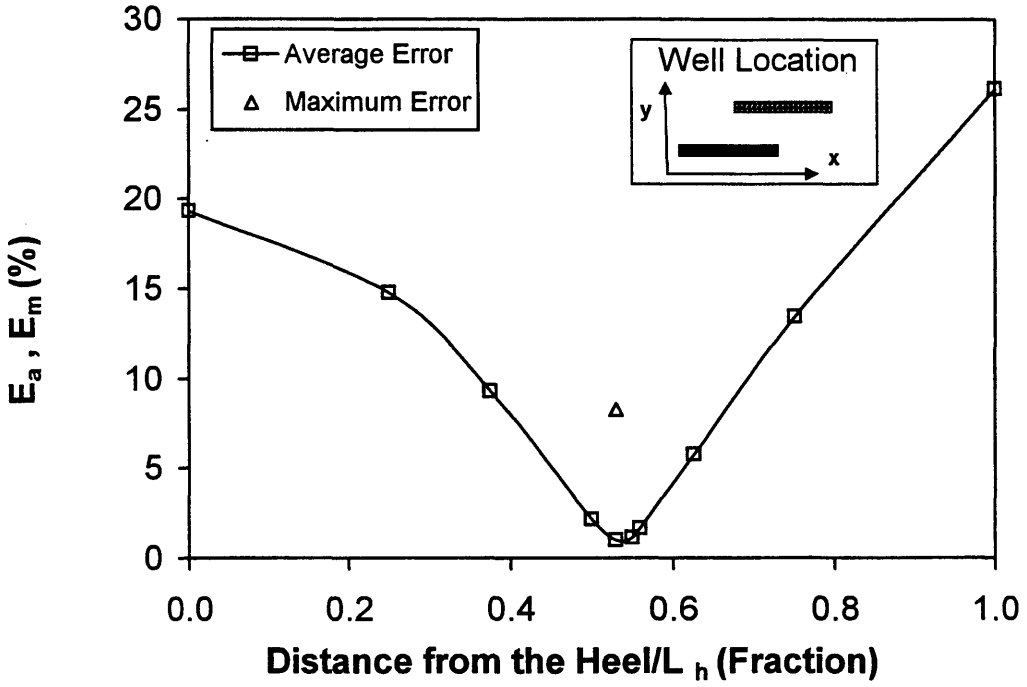

Figure 5-6. Average and maximum error trends for Case 3 of Table 5-1.

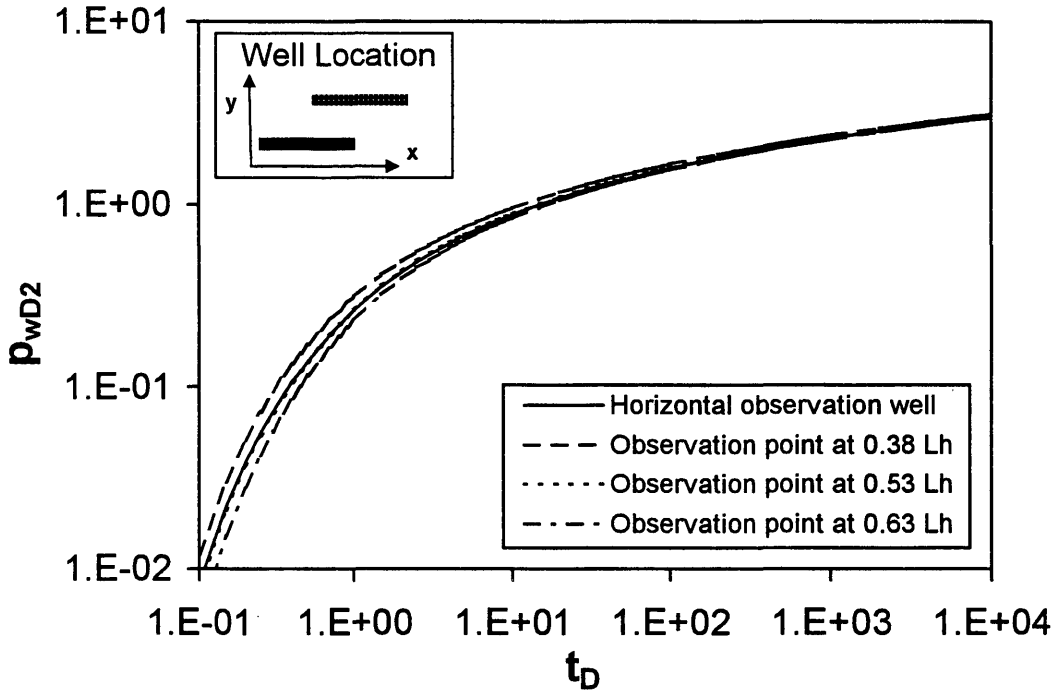

Figure 5-7. Comparison of the dimensionless pressure computed at observation points to actual horizontal observation well responses; Case 3, Table 5-1.

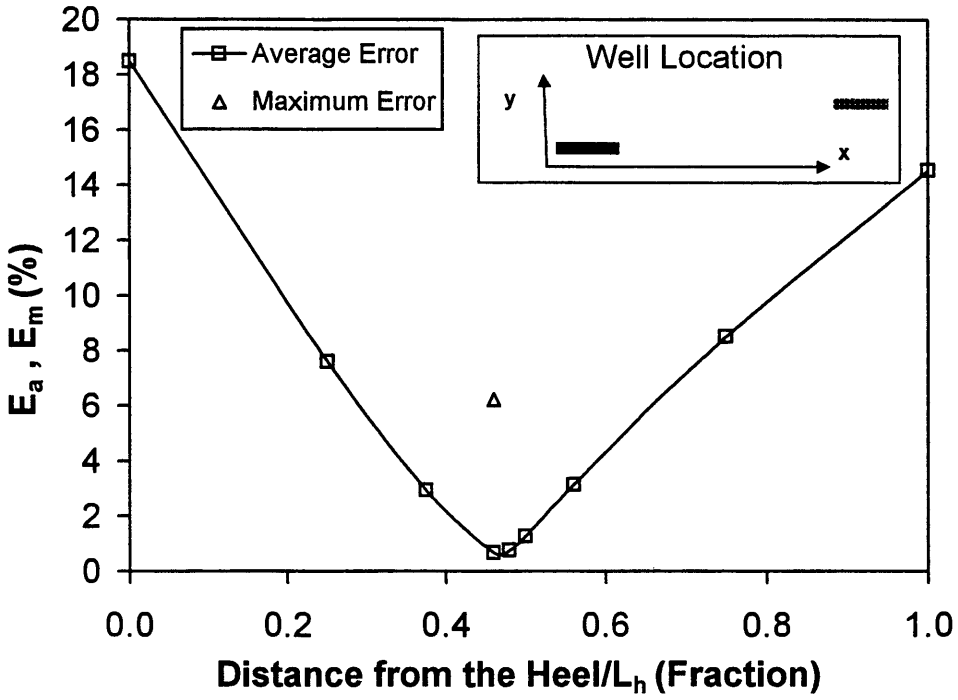

Figure 5-8. Average and maximum error trends for Case 4 of Table 5-1.

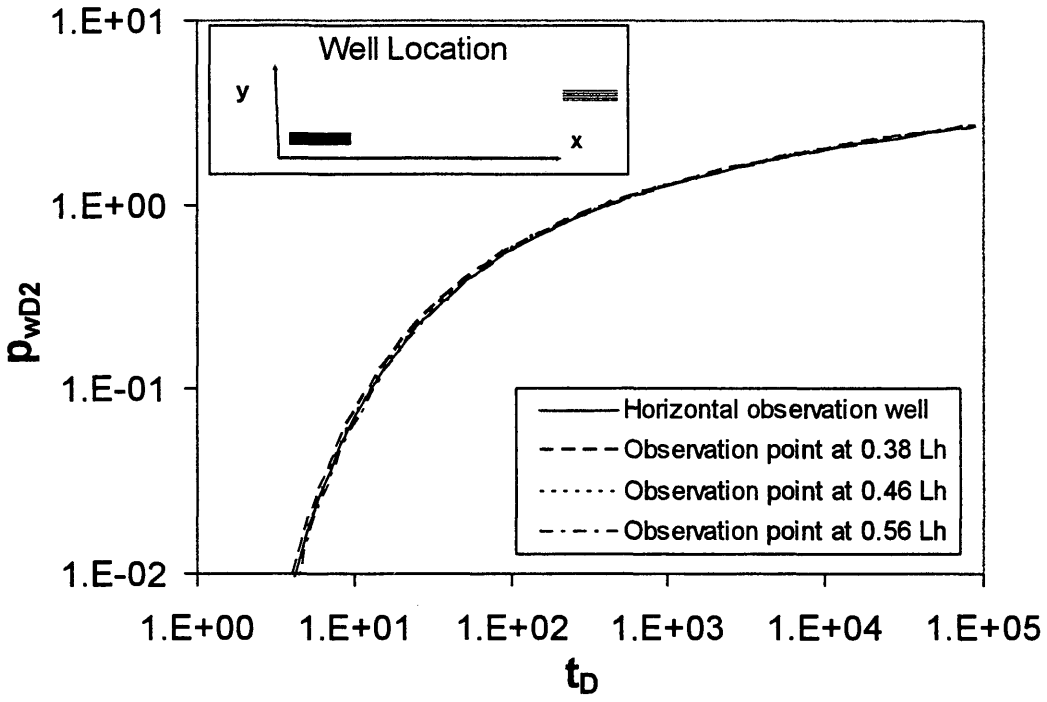

Figure 5-9. Comparison of the dimensionless pressure computed at observation points to actual horizontal observation well responses; Case 4, Table 5-1.

The examples discussed above indicate that a correlation for the optimum observation point may exist. In order to establish this correlation, many cases covering wide ranges of reservoir and well conditions have been investigated and compared. Both anisotropic and isotropic reservoir conditions have been considered. In general, it was found that the permeability anisotropy has no significant effect on the location of the optimum observation point. Similarly, the *z*-direction location was found to be insignificant even for cases when both wells have different locations in the vertical direction. Table 5-2 shows the ranges of the main parameters covered.

The results of this study showed that the optimum observation point may be correlated with the dimensionless well relative locations ($\Delta x_h/L_h$ and $\Delta y_h/L_h$). Figure 5-10 shows this correlation and clearly indicates that the location of the optimum observation point shifts from the toe to the center of the original horizontal observation well as the x- direction shift (Δx_h) increases. Moreover, the correlation shows that the location of the optimum observation point will ultimately reach the center of the actual horizontal observation well when: $\Delta y_h/L_h > 5$ and $\Delta x_h/L_h > 7$. The data of Figure 5-10 is presented in Appendix B.

It is important to quantify the error associated with the use of the optimum observation point determined from the correlation given in Figure 5-10. Figure 5-11, shows that as the distance between the observation and active horizontal wells becomes closer, the error in approximating the horizontal observation well pressure responses by the pressures at the optimum observation point increases. This is valid especially when both wells are closely aligned in the horizontal direction. Also, the location of the average absolute error is found to be a function of both $\Delta y_h/L_h$ and $\Delta x_h/L_h$. It must be noted here that the estimated errors shown in Figure 5-11 are exaggerated by the fact that they deal with pressure changes and not absolute pressure values.

Although the average absolute error values shown in Figure 5-11 are reasonably small, the corresponding maximum error values may be large. In general, high maximum errors are always associated with relatively high average absolute errors. Moreover, the maximum error always occurs at early times where maximum deviation between the two responses transpires. As a rule of thumb, the correlation given in Figure 5-10 may be used with reasonable accuracy in terms of pressure where the maximum error is less than about 6.0 % when $\Delta y_h/L_h \geq 3$.

Table 5-2. Data ranges used to derive the correlation for the optimum observation point.

Parameter	Range
L_h, ft	1000 – 4000
k_x, md	50 - 3000
k_y, md	100 - 3000
k_z, md	25 - 500

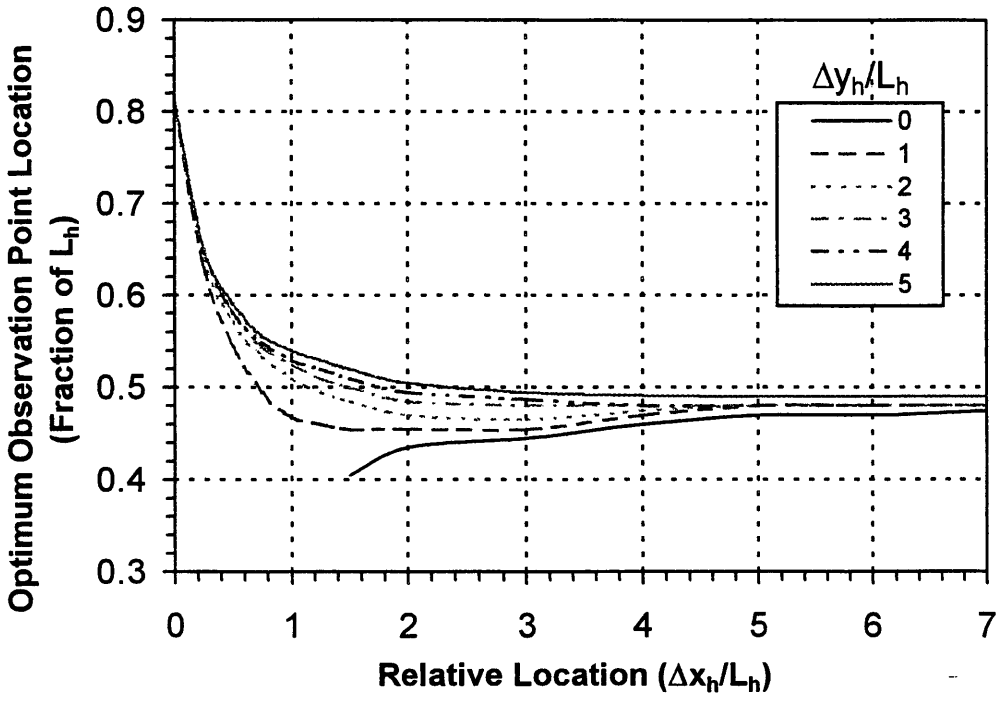

Figure 5-10. Correlation to estimate the optimum observation point.

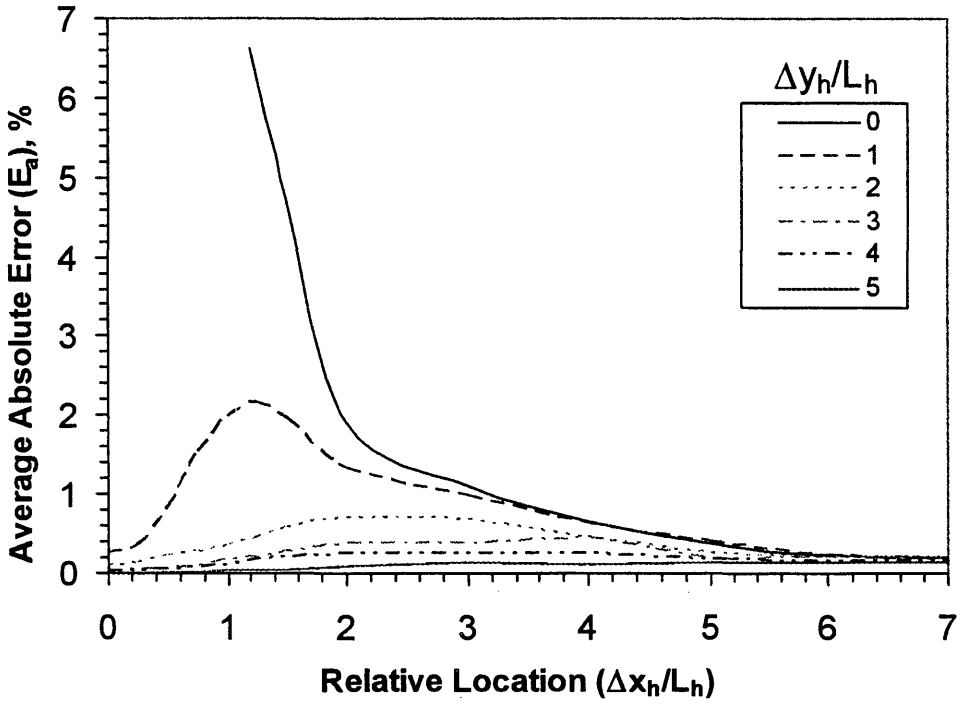

Figure 5-11. Error trend for the optimum observation point correlation.

5.2 Approximation by the Exponential Integral Solution

If the boundary effects do not interfere earlier, horizontal wells develop pseudoradial flow regime at late times.[1,2] Under pseudoradial flow conditions, the equipotential curves are elliptical around the well and circular away from the well. This indicates that if the distance between the active and observation horizontal wells is large enough, by the time the effect of the active well reaches the observation well, pseudoradial flow may have developed in the reservoir and flow may be predominantly radial in the vicinity of the observation well. Under these conditions, the radial flow model represented by the exponential integral solution may be used to approximate the horizontal observation well responses. In other words, if the

distance between the two horizontal wells is large enough, then the geometry of the wells becomes unimportant and the active and observation horizontal wells may be represented by a vertical line source and an observation point, respectively. Then the following exponential integral solution[59,60] (used to model interference between two vertical wells) may also be used to describe interference between two horizontal wells if the distance between the wells is sufficiently large:

$$\tilde{p}_D = -\frac{1}{2} Ei\left(\frac{-\tilde{r}_D^{\,2}}{4\tilde{t}_D}\right), \tag{5-3}$$

here the *Ei* function or the exponential integral is given by

$$Ei(x) = -\int_0^{\infty} \frac{e^{-u}}{u} du\,. \tag{5-4}$$

In Eq. 5-3, the dimensionless variables are defined based on the average horizontal permeability,

$$k_h = \sqrt{k_x k_y} \tag{5-5}$$

and are given by

$$\tilde{p}_D = \frac{k_h}{141.2qB\mu}(p_i - p) \tag{5-6}$$

$$\tilde{t}_D = \frac{6.328\times10^{-3} k_h}{\phi c_t \mu l^2} t \tag{5-7}$$

and

$$\tilde{r}_D = \frac{r}{l} \tag{5-8}$$

where r is the radial distance between the wells. As can be seen here, since in this case the active horizontal well is represented by a line source solution, the relation used (Eq. 5-3) implies no z-direction flow. Therefore, if there is significant contribution of z-direction flow, the approximation of the horizontal observation well responses by the exponential integral solution would result in significant error. This should be the case when the two wells are too close and are not at the same elevation.

In 1992, Malekzadeh[19] investigated the possibility of representing the horizontal observation well responses by the exponential integral solution. He assumed isotropic permeability in the horizontal plane ($k_x = k_y = k_h$) and that both wells are located in the reservoir mid-height. With these assumptions, Malekzadeh concluded that the exponential integral solution could be used to approximate the observation well responses when $t_D/\tilde{r}_D^2$ is greater than or equal to 0.6 and for (x_D, y_D) greater than or equal to (0.7,0.7). He did not, however, comment on how to define the distance between the two horizontal wells, which has been shown to be an important factor in the previous section.

Our objective in this study is to determine if horizontal interference well responses may be correlated by the exponential integral solution. This will be investigated for anisotropic permeabilities in the three principal directions and for different well configurations. The idea here is also to establish the limits when the exponential integral solution can be used to analyze horizontal observation well responses. The criteria used in this study to determine the validity of the exponential integral approximation is to match the dimensionless pressures of the horizontal observation well by the exponential integral solution for at least three log-cycles.

In order to use the exponential integral solution, one has to determine the radial distance between the two horizontal wells. Note that the radial distance between two horizontal wells depends on the choice of the reference points along the horizontal well. In this study, the radial distance is measured between the vertical line passing through the center of the active horizontal well and the location of the optimum observation point defined in the previous section (Figure 5-10). In anisotropic formations, the radial distance needs to be scaled by the directional permeabilities. Based on the geometry shown in Figure 5-12, the radial distance between the two horizontal wells is given by

$$r = \sqrt{\left(\sqrt{\frac{k_h}{k_x}}\Delta x\right)^2 + \left(\sqrt{\frac{k_h}{k_y}}\Delta y\right)^2} \,. \tag{5-9}$$

and the dimensionless radial distance is defined by Eq. 5-8.

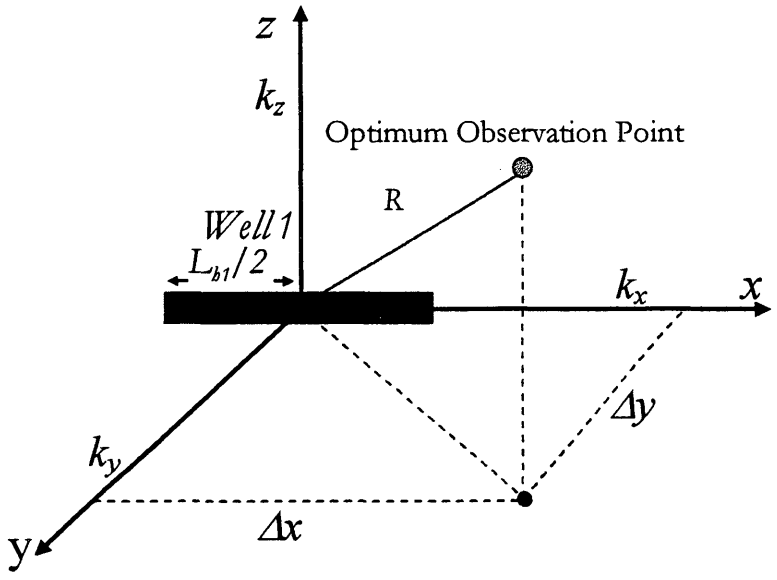

Figure 5-12. 3-D view showing the distance between the active horizontal well and the optimum observation point.

As noted above, to determine if the exponential integral solution is a good approximation for the horizontal observation well responses, we compared the dimensionless pressures calculated from the rigorous model derived in Chapter 2 with the dimensionless pressures obtained from Eq. 5-3 and required a good match for at least three log-cycles. Because the definitions of dimensionless pressure and time used in the two solutions are different (the rigorous model uses $k = \sqrt[3]{k_x k_y k_z}$ while the exponential integral solution uses $k_h = \sqrt{k_x k_y}$) we needed to convert one to the other by using the following simple relations

$$p_D = \frac{k}{k_h} \tilde{p}_D \tag{5-10}$$

and

$$t_D = \frac{k}{k_h} \tilde{t}_D . \tag{5-11}$$

The above two relations have been derived based on the definitions of dimensionless pressure and time given by Eqs. 2-2, 2-3, 5-6 and 5-7.

As expected based on physical intuition, our results indicated that the exponential integral solution could match the rigorous model results only when the radial distance between the two horizontal wells is sufficiently large for the flow convergence to be predominantly radial. The minimum radial distance between the two wells has been found to be a function of the angle θ between the axis of the active well and the line connecting the mid-point of the active well to the projection of the optimum observation point in the horizontal plane (see Figure 5-13). The angle θ is given by

$$\theta = \tan^{-1}\left(\frac{\Delta y}{\Delta x}\right) = \left(\frac{y_{OOP}}{x_{OOP} - \frac{L_{h1}}{2}}\right). \tag{5-12}$$

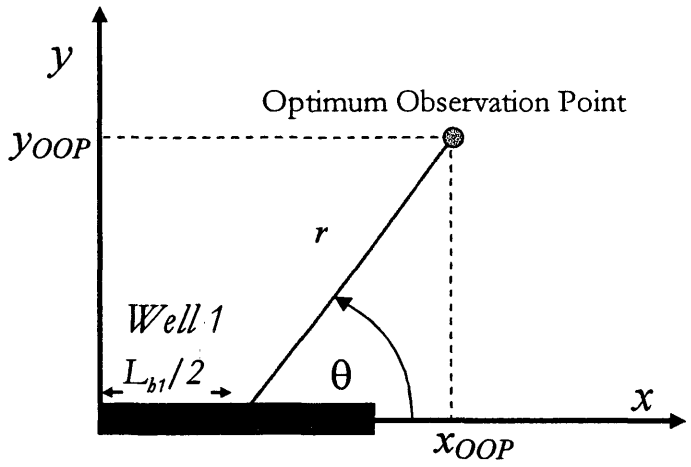

Figure 5-13. 2-D view showing the angle between the active horizontal well and the vertical observation well.

Figure 5-14 summarizes the results of extensive comparisons illustrating when the exponential integral solution may be used to approximate the horizontal observation well responses with reasonable accuracy. The three curves shown in the plot correspond to the average absolute errors of about 2, 5 and 10% with respect to the dimensionless pressures for various well configurations. The data of Figure 5-14 is presented in Appendix D. Figure 5-14 shows that the minimum distance between the two wells, $\tilde{r}_D$, which is required to yield a good match with the exponential integral solution is maximum when both wells are axially aligned (θ = 0°), while it becomes minimum when θ is about 65° (note that all the results here assume that the horizontal wells are always parallel to each other). Therefore, the angle

θ should not be taken as an indicator of the orientation of the observation well. For example, $\theta = 90°$ does not mean that the two wells are perpendicular. It simply means that the optimum observation point is aligned with the midpoint of the active horizontal well in the y-direction.

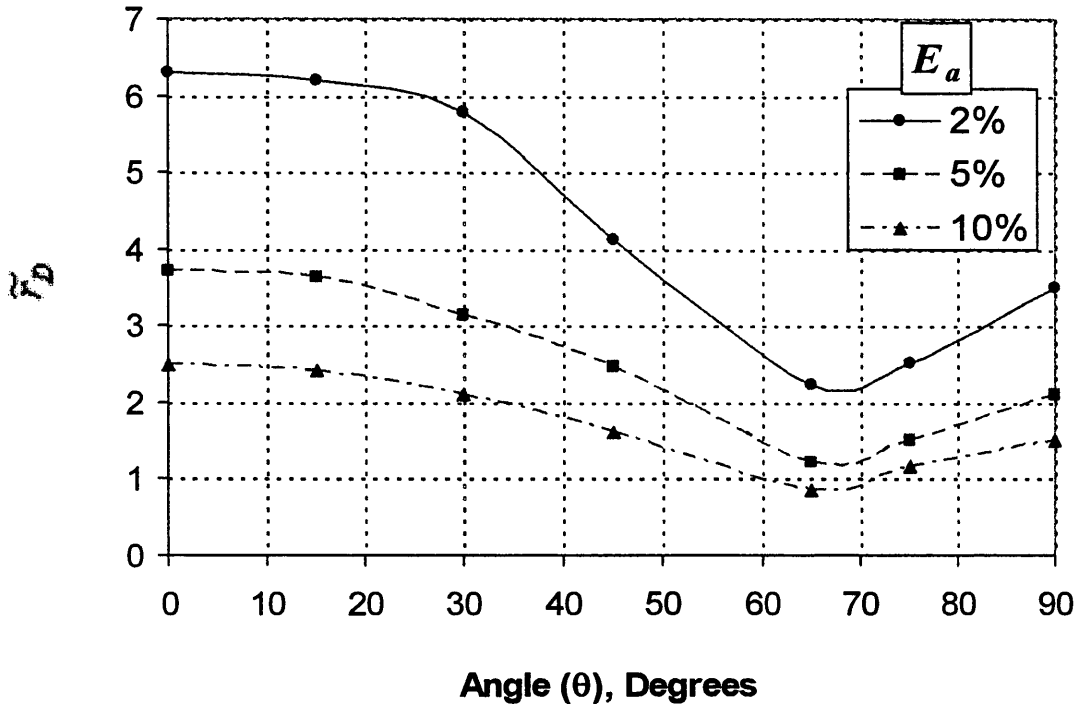

Figure 5-14. Correlation for the minimum radial distance to match the horizontal observation well responses by the exponential integral solution.

In general, when $\tilde{r}_D$ between the two wells is greater than 6.3, the horizontal observation well responses may be approximated by the exponential integral solution for all well orientations with an absolute average error of less than 2%. In general, the error is larger at earlier times and decreases as time increases. Even for the cases in the high error region of Figure 5-14, the late time data may display a reasonably good match while there is relatively

high deviation at early times. Therefore, while the absolute average error in terms of dimensionless pressure match may be relatively small, the maximum error at early times may still be high. For example, the maximum errors corresponding to the three average absolute errors of 2, 5 and 10% shown in Figure 5-14 may reach to 20, 50 and 80%, respectively, at early times. However, the regression and type-curve matching analysis use log-log scales where the early-time errors do not significantly affect the accuracy of the results. These comments will be delineated by the examples discussed in the following sections.

5.3 Application Examples

In the previous two sections, two approximate techniques have been developed to analyze interference tests between two horizontal wells. The intent of this section is to present several examples to demonstrate the capability of the rigorous and approximate methods to estimate the directional permeabilities. Four cases are used in the examples. The data for these cases are presented in Table 5-3. For reference, Figure 5-15 shows where the four cases fall with respect to the applicability of the exponential integral approximation. Example Case 1 is a good candidate to be analyzed by the exponential integral approximation (with less than 2% error). This indicates that the observation well is predominantly influenced by the radial convergence of flow toward the active well. Case 4 represents the conditions where the exponential integral may not yield a good approximation (the error is more than 10%). Cases 2 and 3 are in the region where the exponential integral approximation leads to an error between 2% to 5%.

This section is divided into two parts. The objective of the first part is to discuss the potential of horizontal observation well tests to reveal the directional permeabilities and comment on the uniqueness of the results to be obtained by regression analysis. The rigorous analytical model developed in Chapter 2 is used for these discussions. The second

part demonstrates the use of the approximate analysis techniques developed in the previous sections and documents the errors resulting from the use of these techniques by considering four examples.

Table 5-3. Data for the examples considered in Section 5.3.

Parameter	Case 1	Case 2	Case 3	Case 4
q, B/D	5000	5000	2000	2000
h, ft	200	200	100	100
$L_{h1}=L_{h2}$, ft	2500	2500	2000	2000
k_x, md	500	500	50	300
k_y, md	1000	1000	100	300
k_z, md	250	250	25	100
x_{h1}, ft	0	0	0	0
y_{h1}, ft	0	0	0	0
z_{h1}, ft	80	80	50	50
x_{h2}, ft	2700	6055	3000	2800
y_{h2}, ft	7556	2526	2000	0
z_{h2}, ft	150	150	50	50
r_{w1}, ft	0.265	0.265	0.165	0.165
r_{w2}, ft	0.265	0.265	0.165	0.165
ε, ft	0.00015	0.00015	0.00015	0.00015
ρ_{fluid}, lb/ft3	48	48	48	48

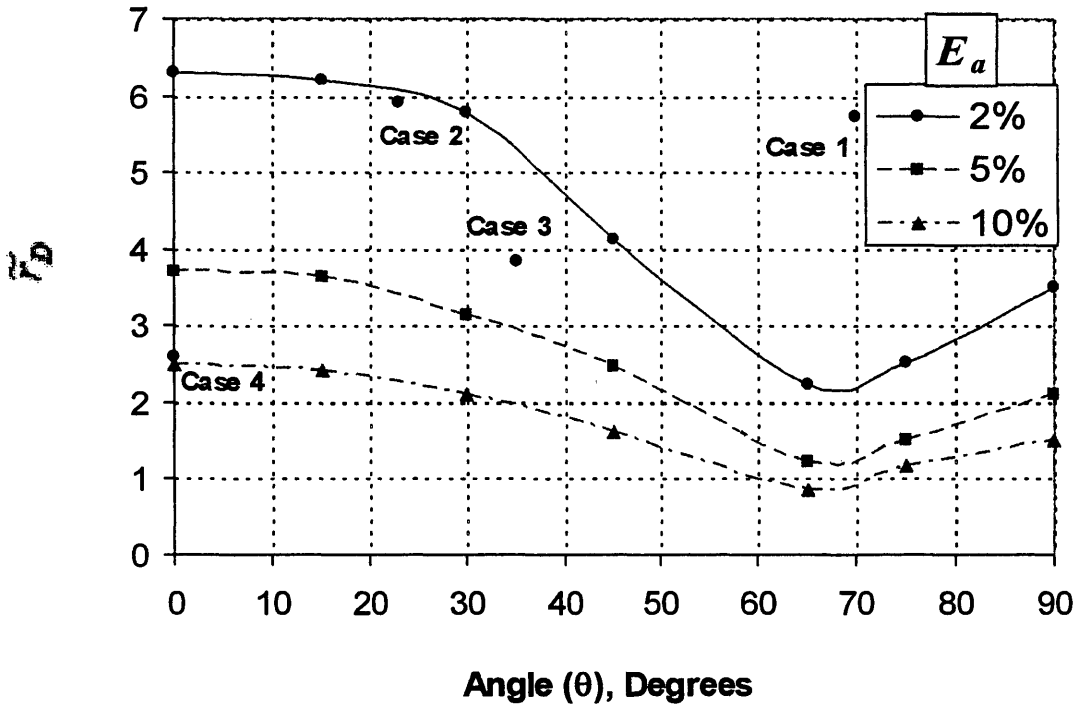

Figure 5-15. Possibility of matching Cases 1 – 4 of Table 5-3 with the exponential integral solution.

5.3.1 Estimation of Directional Permeabilities

The analysis of interference tests normally requires the use of type-curve matching or regression techniques because the span of the data is not sufficient for the application of the straight-line analysis techniques (especially, the semi-log analysis technique during pseudoradial flow). Therefore, the objective of this section is to demonstrate the analysis of horizontal observation well responses by matching with the theoretical solutions.

Two specific concerns need to be addressed in the analysis of horizontal observation well responses. The first concern is the ability of the particular analysis technique to estimate the parameters of interest. Here, we limit the parameters of interest to the directional permeabilities but in practice more parameters may be involved in the list. The second concern is the uniqueness of the results. This concern arises especially in type-curve matching or regression analysis of pressure transient data.

In general, the concerns noted above relate to the issue of the underlying flow regime for the horizontal observation well responses. As noted in Chapter 4, horizontal observation well responses generally display radial/pseudoradial flow convergence characteristics unless the active well is extremely close (as in the case of vertically stacked laterals). The results presented in Section 5.2 also indicate that if the distance between the active and observation wells is sufficiently large, the horizontal observation well responses may be represented by the exponential integral solution given by Eq. 5-3. Then, if the distance between the active and observation wells is sufficiently large, the pressure responses are functions of the average horizontal permeability, k_h, and t/r^2. This indicates that if the radial distance, r, between the center of the active well and the optimum observation point given by Eq. 5-9 is the same, only the horizontal permeability, k_h, may be estimated from the analysis of the data. However, Eq. 5-9 shows that r is a function of the distances between the wells and the horizontal directional permeabilities (k_x and k_y) and therefore the possibility exists to determine the horizontal directional permeabilities from the analysis of the interference data uniquely. In these cases, the techniques used to analyze interference tests between two vertical wells in anisotropic formations[26,28] are applicable to interference tests between two horizontal wells.

Three examples are given below considering two cases. Examples 5-1 and 5-2 consider the conditions where the exponential integral solution is not a good approximation for the observation well responses (Case 4 in Table 5-3) because of non-radial convergence of flow.

Example 5-1 discusses the estimation of the directional permeabilities in the horizontal plane while Example 5-2 investigates the sensitivity of the vertical permeability. In Example 5-3 (Case 1 in Table 5-3), the exponential integral approximation is expected to yield very good results because the flow convergence is predominantly radial and the existence of the observation well does not disturb the flow. Here, the estimation of the horizontal directional permeabilities is discussed because the vertical permeability should have no influence.

It must be emphasized again that the references to the exponential integral solution here are to signify the underlying flow characteristics for the examples considered. Otherwise, for all the results presented in this part, the rigorous model developed in Chapter 2 is used.

Example 5-1. – Non-radial flow convergence (wells are relatively close): This example considers the observation well responses for Case 4 of Table 5-3 (diamonds in Figure 5-16). As shown in Figure 5-15, this case falls in the bad match region (more than 10% error) for the exponential integral approximation, which implies radial flow convergence may not be a good assumption for this case. The lines without data points in Figure 5-16 correspond to two cases where the horizontal permeabilities are changed by keeping the average radial permeability and vertical permeability fixed. The sensitivity of the vertical permeability is investigated in Example 5-2 below.

The results indicate that even when the average horizontal permeability is the same, the pressure responses are sensitive to the individual values of the horizontal permeabilities. This implies that a regression analysis should converge to the correct values of the horizontal directional permeabilities and the result should be unique.

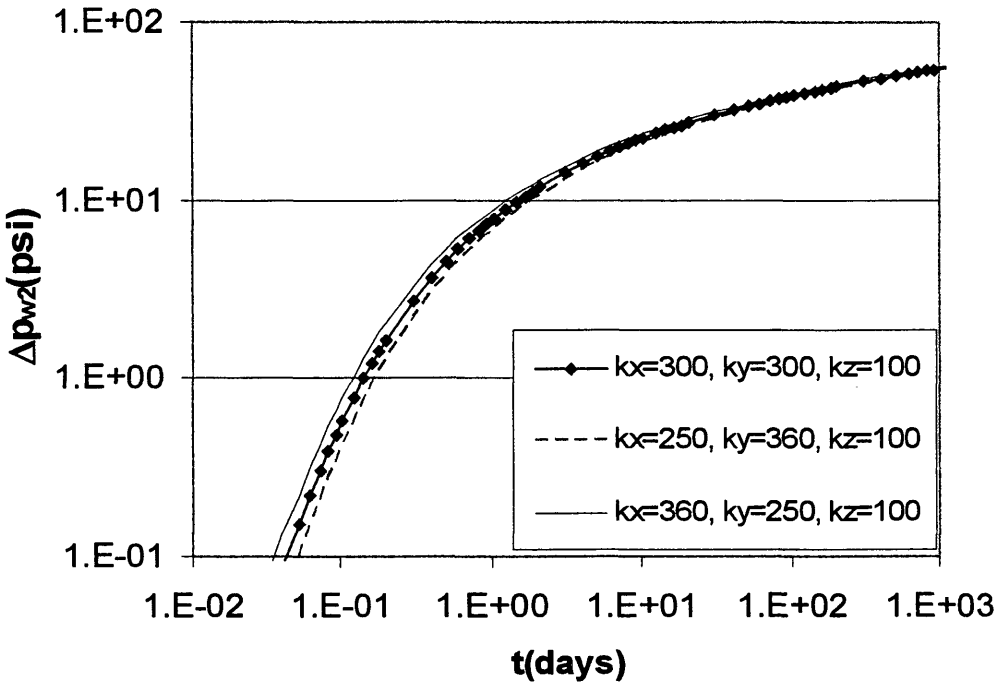

Figure 5-16. The sensitivity of the pressure responses to the horizontal permeabilities; Case 4 of Table 5-3.

It is interesting to note that although the exponential integral solution does not provide a good approximation for this data, plotting the results in terms of t/r^2 causes the responses for different horizontal permeabilities to collapse into one single curve (Figure 5-17). This indicates that although radial flow convergence is not warranted in this case, the responses may be correlated in terms of the equivalent radial distance between the two wells.

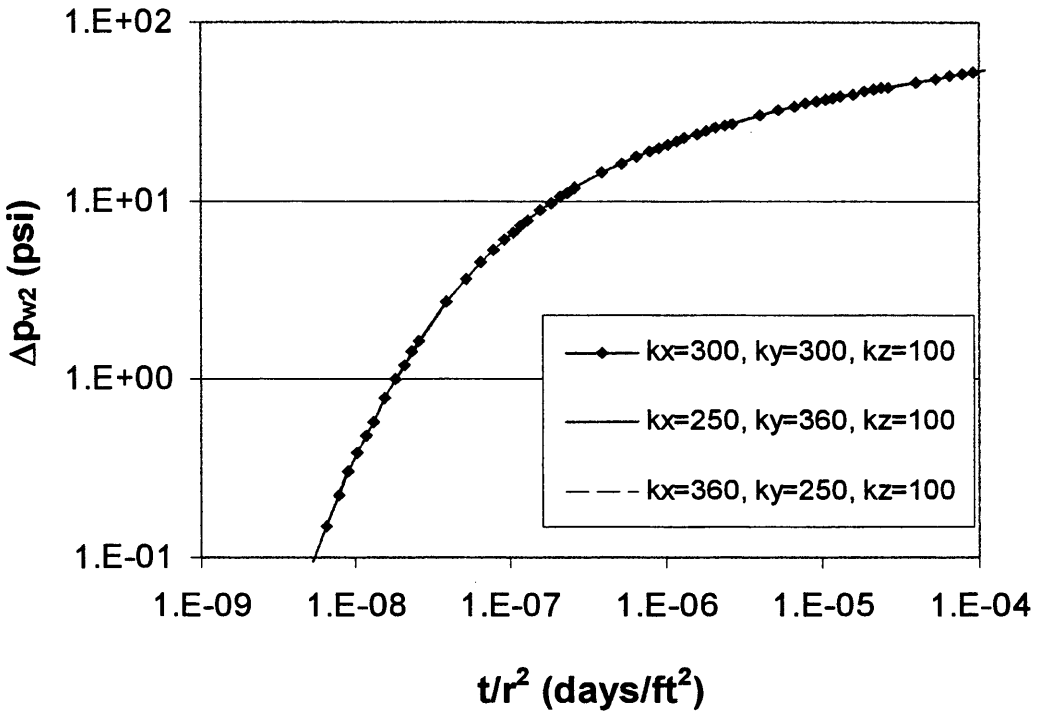

Figure 5-17. The correlation of the pressure responses in terms of t/r^2; Case 4 of Table 5-3.

Example 5-2 – Sensitivity to vertical permeability - Non-radial flow convergence (wells are relatively close): This example investigates the sensitivity of the vertical permeability component in the analysis of horizontal observation well responses for the same case considered in Example 5-1 above. Physical intuition tells us that the vertical convergence of flow should be negligible at relatively small distances from an active horizontal well. Therefore, if the distance between the two horizontal wells is relatively large, then no effect of vertical permeability on the horizontal observation well responses should be expected. In Figure 5-18, the horizontal permeability components are kept constant while changing the vertical permeability. The results are insensitive to the changes in the vertical

permeability indicating that the vertical permeability may not be determined from the analysis of the horizontal observation well responses. The exception to this conclusion is the case where the two wells are extremely close to each other in both horizontal and vertical directions.

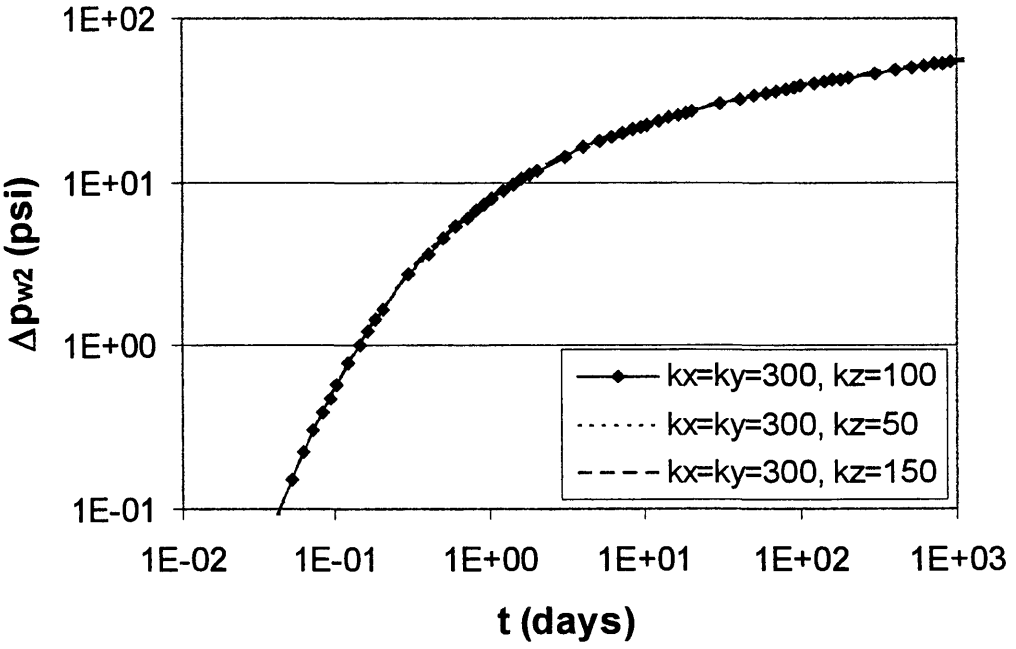

Figure 5-18. The sensitivity of the pressure and derivative responses to the vertical permeability; Case 4 of Table 5-3.

Example 5-3 – Radial flow (wells are considerably far from each other): This example considers Case 1 of Table 5-3 and as indicated by Figure 5-15, falls in the good match region for the exponential integral approximation. The characteristics of the responses shown in Figure 5-18 are the same as those for Example 5-1 (Figure 5-16) and the responses are

sensitive to the directional permeabilities in the horizontal plane even when the average horizontal permeability is fixed. Therefore, the possibility of estimating the horizontal directional permeabilities exists. All the techniques developed for vertical observation well tests should be applicable in this case. (For example, 3 different well tests may be used to determine the individual directional permeabilities as suggested by Ramey.[26]) Because the observation well responses have been shown to be insensitive to the vertical permeability even when the wells are closer as in Example 5-2, the effect of vertical permeability should be negligible here also (it cannot be determined from the observation well test).

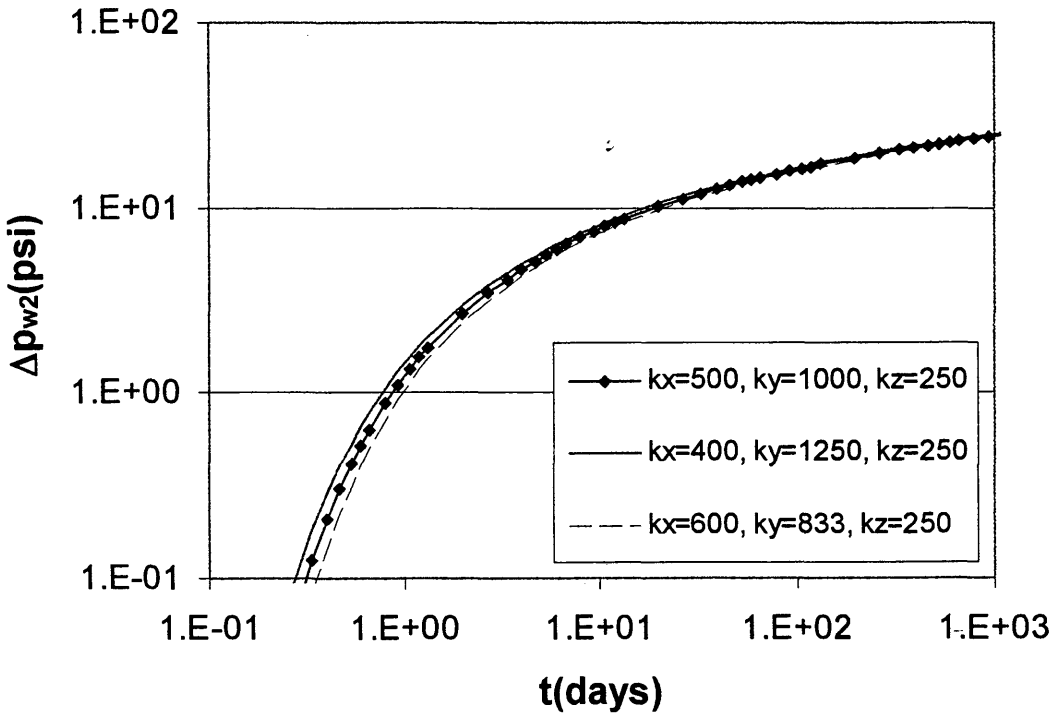

Figure 5-19. The sensitivity of the pressure responses to the horizontal permeabilities; Case 1 of Table 5-3.

Figure 5-20 is the counterpart of Figure 5-17 and shows that the interference responses may be correlated in terms of Δp vs. t/r^2. Although in Example 5-1 (Figure 5-17), this was not an intuitive result, here it is expected from the exponential integral solution given by Eq. 5-3.

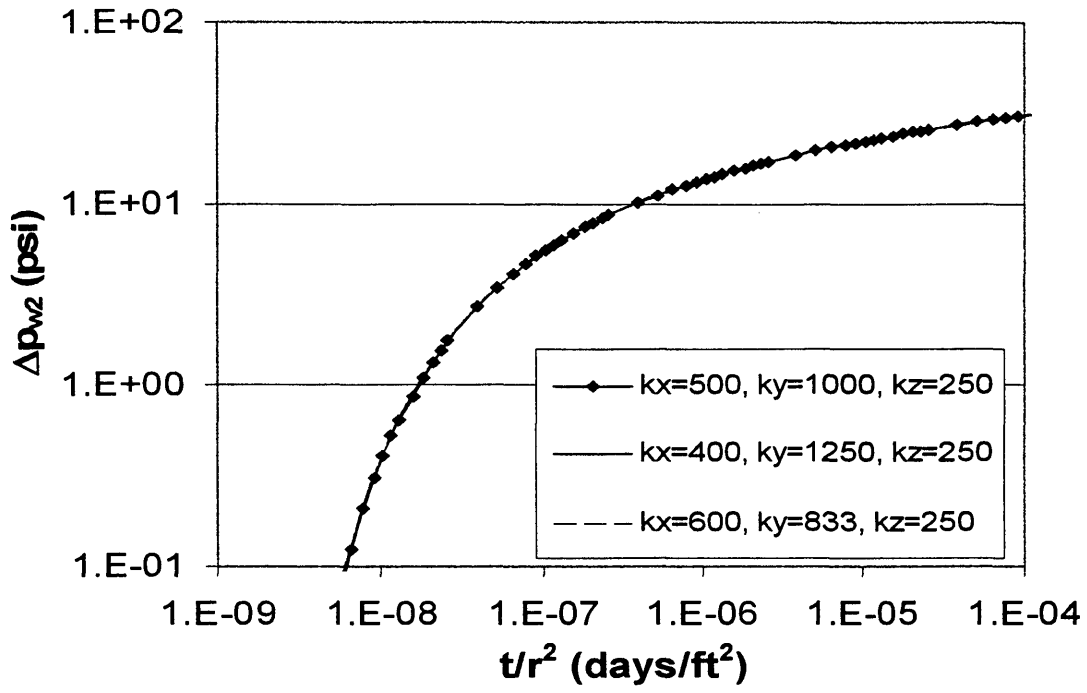

Figure 5-20. The correlation of the pressure and derivative responses in terms of t/r^2; Case 1 of Table 5-3.

5.3.2 Use of the Approximate Analysis Techniques

In this section, four examples are discussed to illustrate the use of the two correlations developed in the previous two sections. Examples are intended to illustrate the magnitude of the expected errors for various well orientations. The first example is Case 1 in Table 5-3

which considers the conditions where the horizontal observation well responses can be approximated by both an observation point and exponential integral solution with an average absolute error less than 2%. In the second example (Case 2 of Table 5-3), the horizontal observation well responses may be matched with the exponential integral solution with an error of about 2%. The third and fourth examples (Cases 3 and 4, respectively) consider cases where the error resulting from the use of the exponential integral approximation is about 5 and 10%, respectively.

To demonstrate the use of the approximate analysis techniques, we have generated synthetic pressure data by using the rigorous model developed in Chapter 2 for Cases 1 – 4 in Table 5-3. We label these results as Horizontal-Horizontal in the examples below and use to represent the field cases to be analyzed by type-curve matching or regression analysis by using the approximate models. We then calculate the pressures at the optimum observation point by using the single horizontal well and exponential integral models and discuss the success of these models by matching the results with the pressures for the Horizontal-Horizontal case.

Example 5-4, Case 1: We first determine the location of the optimum observation point:

$$\text{Relative location } \left(\frac{\Delta x_h}{L_h}\right) = \frac{2700}{2500} = 1.1$$

$$\text{Relative location } \left(\frac{\Delta y_h}{L_h}\right) = \frac{7556}{2500} = 3.0$$

From Figure 5-10, location of the optimum observation point= 0.52 L_h

x-direction location of the optimum observation point = 0.52*2500+2700= 4000 ft

Therefore, the location of the optimum observation point (x_{OOP}, y_{OOP})= (4000,7556)

Estimation of the angle between the optimum observation point and the horizontal active well:

$$\theta = \tan^{-1}\left(\frac{\Delta y}{\Delta x}\right) = \tan^{-1}\left(\frac{y_{OOP}}{x_{OOP} - \frac{L_{h1}}{2}}\right) = \tan^{-1}\left(\frac{7556}{4000 - \frac{2500}{2}}\right) = 70°$$

The dimensionless distance between the active well and the optimum observation point can be estimated from Eq. 5-8 as follows:

$$\tilde{r}_D = \frac{1}{1250}\sqrt{\left(\sqrt{\frac{\sqrt{500*1000}}{500}}2750\right)^2 + \left(\sqrt{\frac{\sqrt{500*1000}}{1000}}7556\right)^2}$$
$$= 5.72$$

Figure 5-15, indicates that the average absolute error to be expected from the exponential integral approximation is less that 2% for this case (Case 1). Figure 5-21 presents comparisons of the actual horizontal observation well responses (Horizontal-Horizontal) and the optimum observation point and exponential integral approximations. Both approximations yield excellent matches with the correct data. The third row of Table 5-4, shows the calculated average absolute and the maximum errors for the optimum observation point and exponential integral approximations. As expected, the average absolute errors are less than 2% for both approximations.

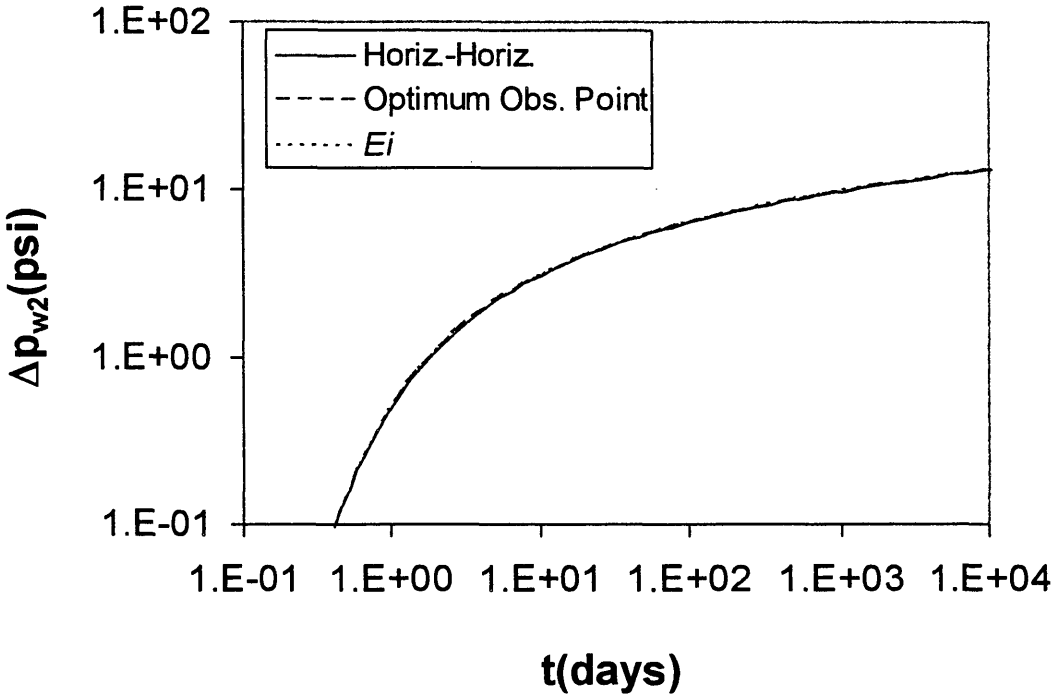

Figure 5-21. Comparison of the approximate model results with the correct pressure responses for Case 1 of Table 5-3.

Table 5-4. Error results for Cases 1 – 4 of Table 5-3.

	Optimum Observation Point		Exponential Integral	
Case	E_a (%)	E_m (%)	E_a (%)	E_m (%)
1	0.26	2.54	0.58	4.12
2	1.19	10.7	2.89	29.8
3	1.89	22.7	4.39	56.2
4	5.16	40.0	10.2	85.4

Example 5-5, Case 2: The location of the optimum observation point is calculated as follows:

$$\text{Relative location } (\frac{\Delta x_h}{L_h}) = \frac{6055}{2500} = 2.4$$

$$\text{Relative location } (\frac{\Delta y_h}{L_h}) = \frac{2526}{2500} = 1.0$$

From Figure 5-10, location of the optimum observation point = 0.455 L_h

x-direction location of the optimum observation point = 0.455*2500+6055= 7193 ft

Therefore location of the optimum observation point (x_{OOP}, y_{OOP})= (7193,2526)

Estimation of the angle between the optimum observation point and the horizontal active well:

$$\theta = \tan^{-1}\left(\frac{\Delta y}{\Delta x}\right) = \tan^{-1}\left(\frac{y_{OOP}}{x_{OOP} - \frac{L_{h1}}{2}}\right) = \tan^{-1}\left(\frac{2526}{7193 - \frac{2500}{2}}\right) = 23°$$

The dimensionless radial distance between the active well and the optimum observation point can be estimated from Eq. 5-8 as follows:

$$\tilde{r}_D = \frac{1}{1250}\sqrt{\left(\sqrt{\frac{\sqrt{500*1000}}{500}}5943\right)^2 + \left(\sqrt{\frac{\sqrt{500*1000}}{1000}}2526\right)^2}$$

$$= 5.90$$

Figure 5-15, shows that the exponential integral approximation should yield and average absolute error close to 2%. Figure 5-22 compares the optimum observation point and exponential integral approximations with the correct data (Horizontal-Horizontal). The match of the approximate results is excellent for all practical purposes. The error estimates are shown in the fourth row of Table 5-4.

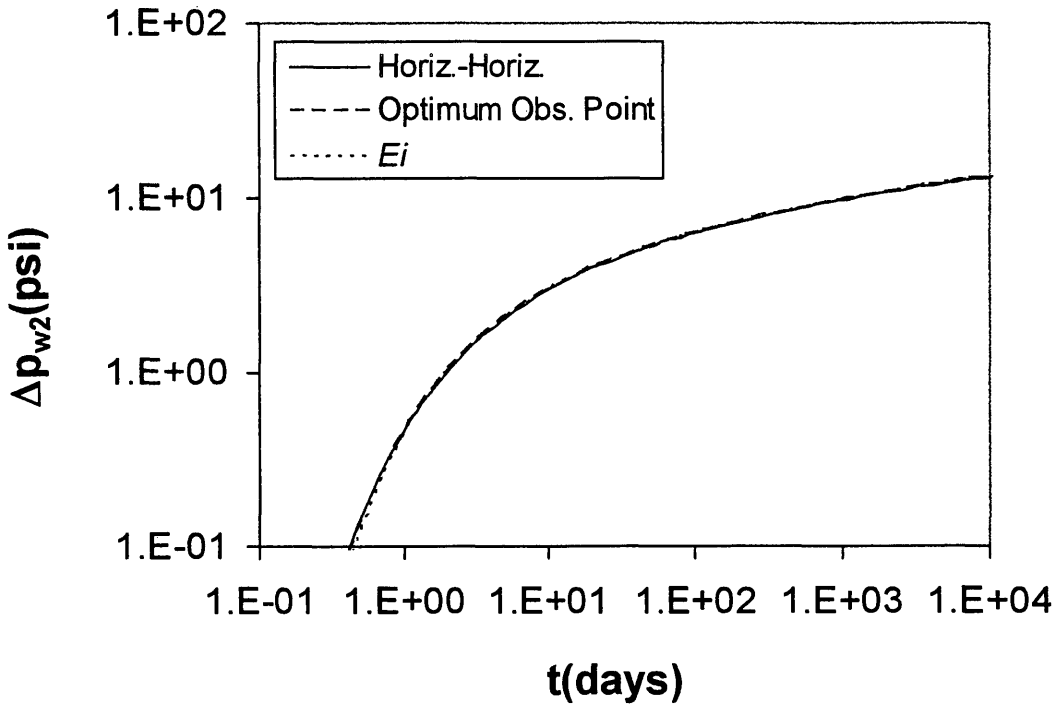

Figure 5-22. Comparison of the approximate model results with the correct pressure responses for Case 2 of Table 5-3.

Example 5-6, Case 3: The location of the optimum observation point is calculated as follows:

$$\text{Relative location } \left(\frac{\Delta x_h}{L_h}\right) = \frac{3000}{2000} = 1.5$$

$$\text{Relative location } (\frac{\Delta y_h}{L_h}) = \frac{2000}{2000} = 1.0$$

From Figure 5-10, the location of the optimum observation point = 0.45 L_h

x-direction location of the optimum observation point = 0.45*2000+3000= 3900 ft

Therefore the location of the optimum observation point $(x_{OOP}, y_{OOP}) = (3900,2000)$

Figure 5-11 indicates that the application of the optimum observation point approximation at this location should cause approximately 2% average absolute error.

Estimation of the angle between the optimum observation point and the horizontal active well:

$$\theta = \tan^{-1}\left(\frac{\Delta y}{\Delta x}\right) = \tan^{-1}\left(\frac{y_{OOP}}{x_{OOP} - \frac{L_{h1}}{2}}\right) = \tan^{-1}\left(\frac{2000}{3900 - \frac{2000}{2}}\right) = 35°$$

The dimensionless radial distance between the active well and the optimum observation point can be estimated from Eq. 5-8 as follows:

$$\tilde{r}_D = \frac{1}{1000}\sqrt{\left(\sqrt{\frac{\sqrt{50*100}}{50}}2900\right)^2 + \left(\sqrt{\frac{\sqrt{50*100}}{100}}2000\right)^2}$$

$$= 3.84$$

According to Figure 5-15, the exponential integral approximation should be expected to lead to an average absolute error between 2 and 5%. Figure 5-23 shows the comparison of the actual horizontal observation well responses and the optimum observation point and

exponential integral approximations. Although both approximations yield acceptable matches, the exponential integral approximation displays more deviation at earlier times leading to an average absolute error of approximately 5% (the fifth row of Table 5-4). The average absolute error resulting from the optimum observation point approximation is still less than 2% (the fifth column of Table 5-4).

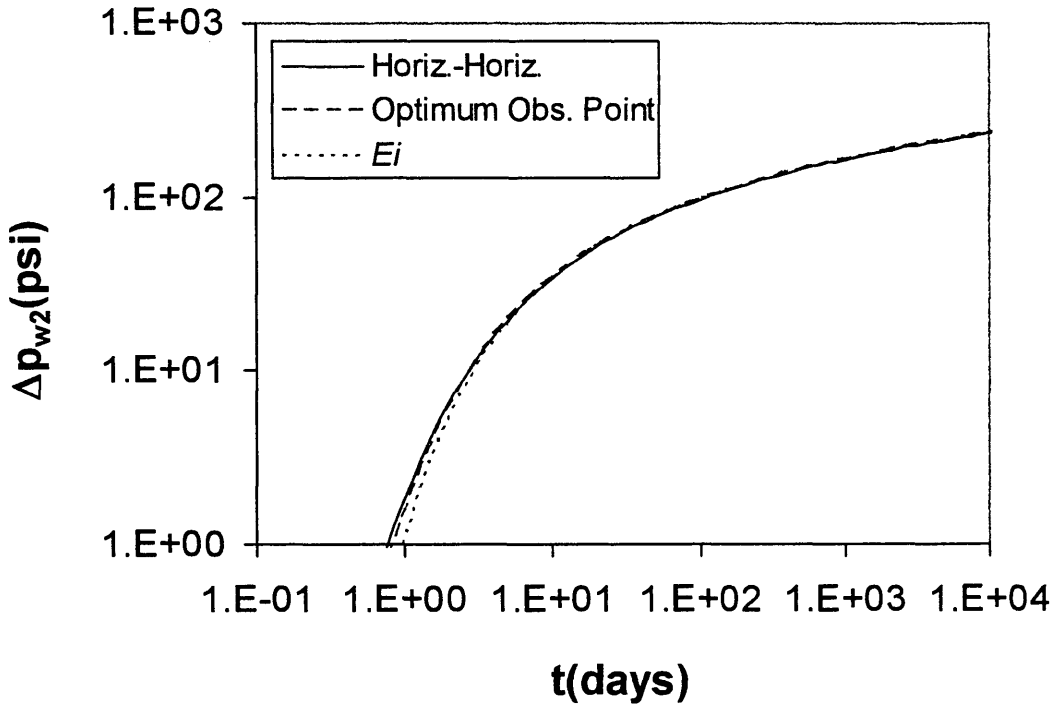

Figure 5-23. Comparison of the approximate model results with the correct pressure responses for Case 3 of Table 5-3.

Example 5-7, Case 4: The location of the optimum observation point is calculated as follows:

$$\text{Relative location } \left(\frac{\Delta x_h}{L_h}\right) = \frac{2800}{2000} = 1.4$$

$$\text{Relative location } (\frac{\Delta y_h}{L_h}) = \frac{0}{2000} = 0.0$$

From Figure 5-10, the location of the optimum observation point = 0.39 L_h

x-direction location of the optimum observation point = 0.39*2000+2800= 3580 ft

Therefore, the location of the optimum observation point $(x_{OOP}, y_{OOP}) = (3580,2000)$

Figure 5-11 indicates that for this case, the optimum observation point approximation should yield an error higher than 5%.

The angle between the optimum observation point and the horizontal active well:

$$\theta = \tan^{-1}\left(\frac{\Delta y}{\Delta x}\right) = \tan^{-1}\left(\frac{y_{OOP}}{x_{OOP} - \frac{L_{h1}}{2}}\right) = \tan^{-1}\left(\frac{0.0}{3580 - \frac{2000}{2}}\right) = 0°$$

The dimensionless radial distance between the active well and optimum observation point can be calculated from Eq. 5-8:

$$\tilde{r}_D = \frac{1}{1000}\sqrt{\left(\sqrt{\frac{300*300}{300}}2580\right)^2 + \left(\sqrt{\frac{300*300}{300}}0\right)^2}$$

$$= 2.58$$

According to Figure 5-15, the application of the exponential integral approximation should yield an average absolute error close to 10%. Figure 5-24 compares the actual horizontal observation well responses and the optimum observation point and exponential integral approximations. The exponential integral approximation is shown to yield a poor match,

especially at early times, while the optimum observation point approach yields relatively closer results to the actual pressure responses. The sixth row of Table 5-4 shows that average absolute errors of the approximations are in the range of the predictions from Figures 5-11 and 5-15.

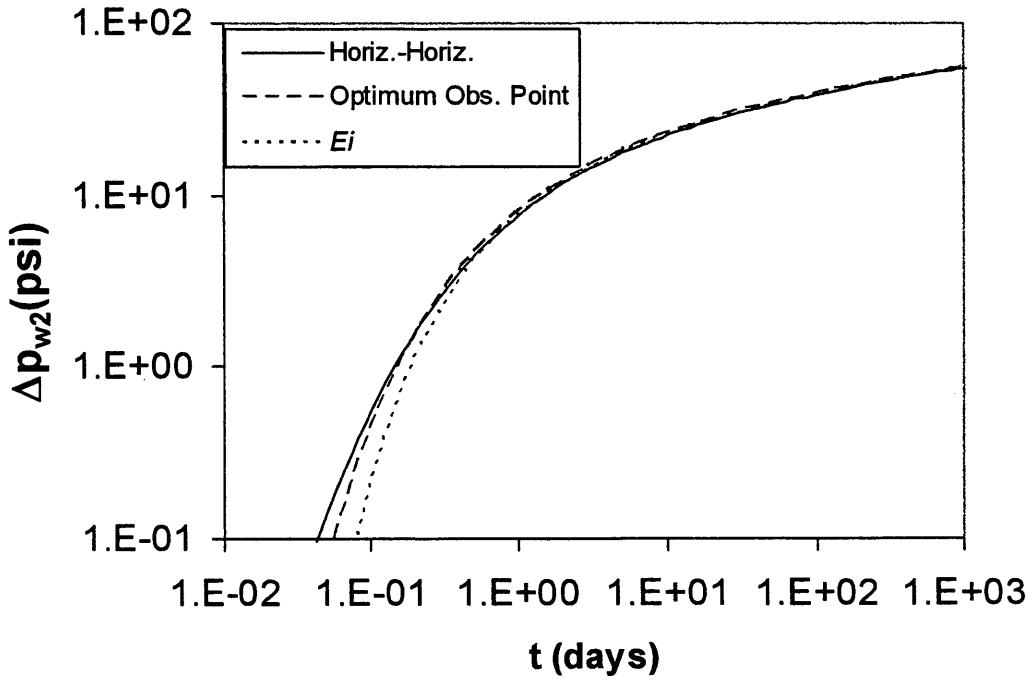

Figure 5-24. Comparison of the approximate model results with the correct pressure responses for Case 4 of Table 5-3.

CHAPTER 6

GENERAL MODEL FOR ARBITRARY WELL AZIMUTH ANGLES IN ANISOTROPIC RESERVOIRS

The discussions in the previous chapters were concerned with the interference effects on the responses of parallel horizontal wells which were aligned with one of the principal permeabilities. Although, ideally one would like to drill horizontal wells normal to the direction of the maximum permeability, this may not be the case in practice for two reasons. First, in most cases the directional permeabilities of the reservoir are not known. Second, the orientation of the horizontal wells may be dictated by several other factors such as reservoir sweep efficiency and drilling constrains as in offshore applications.

In this chapter, a general model is developed to investigate interference between two horizontal wells with arbitrary azimuth angles in an anisotropic reservoir (Figure 6-1). This model is not significantly different from the previous model developed in Chapter 2 in formulation but it is more complex in terms of computational algorithm. This has dictated the approach taken in this dissertation; that is a relatively simpler model was developed first so that it could be used to verify the more complex model.

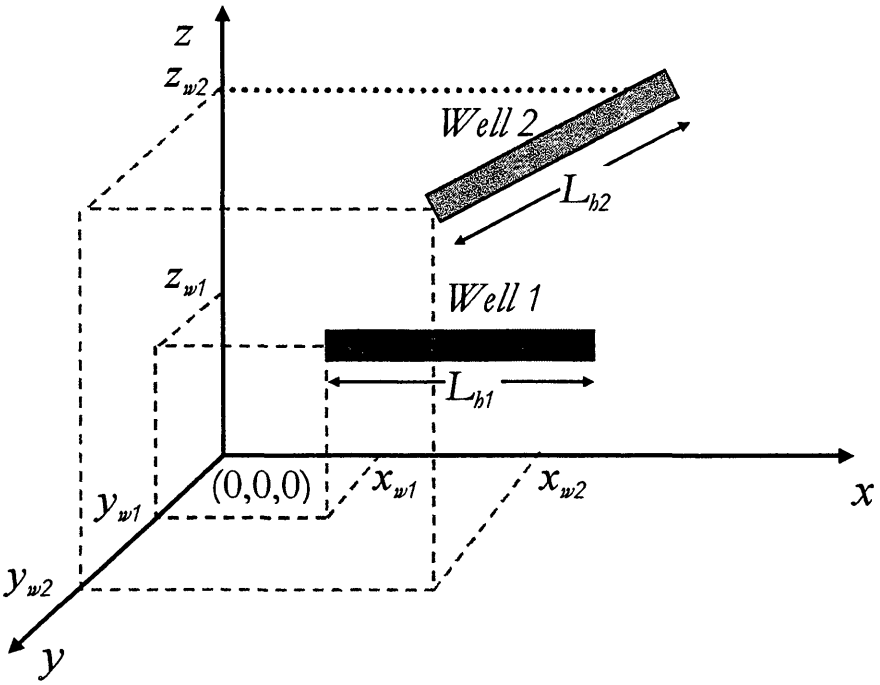

Figure 6-1. Second model horizontal well configuration, 3-D view.

6.1 Permeability Ellipse for Anisotropic Reservoirs

In general, flow in anisotropic reservoirs is considered to be an elliptical flow problem.[23,24,28] In this case the permeability anisotropy can be visualized as a permeability ellipse (Figure 6-2). The size and orientation of the ellipse reflect the magnitude and direction of the permeability anisotropy, respectively. In this case, the major and minor axes of the ellipse correspond to the square root of the maximum and minimum horizontal principal permeabilities (k_{hmax} and k_{hmin}), respectively. The radius of the ellipse is equal to the square root of the radial directional permeability $(k_r)^{1/2}$ defined by

$$\frac{1}{k_r} = \frac{\cos^2\theta}{k_{h\max}} + \frac{\sin^2\theta}{k_{h\min}}. \tag{6-1}$$

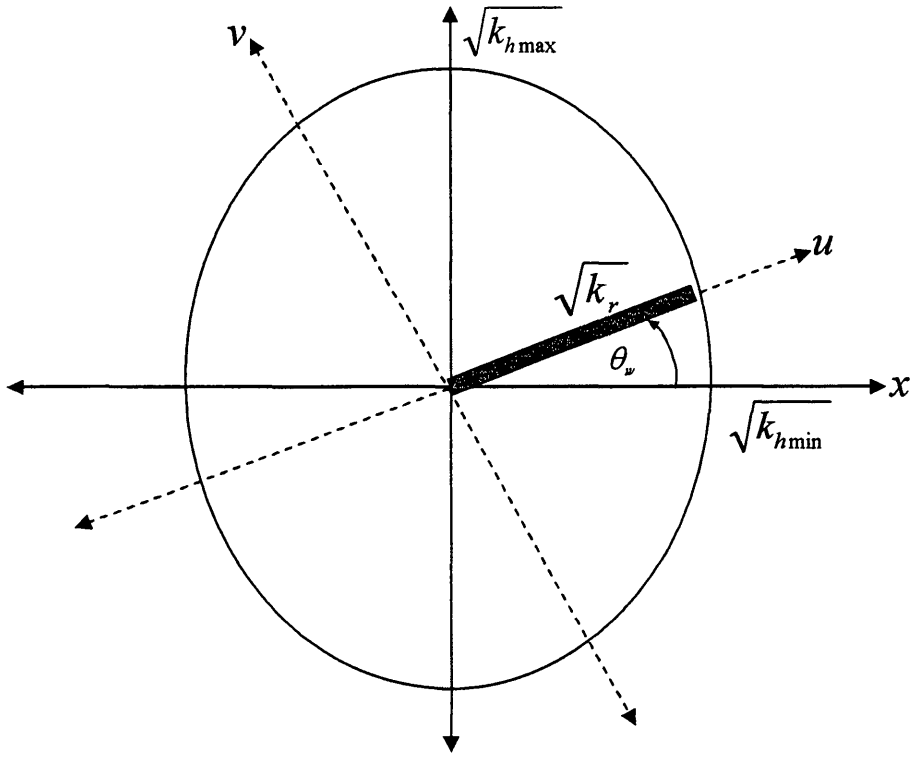

Figure 6-2. Permeability ellipse showing location of horizontal well.

For a horizontal well at an angle θ_w with respect to the minimum horizontal permeability direction, k_{hmin}, evaluating Eq. 6-1 gives the equivalent permeability aligned with the horizontal well direction while evaluating it with $\theta = \theta_w + 90$ gives the equivalent permeability normal to the horizontal well. It is clear also from Eq. 6-1 that for isotropic permeability

cases where $k_{hmax} = k_{hmin} = k_r = k$ the ellipse transforms into a circle with an equivalent area. In this study, we assume that the x-axis coincides with the minimum permeability direction and the y-axis is in the direction of maximum permeability. We also use the notation that u and v denote the directions aligned with and normal to the well axis, respectively (Figure 6-2).

6.2 Semi-Analytical Model

The solution given by Eq. 2-15 may be used to calculate the pressure drop due to a horizontal well with an azimuth angle θ by incorporating the following coordinate transformation (see Figure 6-2):

$$x = u\cos\theta, \tag{6-1}$$

$$y = u\sin\theta. \tag{6-2}$$

Using the definitions of dimensionless variables and

$$\alpha = \frac{u}{l}, \tag{6-3}$$

the dimensionless pressure for a horizontal well with an azimuth angle θ (with respect to the minimum horizontal permeability direction, k_x) is given by

$$p_D(x_D,y_D,z_D,t_D)=\frac{1}{4}\sqrt{\frac{k^2}{k_x k_y}}\int_0^{t_D}\int_0^{2L_D h_D} q_{hD}(\alpha,\tau)\exp\left[-\frac{\left(x_D-x_{wD}-\alpha\cos\theta\sqrt{\frac{k}{k_x}}\right)^2}{4(t_D-\tau)}\right]$$

$$\exp\left[-\frac{(y_D-y_{wD}-\alpha\sin\theta\sqrt{\frac{k}{k_y}})^2}{4(t_D-\tau)}\right]d\alpha$$

$$\left\{1+2\sum_{n=1}^{\infty}\exp\left[-\frac{n^2\pi^2(t_D-\tau)}{h_D^{\,2}}\right]\cos n\pi z_D\cos n\pi z_{wD}\right\}\frac{d\tau}{(t_D-\tau)} \tag{6-4}$$

where

$$q_{hD}=\frac{2q_h l}{qB}. \tag{6-5}$$

Eq. 6-4 is the counterpart of Eq. 2-20 for horizontal wells which are not aligned with either of the horizontal principal permeability directions. In addition, the angle θ now can be written as θ_1 or θ_2 for Well 1 and 2 respectively. The superposition of the two horizontal wells as in Eq. 2-21 can now be carried out by using Eq. 6-4 with $\theta=\theta_1$ and θ_2 for the active and observation horizontal wells respectively.

6.2.1 Coupled Wellbore-Reservoir Models

Following the same lines as in Chapter 2, the pressure drop in the wellbore of the active well is given by the following relation:

$$\frac{dp_{h1}}{du} = Efq_{hc}^2 . \tag{6-6}$$

Where now u represents the location along the horizontal wellbore. By similar lines, Eq. 2.30 can now be written as:

$$p_{wD1}(t_D) - p_{hD1}(u_D, t_D) = \frac{N_{Re1} f_{t1}}{16} \frac{\pi}{C_{hD1}} \left[\frac{2(u_D - u_{wD1})}{L_{D1} h_D} - \frac{1}{L_{D1} h_D} \int_{u_{wD1}}^{u_D} \int_{u_{wD1}}^{u_D'} \left(\frac{D_1}{N_{Re1} f_{t1}} q_{hD1} \right) du_D'' du_D' \right]. \tag{6-7}$$

For the observation well the counterpart of Eq. 2-42 is given by

$$p_{wD2}(t_D) - p_{hD2}(u_D, t_D) = -\frac{\pi}{16 C_{hD2}} \frac{1}{L_{D2} h_D} \int_{u_{wD2}}^{u_D} \int_{u_{wD2}}^{u_D'} D_2 q_{hD2} du_D'' du_D' . \tag{6-8}$$

For simplicity in coupling the wellbore and reservoir models, Eq. 6-7 and 6-8 have been expressed in terms of u (distance in the direction of the well axis) instead of x. In this case, the distances in wellbore and reservoir models can be related by Eq. 6-3. The coupling of the wellbore and reservoir models and the solution of the system can now be carried out in a similar manner to that in Chapter 2. To solve the coupled system, the flux distributions, q_{hD1} and q_{hD2} along the horizontal sections of the active and interference wells, respectively, need to be known. In order to achieve this, a semi-analytical algorithm similar to the one presented in Chapter 2 will need to be developed.

6.2.2 Solution Algorithm

In this section, a semi-analytical algorithm will be developed to estimate the flux distribution along both horizontal wells. For simplicity, Well 1 will be considered first and the center of the coordinate axis in the *x-y* plane will be assumed to be at the heel of Well 1; that is, x_{w1}= y_{w1}=0. In this case Eq. 6-7 simplifies to

$$p_{wD1}(t_D) - p_{hD1}(u_D, t_D) = \frac{N_{Re\,t1} f_{t1}}{16} \frac{\pi}{C_{hD1} L_{D1} h_D} \left[2u_D - \int_{u_{wD1}}^{u_D} \int_{u_{wD1}}^{u_D'} \left(\frac{D_1}{N_{Re\,t1} f_{t1}} q_{hD1} \right) du_D'' du_D' \right]. \tag{6-9}$$

Similar to Eq. 2-33, $p_{hD1}(u_D, t_D)$ may be written at x_{w1}= y_{w1}=0 as

$$\begin{aligned} p_{hD1}(u_D, t_D) = {} & p_{D1}(x_D, y_D, z_{wD1} + r_{wD1}; 0, 0, z_{wD1}, t_D) + q_{hD1}(x_D, t_D) S_1(x_D) \\ & + p_{D2}(x_D, y_D, z_{wD1} + r_{wD1}; x_{wD2}, y_{wD2}, z_{wD2}, t_D) \end{aligned} \tag{6-10}$$

If Well 1 is divided into M segments and the center of segment j is denoted by u_{Dj}, then the double integral in Eq. 6-9 may be written as

$$\int_{u_{wD1}}^{u_{Dj}} \int_{u_{wD1}}^{u_D'} D_1 q_{hD1} du_D'' du_D' = \left[\sum_{i=1}^{j-1} \left(u_{Dj} - i\Delta u_{D1} + \frac{\Delta u_{D1}}{2} \right) \Delta u_{D1} D_{1i} q_{hD1i} + \frac{(\Delta u_{D1})^2}{8} D_{1j} q_{hD1j} \right]. \tag{6-11}$$

Here, D_{1i} and q_{hD1i} are evaluated at the center of the i^{th} interval. Let us assume that the flux, q_{hD}, is constant in each segment, divide Well 1 into M equal segments, and define the following relation:

$$G_{ki}(x_D, y_D, z_D; x_{wDk}, y_{wDk}, z_{wDk}, t_D) = \frac{1}{4}\sqrt{\frac{k^2}{k_x k_y}} \int_{2(i-1)\tilde{L}_{Dk}/M}^{2i\tilde{L}_{Dk}/M} q_{hD}(\alpha, \tau)$$

$$\exp\left[-\frac{\left(x_D - x_{wDk} - \alpha\cos\theta\sqrt{\frac{k}{k_x}}\right)^2}{4(t_D - \tau)}\right] \exp\left[-\frac{(y_D - y_{wDk} - \alpha\sin\theta\sqrt{\frac{k}{k_y}})^2}{4(t_D - \tau)}\right] d\alpha \,, \qquad (6\text{-}12)$$

$$\left\{1 + 2\sum_{n=1}^{\infty}\exp\left[-\frac{n^2\pi^2(t_D - \tau)}{h_D^{\,2}}\right]\cos n\pi z_D \cos n\pi z_{wDk}\right\}\frac{d\tau}{(t_D - \tau)}$$

here

$$\tilde{L}_{Dk} = L_{Dk} h_D \,. \qquad (6\text{-}13)$$

Using Eq. 6-12, p_{Dk} in Eq. 6-10 can be written as follows:

$$p_{Dk}(x_{Dj}, y_D, z_D; x_{wDk}, y_{wDk}, z_{wDk}, t_D) = \int_0^{t_D}\sum_{i=1}^{M} q_{hDki}(\tau) G_{ki}(x_{Dj}, y_D, z_D; x_{wDk}, y_{wDk}, z_{wDk}, t_D - \tau) d\tau \,. \qquad (6\text{-}14)$$

Eq. 6-14 may be discretized in time as follows:

$$p_{Dk}(x_{Dj}, y_D, z_D; x_{wDk}, y_{wDk}, z_{wDk}, t_D) = \sum_{l=1}^{N}\int_{t_{Dl-1}}^{t_{Dl}}\sum_{i=1}^{M} q_{hDki}(\tau) G_{ki}(x_{Dj}, y_D, z_D; x_{wDk}, y_{wDk}, z_{wDk}, t_D - \tau) d\tau \,. \qquad (6\text{-}15)$$

Assuming q_{hDki} is constant in each time interval (t_{Dl}-t_{Dl-1}), Eq. 6-15 can be written as

$$p_{Dk}\left(x_{Dj},y_D,z_D;x_{wDk},y_{wDk},z_{wDk},t_D\right)=\tilde{p}_{Dk}\left(x_{Dj},y_D,z_D;x_{wDk},y_{wDk},z_{wDk},t_D\right)$$
$$+\sum_{i=1}^{M}q_{hDki}\left(t_{DN}\right)\int_{0}^{t_{DN}-t_{DN-1}}G_{ki}\left(x_{Dj},y_D,z_D;x_{wDk},y_{wDk},z_{wDk},\tau\right)d\tau \quad (6\text{-}16)$$

In Eq. 6-16,

$$\tilde{p}_{Dk}\left(x_{Dj},y_D,z_D;x_{wDk},y_{wDk},z_{wDk},t_D\right)=\sum_{l=1}^{N-1}\sum_{i=1}^{M}q_{hDki}\left(t_{Dl}\right)$$
$$\left[\int_{0}^{t_{DN}-t_{DN-1}}G_{ki}\left(x_{Dj},y_D,z_D;x_{wDk},y_{wDk},z_{wDk},\tau\right)d\tau-\int_{0}^{t_{DN}-t_{Dl}}G_{ki}\left(x_{Dj},y_D,z_D;x_{wDk},y_{wDk},z_{wDk},\tau\right)d\tau\right] \quad (6\text{-}17)$$

Substituting Eqs. 6-10, 6-11, 6-16 and 6-17 into Eq. 6-9, we obtain:

$$\begin{aligned}
&p_{wD1}(t_{DN})-\tilde{p}_{D1}\left(x_{D1j},y_{D1j},z_{wD1}+r_{wD1};0,0,z_{wD1},t_D\right)\\
&-\sum_{i=1}^{M}q_{hD1i}\left(t_{DN}\right)\int_{0}^{t_{DN}-t_{DN-1}}G_{1i}\left(x_{D1j},y_{D1j},z_D;0,0,z_{wDk},\tau\right)d\tau\\
&-q_{hD1j}S_{1j}-\tilde{p}_{D2}\left(x_{D1j},y_{D1j},z_{wD1}+r_{wD1};x_{wD2j},y_{wD2j},z_{wD2},t_D\right)\\
&-\sum_{i=1}^{M}q_{hD2i}\left(t_{DN}\right)\int_{0}^{t_{DN}-t_{DN-1}}G_{2i}\left(x_{D1j},y_{D1j},z_{wD1}+r_{wD1};x_{wD2j},y_{wD2j},z_{wD2},\tau\right)d\tau=\\
&\frac{\pi N_{Re\,t1}f_{t1}}{8C_{hD1}}\frac{1}{L_{D1}h_D}u_{D1j}\\
&-\frac{\pi}{16C_{hD1}}\frac{1}{L_{D1}h_D}\left[\sum_{i=1}^{j-1}\left(u_{D1j}-i\Delta u_{D1}+\frac{\Delta u_{D1}}{2}\right)\Delta u_{D1}D_{1i}q_{hD1i}+\frac{(\Delta u_{D1})^2}{8}D_{1j}q_{hD1j}\right]
\end{aligned} \quad (6\text{-}18)$$

where the reference point is at the heel of Well 1 and

$$S_{1j}=S_1(u_{D1j}). \quad (6\text{-}19)$$

By similar lines, we derive the following counterpart of Eq. 6-18 for Well 2:

$$
\begin{aligned}
&p_{wD2}(t_{DN}) - \tilde{p}_{D1}\left(x_{D2j}, y_{D2j}, z_{wD2} + r_{wD2}; x_{wD1}, y_{wD1}, z_{wD1}, t_D\right) - \\
&\sum_{i=1}^{M} q_{hD1i}(t_{DN}) \int_0^{t_{DN}-t_{DN-1}} G_{1i}\left(x_{D2j}, y_{D2j}, z_{wD2} + r_{wD2}; x_{wD1}, y_{wD1}, z_{wD1}, \tau\right) d\tau \\
&- \tilde{p}_{D2}\left(x_{D2j}, y_{D2j}, z_{wD2} + r_{wD2}; 0, 0, z_{wD2}, t_D\right) \\
&- \sum_{i=1}^{M} q_{hD2i}(t_{DN}) \int_0^{t_{DN}-t_{DN-1}} G_{1i}\left(x_{D2j}, y_{D2j}, z_{wD2} + r_{wD2}; 0, 0, z_{wD2}, \tau\right) d\tau - q_{hD2j} S_{2j} = \\
&\frac{\pi}{16 C_{hD2}} \frac{1}{L_{D2} h_D} \left[\sum_{i=1}^{j-1} \left(u_{D2j} - i\Delta u_{D2} + \frac{\Delta x_{D2}}{2} \right) \Delta u_{D2} D_{2i} q_{hD2i} + \frac{(\Delta u_{D2})^2}{8} D_{2j} q_{hD2j} \right]
\end{aligned}
\tag{6-20}
$$

Again here, the reference point is at the heel of Well 2. In addition, x_{wD} and y_{wD} in Eqs. 6-18 and 6-20 now represent the distance between Well 1 and 2 at a particular reference point. Although the left hand sides of Eq. 6-18 and 6-20 are expressed in terms of x and y while the right hand sides of the equations are expressed in terms of u, they can be easily related using Eq. 6-3.

The solution of Eqs. 6-18 and 6-20 is similar to that presented in Chapter 2. We discretize both horizontal wells into M segments and evaluate Eqs. 6-18 and 6-20 at the center of each segment i (u_{Dki}). The discretized flow equations yield $2M$ expressions in $2M+2$ unknowns, p_{wD1}, p_{wD2}, q_{hD1i}, and q_{hD2i} (i=1, M). Two additional expressions may be obtained from the condition that the sum of the fluxes along the active well must be equal to the total production rate and the sum of the fluxes along the observation well must be zero. These conditions may be expressed, respectively, as follows:

$$
\sum_{i=1}^{M} q_{hD1i} = \frac{M}{L_{D1} h_D}, \tag{6-21}
$$

and

$$
\sum_{i=1}^{M} q_{hD2i} = 0, \tag{6-22}
$$

where q_{hDki} is the flux of Well k at the center of the i^{th} segment (u_{Dki}).

The discretized forms of Eqs. 6-18 and 6-20 with Eqs. 6-21 and 6-22 provide $2M+2$ equations in $2M+2$ unknowns. This system of equations needs to be solved by an iteration process because Eqs. 6-18 and 6-20 are non-linear (D_1 and D_2 are functions of q_{hD1}, and q_{hD2}, respectively). The iteration algorithm is the same as that presented in Chapter 2.

6.3 Validation of the General Model

Although the general lines of the model development in this chapter are similar to those for the simpler model discussed in Chapter 2, because of the arbitrary azimuth angle of the wells, a double integral need to be evaluated in Eqs. 6-18 and 6-20 (note that G_{ki} given in Eq. 6-12 also requires the evaluation of an integral). Because the integrals are evaluated numerically, their accuracy is an important requirement for the convergence of the iterative solution technique used to evaluate the general model. After verifying the accuracy of the numerical integrations, we compared the results of the general model developed in this chapter with the results of the model developed in Chapter 2. For isotropic reservoirs and using the same azimuth angle for both wells (parallel orientation), the results of the two models displayed excellent agreement. In addition, similar observation was also found for anisotropic reservoirs and when both wells are rotated by 90°. For other non-zero azimuth angles in anisotropic reservoirs, the effect of the well orientations with respect to the permeability directions discussed in the next chapter were consistent with our physical expectations. These results validated the general model developed in this chapter to investigate interference between two horizontal wells with arbitrary azimuth angles.

CHAPTER 7

EFFECT OF PERMEABILITY ANISOTROPY AND WELL AZIMUTH ANGLES

In this chapter, the effect of the well azimuth angles on the interference between two horizontal wells in an anisotropic reservoir will be investigated. The model developed in Chapter 6 will be used to generate the data for the discussions. Several examples are also presented to illustrate the effect of the azimuth angles with respect to any of the two horizontal principal permeability directions. Attempt was also made to verify the validity of the correlations developed in the previous section to handle the more general cases simulated with the second model developed in Chapter 6. The applicability of the analysis procedures and the extension of the correlations developed in Chapter 5 is also discussed.

7.1 Flux Distribution

For a thorough investigation, we start with discussing the effect of azimuth angles on the flux distribution along the active and observation wells. Figure 7-1, shows a plot of the flux distribution for the base case (Case 1) presented in Table 4-1 except with both wells having an azimuth angel of 45° from the x direction. The same case was considered in Figure 4-1 for zero azimuth angles. By comparing Figure 4-1 with Figure 7-1, we make the following observations. Although there are no significant changes in the dimensionless flux distributions in the active well at both early and late times, the dimensionless flux distribution along the observation well for $\theta_1 = \theta_2 = 45°$ case (Figure 7-1) shows smaller flux variation especially at the tips of the well at late times. Figure 7-2 considers flux distribution

at late times for $\theta_1 = \theta_2 = 0$, 45 and 90° for the same case in Figure 7-1. The highest degree of change in the flux distribution along the observation well occurs at 0° and the smallest change occurs at 45°. Figure 7-3 is similar to Figure 7-2 except the distance between the two wells is relatively larger (Case 2 in Table 4-1). Observations from Figure 7-3 are the same as those from Figure 7-2.

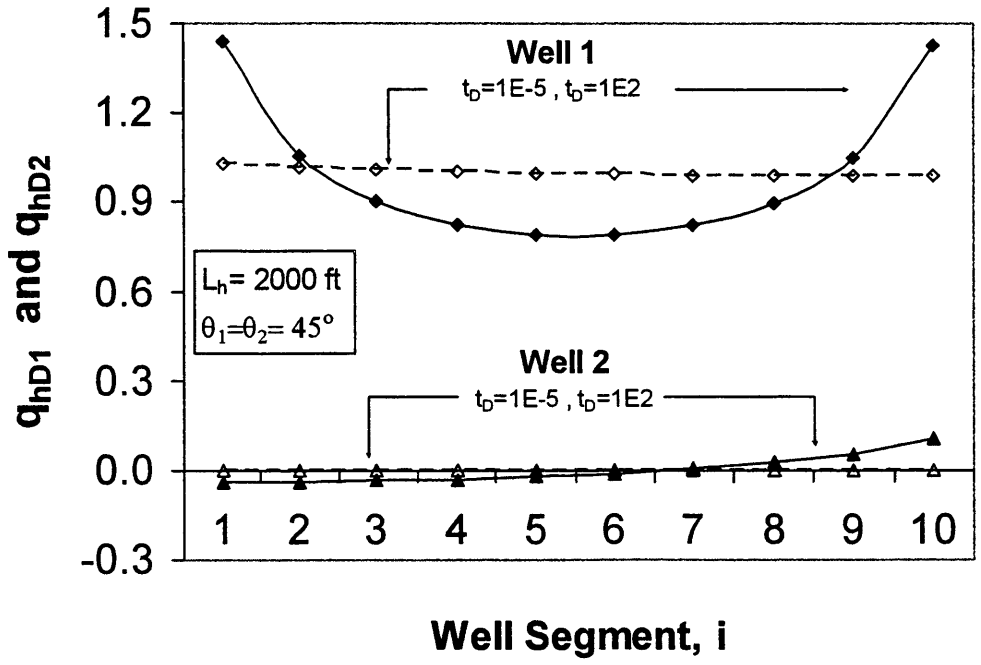

Figure 7-1. Flux distributions along the active and observation wells; Case 1, Table 4-1.

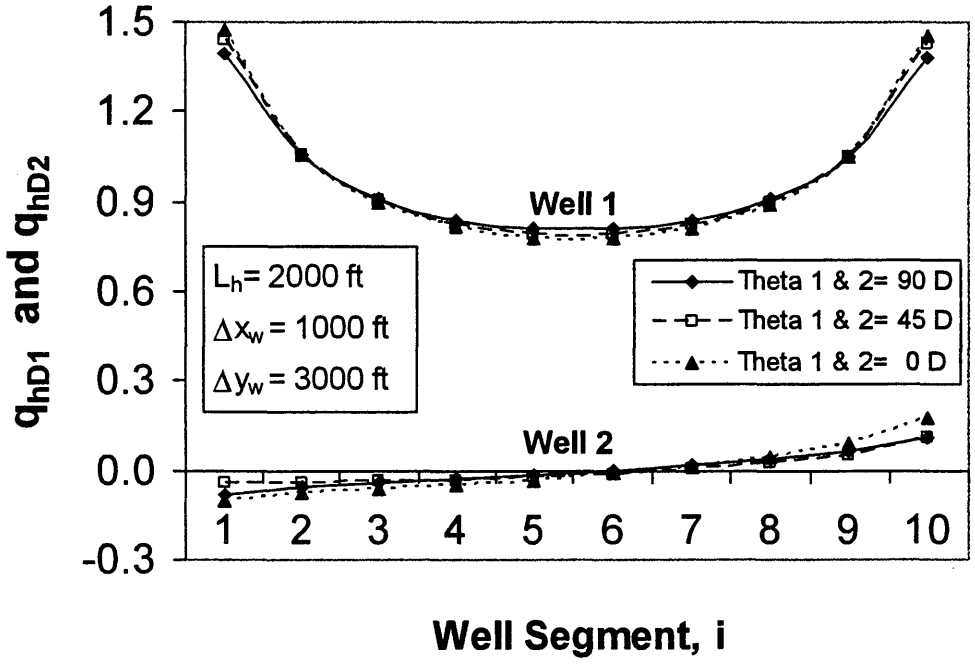

Figure 7-2. Flux distributions along the active and observation wells for three orientations; Case 1, Table 4-1, t_D=100.

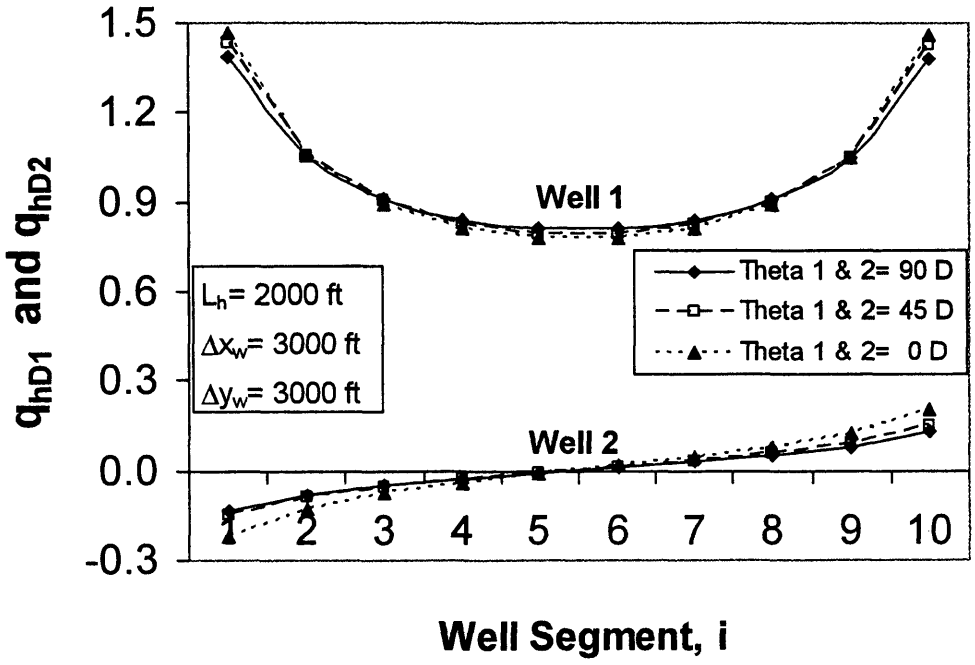

Figure 7-3. Flux distributions along the active and observation wells for three orientations; Case 2, Table 4-1, t_D=100.

Another interesting case for investigation is the base case (Case 1) presented in Table 4-1 but now the observation well is rotated at three angles; 0°, 45° and 90°, while the active well is maintained parallel to the x direction. Although it was expected that the lengths of the positive and negative flux segments along the observation well may change when the observation well is rotated while maintaining the active well at the same orientation, results in Figure 7-4 did not verify this expectations. For all cases investigated, about half of the well always shows positive flux while the other half shows negative flux (even for the case when the observation well is normal to the active well). Comparing the results in Figure 7-4 and 7-2, however, it can be concluded that the magnitudes of the influx and outflux change as the relative orientation of the observation well with respect to active well changes (the total flux is still zero)

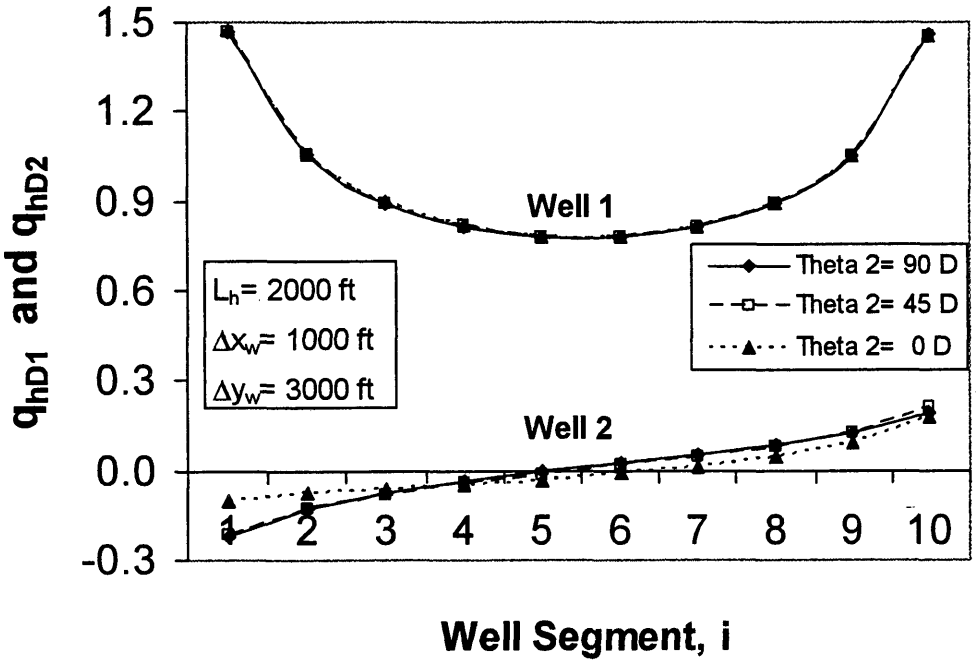

Figure 7-4. Flux distributions along the active and observation wells for three orientations of the observation well, t_D=100.

Finally, we consider a horizontal isotropic reservoir and change the azimuth angle of the horizontal observation well while the active well is aligned with the minimum permeability direction (Figure 7-5). Interesting to note is that for this particular well layout, the 90° orientation gave the highest flux variation along the observation well in spite of the fact that the permeability in the horizontal plane is isotropic. It should be emphasized, however, that the magnitude of the flux along the observation well is small and as noted in the beginning of this section, the discussion of the flux distribution along the observation well has been presented for completeness.

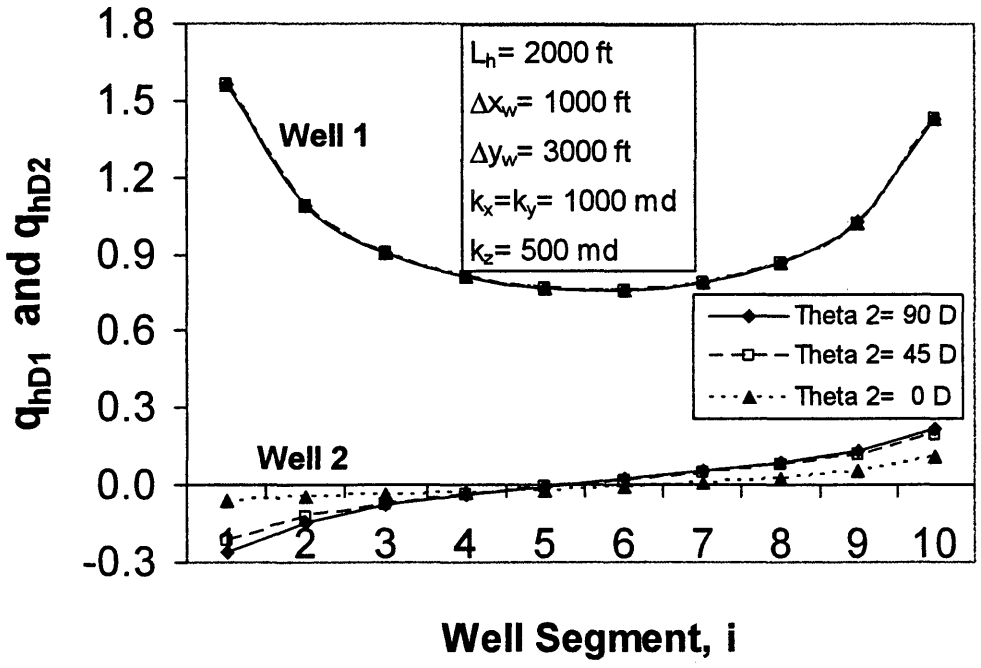

Figure 7-5. Flux distributions along the active and observation wells for three orientations of the observation well, t_D=100.

7.2 Transient Pressure Responses

In this section, the effect of well azimuth angles on transient pressure responses of the active and observation horizontal wells is investigated. Figure 7-6 shows the pressure and derivative responses for Case 1 in Table 4-1 with both wells having an azimuth angle of 45° (sample output data of this case is presented in Appendix E for those who may wish to compare their models with the one given here). Figure 7-6 shows two interesting features. First, the active well dimensionless pressure responses for θ_1 =45° shows an increase similar to that would be expected from non-uniform skin effect (Figure 4-11) or wellbore hydraulics (Figure 4-17). This observation is consistent with the results reported in the literature. [46] Second, the pressure transient response of the observation well appears not to be affected by the rotation of both wells provided that the distance between the two wells remain the same (see Figure 7-7).

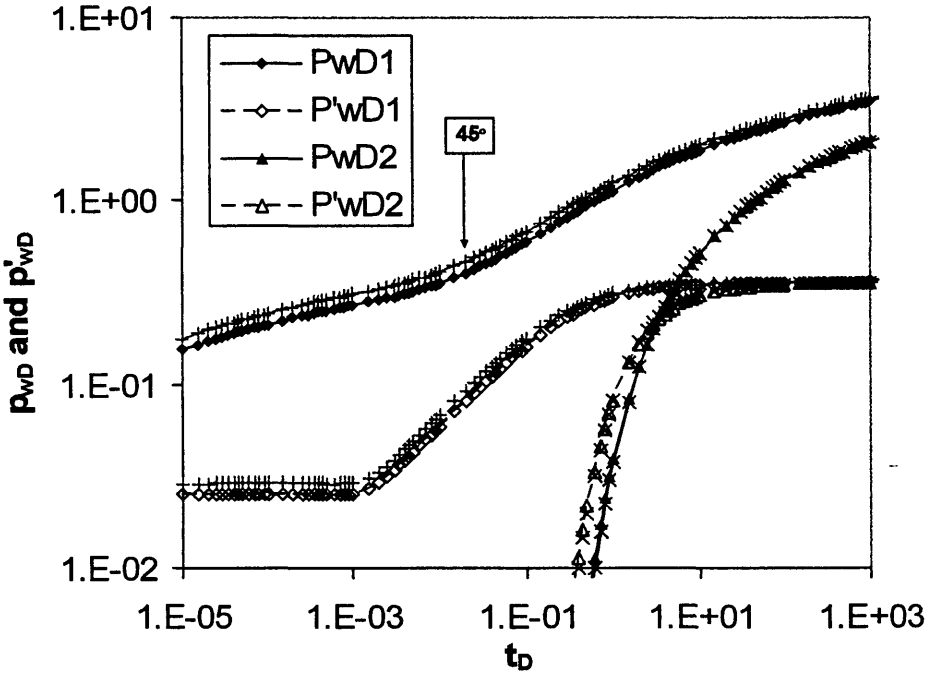

Figure 7-6. Effect of well azmuth angles on the pressure transient responses of the active and observation wells, Case 1.

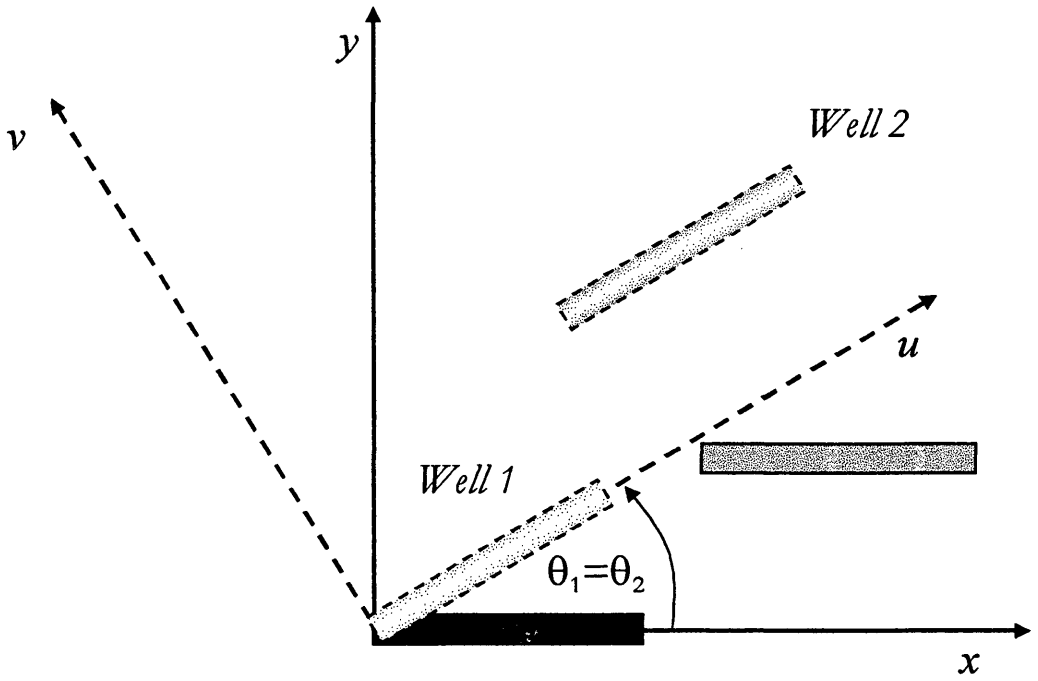

Figure 7-7. Well orientation when rotating both wells at the same angle.

Figures 7-8 and 7-9 consider the same cases as in Figure 7-6 (Case 1 of Table 4-1) for the pressure and derivative responses of the active and observation wells, respectively, with three different azimuth angles; $\theta_1 = \theta_2 = 0$, 45 and 90° (wells are still parallel to each other). It can be seen from these figures that increasing the azimuth angle of the wells from 0 to 90° (that is, changing the alignment of the wells from the minimum to maximum permeability direction) causes higher pressure drop in the active well while the observation well responses remain practically unaffected. Similarly, this observation is also supported by the observation well responses for Case 2 in Table 4-1 shown in Figure 7-10. As expected, the fact that the

observation well responses are not affected by the azimuth angle of the wells as long as the wells are parallel to each other is valid if the distance between the two wells is reasonably large. For smaller distances between the wells than those in Figures 7-9 and 7-10, the early time responses of the observation well may display more dependence on θ. For larger distances, on the other hand, the dependency on θ would completely disappear as shown in Figure 7-11 for Case 2 of Table 4-1 where the distance between the wells is increased to 10,000 ft.

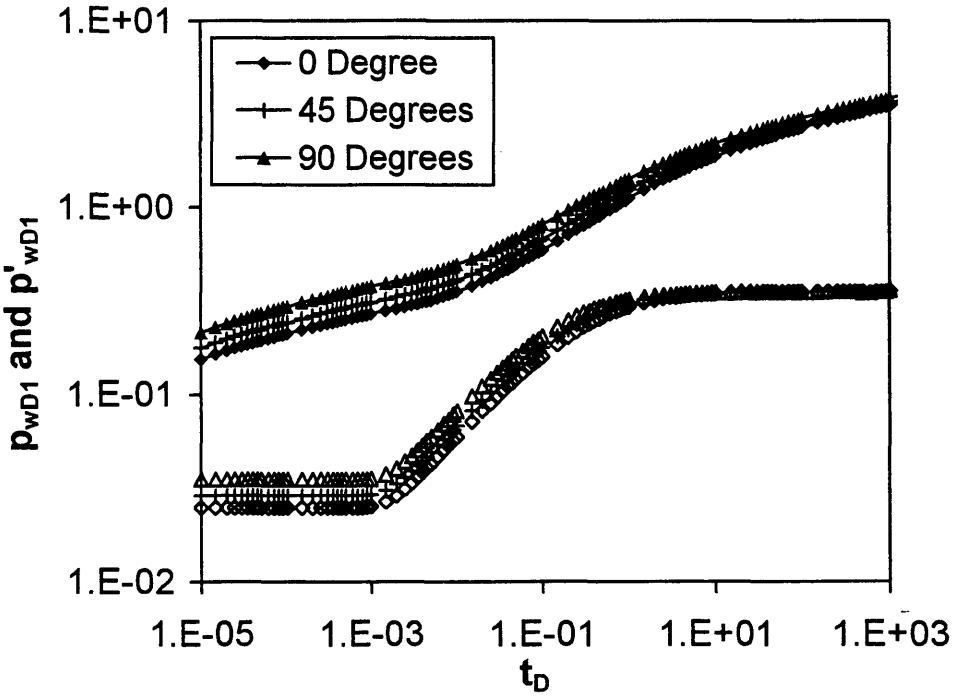

Figure 7-8. Effect of well azmuth angles on the pressure transient responses of the active well; Case 1, Table 4-1.

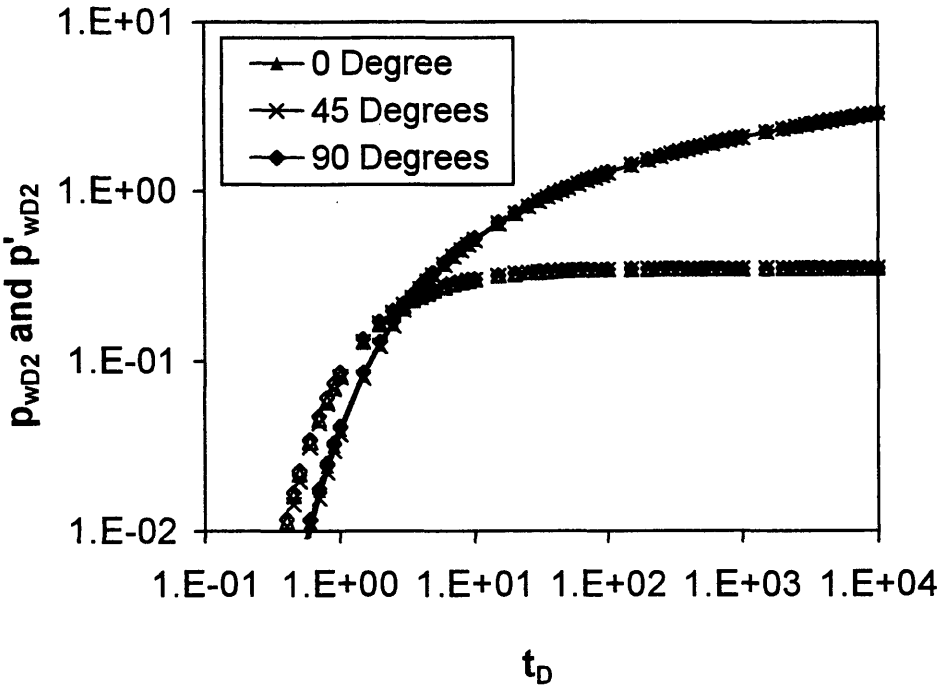

Figure 7-9. Effect of well azmuth angles on the pressure transient responses of the observation well; Case 1, Table 4-1.

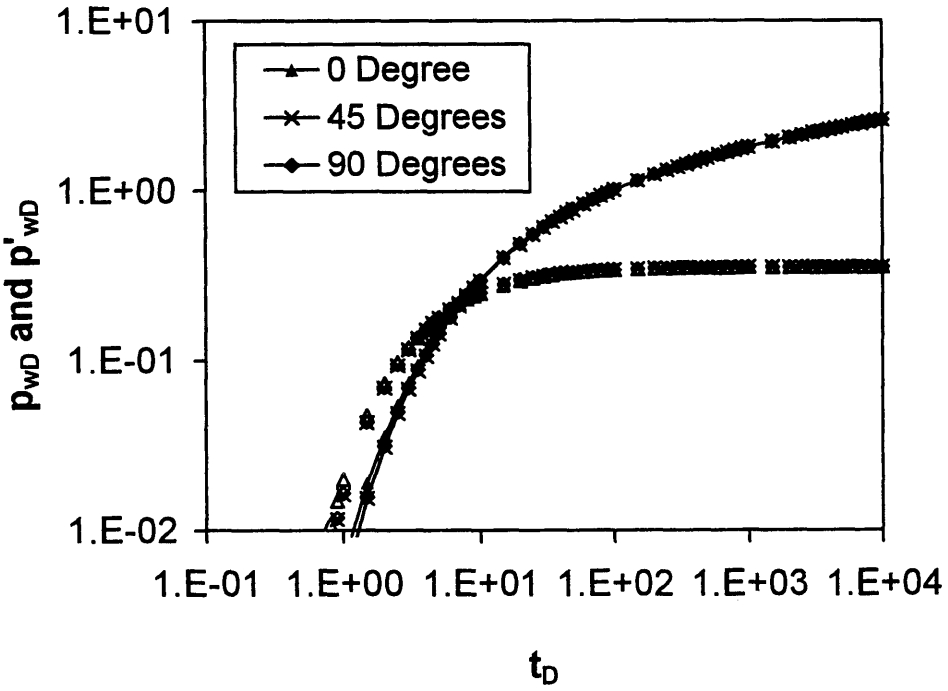

Figure 7-10. Effect of well azmuth angles on the pressure transient responses of the observation well; Case 2, Table 4-1.

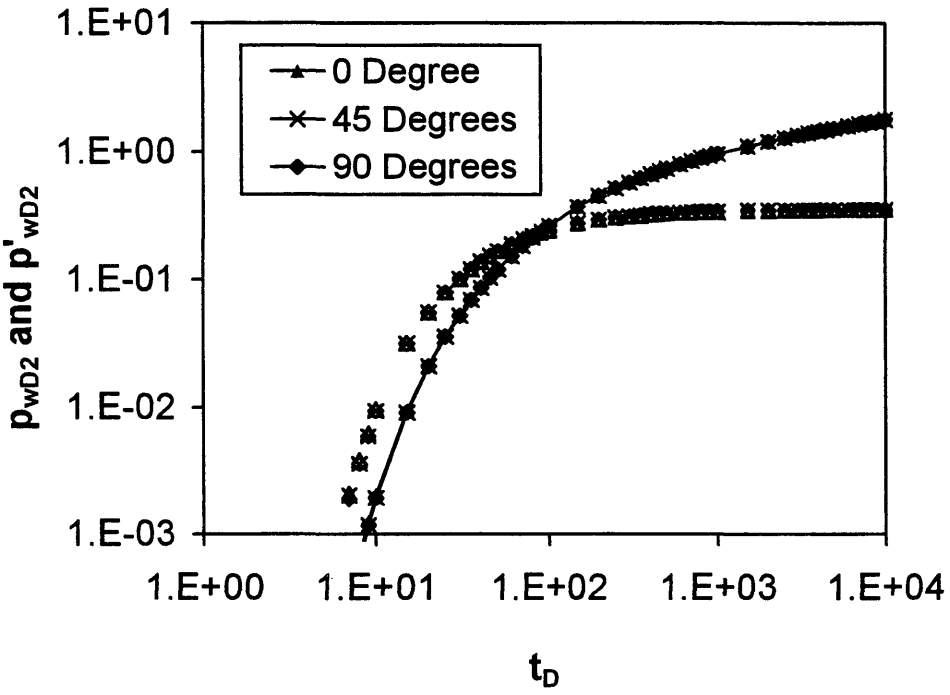

Figure 7-11. Effect of well azimuth angles on the pressure transient responses of the observation well; ; Case 2, Table 4-1 ($\Delta x = \Delta y = 10{,}000$ ft).

The above observations are important in that they imply the applicability of the optimum equivalent observation point (Figure 5-10) and the exponential-integral (5-14) approximation techniques to the case where the wells are not aligned with one of the principal permeabilities but still parallel to each other. The only requirement in this case is that the distance between the two wells is calculated in the *u-v* coordinates shown in Figure 7-7.

It is desirable to extend the approximate analysis techniques developed in Chapter 5 to the cases where the azimuth angles of the wells are completely arbitrary. Because of the large number of parameters and the complex interaction among them, it has not been possible to

obtain a more general approximation in this research. Below, some results are presented to discuss, in general, the effect of completely arbitrary azimuth angles.

Figure 7-12 considers a horizontal isotropic reservoir where the active well is aligned with one of the horizontal permeability directions while the observation well may have three different azimuth angles; θ_2 = 0, 45 and 90° (this is the same cases as in Figure 7-5). In this particular case, the responses of the observation well are delayed as the azimuth angle increases. This result, however, is strictly valid when the active well is always aligned with the minimum permeability direction.

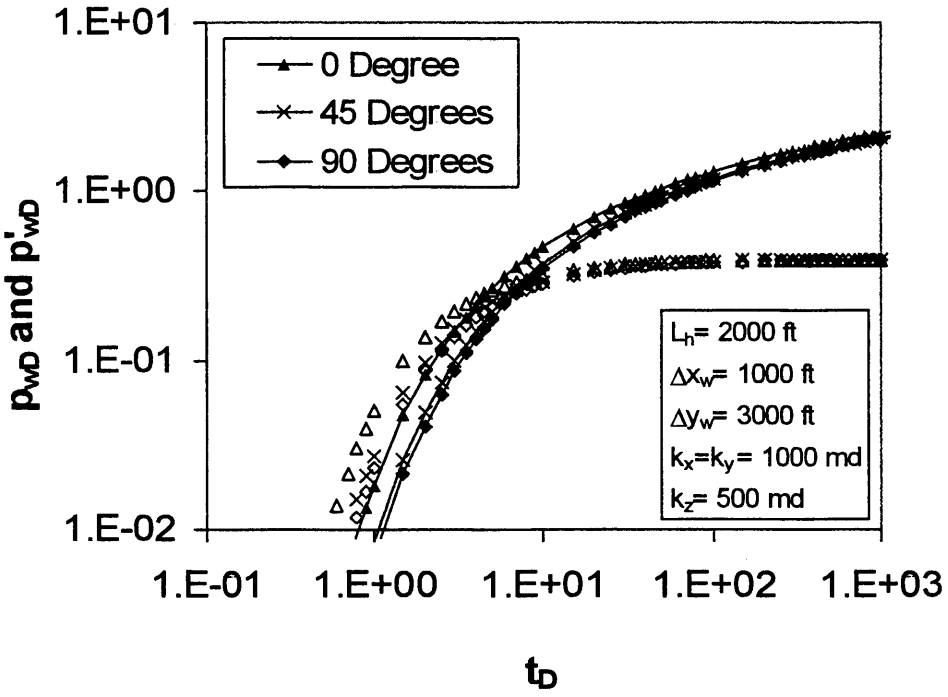

Figure 7-12. Effect of observation well azimuth angle on the pressure transient responses.

In general, a deviation in the alignment of the active well from the minimum permeability direction causes an increase in the pressure drop of the active well. The pressure responses of the horizontal observation well, however, depend on the active and observation well azimuth angles, horizontal permeability anisotropy, and the relative location of the wells. For the active horizontal well, Refs. 23 and 24 indicate that the transient pressure solution for a horizontal well at an arbitrary orientation in an anisotropic reservoir can be obtained from the solution for isotropic reservoirs by simple coordinate transformations. However, for the observation well, this method is not applicable because the well is strongly influenced by its orientation as well as by the active well orientation. Because of this reason, the approximate analysis procedures developed in Chapter 5 may not be generalized for the cases where the azimuth angles the wells have are not the same.

Before concluding this chapter, another interesting result to report is Case 3 of Table 4-1. Here, we consider vertically stacked laterals and investigate the effect of changing the azimuth angle of the observation well only. Figure 7-13 shows pressure and derivative responses of the observation well for three azimuth angles: 0°, 3° and 10°. The results indicate that a small deviation of even 3° from the minimum permeability direction (and also from the direction of the active well) is sufficient to cause significant change in the pressure and derivative responses at early times.

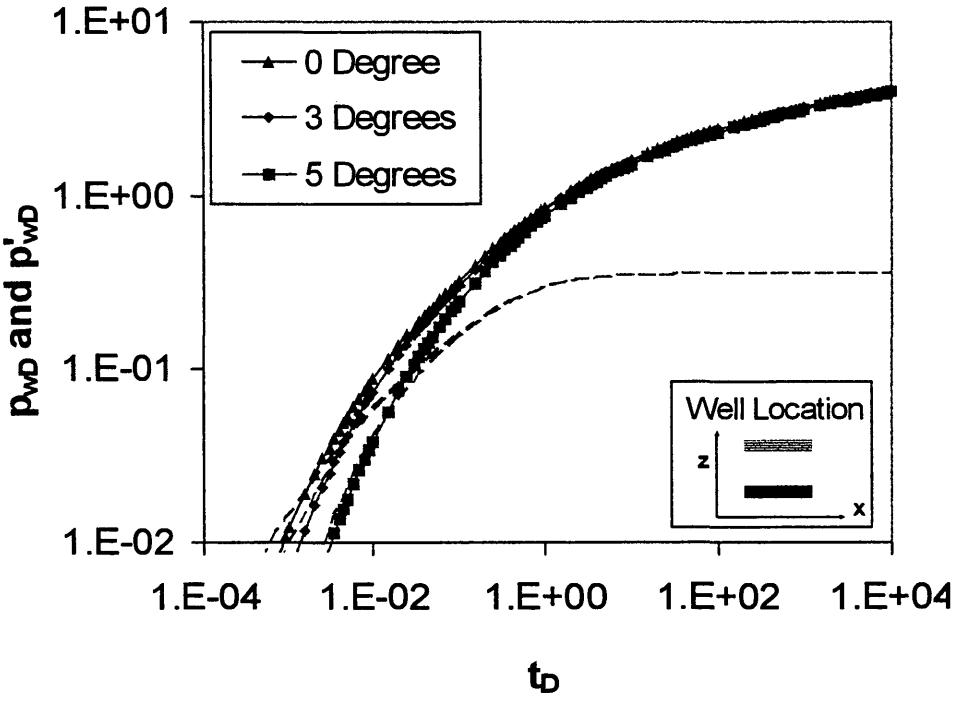

Figure 7-13. Effect of well azmuth angles on the pressure transient responses of the observation well, Case 3, Table 4-1.

CHAPTER 8

CONCLUSIONS

The objective of this dissertation was to investigate interference between two horizontal wells and develop methods to analyze interference tests conducted in horizontal observation wells. To achieve this objective, two semi-analytical models have been developed. The models incorporate the effects of anisotropy, finite wellbore conductivity, arbitrary azimuth angles for the wells, and variable skin distribution along the wells. Wellbore storage effects have been assumed to be negligible in both wells.

The results presented here not only improve our understanding of horizontal observation well responses but also provide data to calibrate numerical models. The analysis of horizontal observation well responses has been discussed and rigorous and approximate analysis procedures have been presented. The application examples presented should help the analysts use the techniques proposed in this work.

Although some of the procedures presented in this dissertation have been discussed in the literature, they were misinterpreted and misapplied. In addition, no rigorous justification has been provided for the approximate analysis techniques. This work has provided the basis for the simplified analysis methods, delineated their limitations and ranges of application, and established the procedures and correlations for their appropriate applications.

The following are the specific conclusions of this work:

1. Active well responses are basically unaffected by the presence of an observation well even when the two wells are relatively close to each other.

2. Aligning the active horizontal well at an angle with respect to the minimum horizontal permeability direction increases the pressure drop and causes a distortion in the characteristics of the early and intermediate time flow regimes. This distortion is similar to the effects of non-uniform skin and wellbore hydraulics.

3. The pressure transient responses of horizontal observation wells are not significantly influenced when both active and observation horizontal wells are rotated by the same azimuth angle if the wells are parallel. If the azimuth angle of the observation well is changed while keeping the azimuth angle of the active well constant, the pressure responses of the observation well may be significantly affected.

4. For most practical cases, the observation well responses display radial or pseudoradial flow characteristics. However, in cases where the distance between the two wells is relatively short, as in the case of vertically stacked laterals, the observation well responses may also display a linear flow regime if the two wells are parallel. A small deviation from the parallel alignment of the wells destroys the linear flow regime and causes considerable change in the observation well responses.

5. In the absence of wellbore storage, skin distribution on the active and/or observation well has insignificant effect on the observation well pressure responses, but may influence the flux distribution along the well. On the other hand, non-uniform skin distribution in the active well could influence its early time flow characteristics.

6. Effect of wellbore hydraulics may be significant on the active well responses but it is negligible for all practical purposes of evaluating the observation well responses.

7. If the distance between the active and interference horizontal wells is reasonably large and the wells are parallel, then the geometry of the observation well may be ignored and treated as a point. In this case, the choice of the observation point along the original horizontal observation well strongly affects the accuracy of the analysis. Therefore, the use of the heel or the center of the horizontal observation well as an observation point as suggested in some earlier works is not justified. This work provides a correlation to calculate the optimum location of the observation point.

8. When the location of the optimum observation point is known, then the conventional single-horizontal well models may be used to approximate the interference horizontal well responses. Because of the considerable simplicity of the single-horizontal well models, this approach provides great convenience for implementation with the regression algorithms used in commercial well-test analysis software.

9. If the distance between the two wells is large enough, then the geometry of both wells may be ignored and the exponential integral solution may be used to analyze horizontal-well interference test responses. In this case, the effective radial distance between the two wells is defined based on the distance between the optimum observation point and the center of the active well and is influenced by the directional permeabilities. The formula to calculate the effective radial distance between the wells presented in this study is useful to apply the exponential integral approximation correctly.

10. Unlike the claim in the literature[19], the applicability of the exponential integral solution is not only a function of the radial distance between the two wells, but also a function of their relative orientations. The error limits for the exponential integral approximation may be determined from the correlation provided in this study.

11. Unless the two horizontal wells are extremely close in the horizontal and vertical directions, interference tests between two horizontal wells do not provide information about the vertical permeability. The estimation of the horizontal directional permeabilities, however, should be possible even when the distance between the two wells is large.

Although a detailed evaluation of interference tests between horizontal wells have been provided in this work, the following items are proposed for future research:

1. Incorporate wellbore storage into the analytical models and investigate the combined effects of wellbore storage and skin on horizontal observation well responses.

2. Develop more general correlations for the optimum observation point to be used with the single-horizontal well solutions and exponential integral approximation when the horizontal wells are not parallel.

NOMENCLATURE

p_D	:	dimensionless pressure
t_D	:	dimensionless time
q_D	:	dimensionless rate
u_D	:	dimensionless distance along the horizontal well
x_D	:	dimensionless distance in the x direction
y_D	:	dimensionless distance in the y direction
z_D	:	dimensionless distance in the z direction
h_D	:	dimensionless formation thickness
L_D	:	dimensionless horizontal well length
r_{wD}	:	dimensionless wellbore radius
C_{hD}	:	dimensionless horizontal well conductivity
c_t	:	total compressibility, psi-1
L_h	:	horizontal well length, ft
ℓ	:	horizontal well half length, ft
h	:	formation thickness, ft
k	:	permeability, md
p	:	pressure, psi
q	:	production rate, stb/d
B	:	formation volume factor, RB/stb
N_{Re}	:	Reynolds number
f	:	fanning friction factor

ε_D	:	dimensionless roughness factor
r	:	wellbore radius, ft
r_{we}	:	equivalent wellbore radius, ft
t	:	time, hr
S		skin factor

Greek symbols

ϕ	:	porosity
μ	:	viscosity, cp
ε	:	roughness factor, ft
ρ	:	fluid density, lb/ft^3
θ		angle, °

Subscripts and superscripts

D	:	dimensionless
i	:	initial
x	:	x direction
y	:	y direction
z	:	z direction
r	:	radial
h	:	horizontal
w	:	wellbore

REFERENCES

1. Clonts, M. D. and Ramey, H. J. Jr.: "Pressure Transient Analysis for Wells With Horizontal Drainholes," Paper SPE 15116 presented at the 1986 SPE California Regional Meeting, Oakland, CA, April 2-4, 1986.
2. Ozkan, E., Raghavan, R.., and Joshi, S. D.: "Horizontal Well Pressure Analysis," SPE Formation Evaluation, Dec. 1989, 567-575.
3. Ozkan, E.: "Analysis of Horizontal Well Responses: Contemporary vs. Conventional," paper SPE 52199 presented at the 1999 SPE Mid-Continent Operations Symposium, Oklahoma City, OK, March 28-31, 1999.
4. Umnuayponwiwat, S., Ozkan, E., and Raghavan, R.: "Pressure Transient Behavior and Inflow Performance of Multiple Wells in Closed Systems," paper SPE 62988 presented at the 2000 SPE Annual Technical Conference and Exhibition, Dallas, TX, Oct. 1-4, 2000.
5. Daviau, F., Mouronval, G., Bourdarot, G., and Curutchet, P.: "Pressure Analysis for Horizontal Wells," paper SPE 14251 presented at the 1985 SPE Annual Technical Conference and Exhibition, Las Vegas, Sept 22-25.
6. Goode, P. A. and Thambynayagam, R. K. M.: "Pressure Drawdown and Buildup Analysis of Horizontal Wells in Anisotropic Media," SPEFE (Dec. 1987) 683.
7. Carvalho, R. S. and Rosa, A. J.: "Transient Pressure Behavior for Horizontal Wells in Naturally Fractured Reservoirs," paper SPE 18302 presented at the 1988 SPE Annual Technical Conference and Exhibition, Houston, TX, Oct. 2-5, 1988.
8. Carvalho, R. S. and Rosa, A. J.: "A Mathematical Model for Pressure Evaluation in an Infinite-Conductivity Horizontal Well," SPEFE (Dec. 1989) 567.

9. Odeh, A. S. and Babu, D. K.: "Transient Flow behavior of Horizontal Wells: Pressure Drawdown and Buildup Analysis," SPEFE (March 1990) 7.
10. Ozkan, E. and Raghavan, R.: "Performance of Horizontal Wells Subject to Bottomwater Drive," SPERE (August 1990) 375.
11. Kuchuk, F. J., Goode, P. A., Brice, B. W., Sherard, D. W., and Thambynayagam, R. K. M.: "Pressure-Transient Analysis for Horizontal Wells," JPT (Aug. 1990) 974.
12. Kuchuk, F. J., Goode, P. A., Wilkinson, D. J., and Thambynayagam, R. K. M.: "Pressure-Transient Behavior of Horizontal Wells With and Without Gas Cap or Aquifer," SPEFE (March 1991) 86.
13. Aguilera, R. and Ng, M. C.: "Transient Pressure Analysis of Horizontal Wells in Anisotropic Naturally Fractured Reservoirs," SPEFE (March 1991) 95.
14. Joshi, S. D.: Horizontal Well Technology, Penn Well Publishing Company, Tulsa, Oklahoma, 1991.
15. Du, K. and Stewart, G.: "Transient Pressure Response of Horizontal Wells in Layered and Naturally Fractured reservoirs with Dual-Porosity Behavior," paper SPE 24682 presented at the 1992 SPE Annual Technical Conference and Exhibition, Washington, DC, Oct. 4-7, 1992.
16. Kuchuk, F. J.: "Well Testing and Interpretation for Horizontal Wells," JPT (Jan. 1995) 36. SPE 52199
17. Kuchuk, F. J. and Habashy, T.: "Pressure Behavior of Horizontal Wells in Multilayer Reservoirs with Crossflow," SPEFE (March 1996) 55.
18. Malekzadeh, D. and Tiab, D.: "Interference Testing of Horizontal Wells," paper SPE 22733 presented at the 66th Annual Technical Conference and Exhibition of SPE, Dallas, TX, October 6-9, 1991.
19. Malekzadeh, D.: "Deviation of Horizontal Well Interference Testing From the Exponential Integral Solution," paper SPE 24372 presented at the SPE Rocky Mountain Regional Meeting, Casper, Wyoming, May 18-21, 1992.

20. Besson, J.: "Performance of Slanted and Horizontal Wells on an Anisotropic medium," paper SPE 20965 presented at the SPE Europec 90, The Hague, Netherlands, October 22-24, 1990.
21. Economides, M. J., Brand, C. W. and Frick, T. P.: "Well Configurations in Anisotropic Reservoirs," SPE Formation Evaluation, December 1996.
22. Zhang, L. and Dusseault, M. B.: "Anisotropic Permeability Estimation by Horizontal Well Tests," paper SPE 37071 presented at the SPE International Conference on Horizontal Well Technology, Calgary, Canada, November 18-20, 1996.
23. Yildiz, T. and Ozkan, E.: "Influence of Areal Anisotropy on Horizontal Well performance," paper SPE 38671 at the SPE Annual Technical Conference and Exhibition, San Antonio, Texas, October 5-8, 1997.
24. Spivey, J. P. and Lee, W. J.: "Estimating the Pressure-Transient Response for a Horizontal or a Hydraulically Fractured Well at an Arbitrary Orientation in an Anisotropic Reservoir," SPE Reservoir Evaluation and Engineering, Vol. 2, No. 5, October 1999.
25. Cline, S. B. and Tiab, D.: "Studies in Vertical and Horizontal Well-Flow Behavior in Cases of Permeability Anisotropy," paper SPE 71085 presented at the SPE Rocky Mountain Petroleum Technology Conference, Keystone, Colorado, May 21-23, 2001.
26. Ramey, H. J., Jr.: "Interference Analysis for Anisotropic Formations- A Case History," J. Pet. Tech., (Oct. 1975) 1290-1298; Trans., AIME, 259.
27. Bandiziol, D. and Massonnat, G.: "Horizontal Permeability Anisotropy Characterization by pressure Transient testing and Geological Data," paper SPE 24667 presented at the SPE 67th Annual Technical Conference and Exhibition, Washington, DC, October 4-7, 1992.
28. Chen, H., Hidayati, D. T. and Lawrence, W.: "A Quick Method to Diagnose Flow Anisotropy Using pressure Interference Data," paper SPE 60290 presented at the SPE Rocky Mountain Regional/Low Permeability Reservoirs Symposium and Exhibition, Denver, Colorado, March 12-15, 2000.

29. Mukherjee, H. and Economides, M. J.: "A Parametric Comparison of Horizontal and Vertical Well Performance," SPE Formation Evaluation, June 1991.
30. Retnanto, A. and Economides, M. J.: "Performance of Multiple Horizontal Well Laterals in Low-to Medium–Permeability Reservoirs," SPE Reservoir Engineering, May 1996.
31. Retnanto, A., Frick, T. P., Brand, C. W. and Economides, M. J.: "Optimal Configuration of Multiple-Lateral Horizontal Wells," paper SPE 35712 presented at the Western Regional Meeting, Anchorage, U.S.A., May 22-24, 1996.
32. Retnanto, A. and Economides, M. J.: "Inflow Performance Relationships of horizontal and Multibranched Wells in a Solution-Gas-Drive Reservoir," paper SPE 50659 presented at the SPE European Petroleum Conference, The Hague, The Netherlands, , October 20-22, 1998.
33. Alkhonifer, J. and Ershaghi, I.: "Detection of Channel Sands and Vertical Shale Continuity Using a New Approach in Interference Analysis of Parallel Horizontal Wells," paper SPE 53928 presented at Latin America and Caribbean Petroleum Engineering Conference, Caracas, Venezuela, April 21-23, 1999.
34. Hatzignatiou, D. G.: "Reservoir Engineering Aspects of Horizontal Wells in Stochastic Naturally Fractured Gas Reservoirs," paper SPE 54626 presented at the Western Regional Meeting, Anchorage, Alaska, May 26-28, 1999.
35. Al-Khamis, M. N., Ozkan, E. and Raghavan, R.: "Interference Testing with Horizontal Observation Wells," paper SPE 71581 presented at the 2001 SPE Annual Technical Conference and Exhibition, New Orleans, Louisiana, 30 Septemebr-3 October, 2001.
36. Erwin, M. D., Sanders, L. A. and Redman, R. S.: "Multiwell Interference Test in the Colville River Field, Alaska," paper SPE 77453 at the SPE Annual Technical Conference and Exhibition, San Antonio, Texas, 29 Septemebr-2 October, 2002.
37. Dikken, B. J.: "Pressure Drop in Horizontal Wells and its Effect on Production Performance," JPT (November 1990) 1426.

38. Ozkan, E., Sarica, C, Haciislamoglu, M., and Raghavan, R.: "Effect of Conductivity on Horizontal-Well Pressure-Behavior," SPE Advanced Technology Series, Vol 3, No. 1, p.85-94, 1995.
39. Ozkan, E., Sarica, C, Haciislamoglu, M., and Raghavan, R.: "Supplement to SPE 24683 Effect of Conductivity on Horizontal-Well Pressure-Behavior," paper SPE 30230, 1995.
40. Ding, Y.: "Transient Pressure Solution in the Presence of Pressure Drop in the Wellbore," paper SPE 56614 presented at the 1999 SPE Annual Technical Conference and Exhibition, Houston, Texas, October 3-6, 1999.
41. Ozkan, E., Sarica, C., and Haciislamoglu, M.: "The Influence of Pressure Drop Along the Wellbore on Horizontal Well Productivity," SPEJ (Sept. 1999) 180.
42. Penmatcha, V. R., Arbabi, S. and Aziz, K.: "Effects of Pressure Drop in Horizontal Wells and optimum Well Length," SPE Journal, Vol. 4, No.3 September 1999.
43. Saavedra, N. F. and Reyes, D. A.: "Drainage Area for Horizontal Wells With Pressure Drop in the Horizontal Section," paper SPE 69431 presented at Latin America and Caribbean Petroleum Engineering Conference, Buenos Aires, Argentina, March 25-28, 2001.
44. Horn, R. N.: Modern Well Test Analysis, A Computer-Aided Approach, California, Petroway, Inc., Second edition (1995), 107-114.
45. Peaceman, D.: "Interpretation of Well-Block Pressures in Numerical Reservoir Simulation with Nonsquare Grid Blocks and Anisotropic Permeability," SPEJ (June 1983) 531.
46. Gringarten, A. C. and Ramey, H. J. Jr.: "The Use of Source and green's Functions in Solving Unsteady-Flow problems in Reservoirs," SPEJ (Oct. 1973) 285-96; Trans., AIME, 255.
47. Ozkan, E. and Raghavan, R.: "Estimation of Formation Damage in Horizontal Wells," paper SPE 37511 presented at the Production Operations Symposium, Oklahoma City, OK, March 9-11, 1997.

48. Brill, J. P. and Mukherjee, H.: Multiphase Flow In Wells, Monograph Vol. 17, SPE, Richardson, Texas (1999), 6-7.
49. Blasius, H.: Z. Math. Phys. (1908) 56,1.
50. Calvin, K. and Gary, F.: "New Fullbore Production Logging Sensor Improves the Evaluation of Production in Deviated and Horizontal Wells," paper SPE 29815 presented in the Middle East Oil Technical Conference and Exhibition, Manama, Bahrain, March 11-14, 1995.
51. Gardner, D., Fallet, T. and Nyhavn, F.: "Production Logging Tool Developments for Horizontal Wells and Hostile Environments," paper SPE 36564 presented at the SPE Annual Technical Conference and Exhibition, Denver, Colorado, October 6-9, 1996.
52. Carnegei, A., Roberts, N. and Clyne, I.: "Application of New Generation Technology to Horizontal Well Production Logging-Examples from the North West Shelf of Australia," paper SPE 50178 presented at the SPE Asia Pacific Oil and Gas Conference and Exhibition, Perth, Australia, October 12-14, 1998.
53. Carnegei, A.: "Advanced Horizontal Well Production Logging-An Australian Offshore Example," paper SPE 54326 presented at the SPE Asia Pacific Oil and Gas Conference and Exhibition, Jakarta, Indonesia, April 20-22, 1999.
54. Rosa, A. J. and Carvalho, R. D.: "A Mathematical Model for pressure Evaluation in an Infinite-Conductivity Horizontal Well," SPE Formation Evaluation, December 1989.
55. Yildiz, T. and Ozkan, E.: "A Simple Correlation to Predict Wellbore Pressure Drop Effects on Horizontal Well Productivity," paper SPE 48938 at the SPE Annual Technical Conference and Exhibition, New Orleans, Louisiana, September 27-30, 1998.
56. Jargon, J. R.: "Effect of Wellbore Storage and Wellbore Damage at the Active Well on Interference Test Analysis," Jour. Of Pet. Tech. (Aug. 1976) 851-858.
57. Tongpenyai, Y. and Raghavan, R.: "The Effect of Wellbore Storage and Skin on Interference Test Data," Jour. Of Pet. Tech. (Jan. 1981) 151-160.
58. Lee, J.: Well Testing, Textbook series Vol. 1, SPE, Dallas (1982), 3.

59. Earlougher, R. C. Jr.: Advances in Well Test Analysis, Monograph Vol. 5, Henry L. Doherty Series, SPE, Dallas (1977), 106-111.

60. Matthews, C. S. and Russell, D. G.: Pressure Buildup and Flow Tests in Wells, Monograph Vol. 1, SPE, Dallas (1967), 11.

APPENDICES

Appendix A:

Using the definition of dimensionless distance Eq. 2-4

$$\frac{\partial f}{\partial x_D} = \frac{\partial f}{\partial\left(\frac{x}{l}\sqrt{\frac{k}{k_x}}\right)} = \frac{1}{\left(\frac{1}{l}\sqrt{\frac{k}{k_x}}\right)}\frac{\partial f}{\partial x} \tag{A-1}$$

Using the property of product of derivatives

$$\frac{\partial f}{\partial x} = \frac{\partial f}{\partial N_{\mathrm{Re}}}\frac{\partial N_{\mathrm{Re}}}{\partial x} \tag{A-2}$$

The second term in Eq. A-2

$$\frac{\partial N_{\mathrm{Re}}}{\partial x} = 6.157\times10^{-2}\frac{\rho}{\mu r_w}\frac{\partial q_{hc}(x)}{\partial x} = -6.157\times10^{-2}\frac{\rho}{\mu r_w}q_h \tag{A-3}$$

where q_h is the flux, rate per unit length which has a negative slop (flux is decreasing from in the direction from heel of the well to the toe). Substituting Eq. A-3 in A-2 gives:

$$\frac{\partial f}{\partial x} = -6.157\times10^{-2}\frac{\rho}{\mu r_w}q_h\frac{\partial f}{\partial N_{\mathrm{Re}}}. \tag{A-4}$$

Combining Eq. A-1 and A-4 gives:

$$\frac{\partial f}{\partial x_D} = \frac{-6.157\times10^{-2}}{\left(\frac{1}{l}\sqrt{\frac{k}{k_x}}\right)}\frac{\rho}{\mu r_w}q_h\frac{\partial f}{\partial N_{\mathrm{Re}}}. \tag{A-5}$$

Therefore,

$$\frac{N_{\mathrm{Re}1}}{N_{\mathrm{Re}t1}f_1}\left(\frac{df_1}{dx_D}\right)-q_{hD1}=\frac{q_{hc1}}{q_{t1}f_1}\left(\frac{-6.157\times10^{-2}}{\left(\frac{1}{l}\sqrt{\frac{k}{k_x}}\right)}\frac{\rho}{\mu r_w}q_{h1}\frac{\partial f}{\partial N_{\mathrm{Re}1}}\right)-q_{hD1}$$

$$=\frac{q_{hc1}}{q_{t1}f_1\left(\frac{1}{l}\sqrt{\frac{k}{k_x}}\right)}\frac{-6.157\times10^{-2}\rho}{\mu r_w}\left(q_{h1}\frac{\partial f}{\partial N_{\mathrm{Re}1}}\right)-q_{hD1}$$

$$=\frac{-N_{\mathrm{Re}1}}{q_{t1}f_1\left(\frac{1}{l}\sqrt{\frac{k}{k_x}}\right)}\left(q_{h1}\frac{\partial f}{\partial N_{\mathrm{Re}1}}\right)-q_{hD1}=\frac{-N_{\mathrm{Re}1}}{2f_1}\left(\frac{2q_{h1}l}{q_{t1}}\sqrt{\frac{k_x}{k}}\frac{\partial f}{\partial N_{\mathrm{Re}1}}\right)-q_{hD1}$$

$$=\frac{-N_{\mathrm{Re}1}}{2f_1}\left(q_{hD1}\frac{\partial f}{\partial N_{\mathrm{Re}1}}\right)-q_{hD1}=-\frac{1}{2}\left(\frac{N_{\mathrm{Re}1}}{f_1}\frac{df}{dN_{\mathrm{Re}1}}+2\right)q_{hD1} \qquad \text{(A-6)}$$

Appendix B:

t_D	p_{wD1}	p'_{wD1}	p_{wD2}	p'_{wD2}
1.00E-05	0.1545	0.0250		
1.50E-05	0.1646	0.0250		
2.00E-05	0.1718	0.0250		
2.50E-05	0.1774	0.0250		
3.00E-05	0.1819	0.0250		
3.50E-05	0.1858	0.0250		
4.00E-05	0.1891	0.0250		
4.50E-05	0.1921	0.0250		
5.00E-05	0.1947	0.0250		
6.00E-05	0.1993	0.0250		
7.00E-05	0.2031	0.0250		
8.00E-05	0.2064	0.0250		
9.00E-05	0.2094	0.0250		
1.00E-04	0.2120	0.0250		
1.50E-04	0.2222	0.0250		
2.00E-04	0.2294	0.0250		
2.50E-04	0.2349	0.0250		
3.00E-04	0.2395	0.0250		
3.50E-04	0.2433	0.0250		
4.00E-04	0.2467	0.0250		
4.50E-04	0.2496	0.0250		
5.00E-04	0.2523	0.0250		
6.00E-04	0.2568	0.0250		
7.00E-04	0.2607	0.0250		
8.00E-04	0.2640	0.0251		
9.00E-04	0.2670	0.0252		
1.00E-03	0.2696	0.0253		
1.50E-03	0.2801	0.0269		
2.00E-03	0.2880	0.0289		
2.50E-03	0.2947	0.0314		
3.00E-03	0.3007	0.0339		
3.50E-03	0.3061	0.0363		
4.00E-03	0.3110	0.0386		
4.50E-03	0.3157	0.0408		

5.00E-03	0.3201	0.0429		
6.00E-03	0.3283	0.0468		
7.00E-03	0.3358	0.0503		
8.00E-03	0.3427	0.0535		
9.00E-03	0.3492	0.0565		
1.00E-02	0.3553	0.0594		
1.50E-02	0.3817	0.0718		
2.00E-02	0.4037	0.0816		
2.50E-02	0.4228	0.0901		
3.00E-02	0.4399	0.0975		
3.50E-02	0.4554	0.1043		
4.00E-02	0.4697	0.1104		
4.50E-02	0.4831	0.1160		
5.00E-02	0.4956	0.1212		
6.00E-02	0.5185	0.1306		
7.00E-02	0.5393	0.1389		
8.00E-02	0.5583	0.1464		
9.00E-02	0.5759	0.1532		
0.1	0.5924	0.1595		
0.15	0.6620	0.1845	0.0000	0.0001
0.2	0.7177	0.2031	0.0001	0.0007
0.25	0.7646	0.2177	0.0003	0.0019
0.3	0.8054	0.2295	0.0008	0.0041
0.35	0.8415	0.2393	0.0016	0.0073
0.4	0.8740	0.2476	0.0028	0.0114
0.45	0.9036	0.2548	0.0044	0.0161
0.5	0.9308	0.2609	0.0064	0.0217
0.6	0.9793	0.2711	0.0113	0.0335
0.7	1.0217	0.2794	0.0173	0.0454
0.8	1.0595	0.2862	0.0241	0.0577
0.9	1.0936	0.2917	0.0316	0.0701
1	1.1246	0.2962	0.0396	0.0820
1.5	1.2478	0.3112	0.0823	0.1301
2	1.3388	0.3202	0.1248	0.1652
2.5	1.4109	0.3257	0.1647	0.1915
3	1.4707	0.3296	0.2015	0.2115
3.5	1.5217	0.3324	0.2353	0.2272
4	1.5663	0.3347	0.2665	0.2399

4.5	1.6058	0.3364	0.2954	0.2502
5	1.6413	0.3378	0.3223	0.2588
6	1.7031	0.3401	0.3708	0.2723
7	1.7557	0.3418	0.4136	0.2826
8	1.8014	0.3431	0.4519	0.2906
9	1.8419	0.3442	0.4865	0.2969
10	1.8782	0.3450	0.5180	0.3019
15	2.0187	0.3476	0.6440	0.3177
20	2.1189	0.3492	0.7369	0.3265
25	2.1970	0.3500	0.8104	0.3318
30	2.2608	0.3506	0.8712	0.3353
35	2.3149	0.3510	0.9231	0.3379
40	2.3618	0.3513	0.9684	0.3399
45	2.4032	0.3516	1.0085	0.3413
50	2.4403	0.3518	1.0445	0.3425
60	2.5044	0.3521	1.1072	0.3443
70	2.5587	0.3523	1.1603	0.3456
80	2.6058	0.3524	1.2066	0.3466
90	2.6473	0.3526	1.2474	0.3474
100	2.6844	0.3523	1.2841	0.3480
150	2.8268	0.3523	1.4256	0.3498
200	2.9284	0.3531	1.5264	0.3507
250	3.0072	0.3532	1.6047	0.3513
300	3.0716	0.3533	1.6688	0.3517
350	3.1261	0.3533	1.7230	0.3520
400	3.1732	0.3533	1.7700	0.3522
450	3.2149	0.3534	1.8115	0.3523
500	3.2521	0.3511	1.8486	0.3524
600	3.3154	0.3505	1.9129	0.3526
700	3.3699	0.3534	1.9673	0.3528
800	3.4171	0.3535	2.0144	0.3529
900	3.4587	0.3535	2.0560	0.3529
1000	3.4959	0.3591	2.0931	0.3531

Appendix C:

$\Delta x_h/L_h$	$\Delta y_h/L_h$					
	0	1	2	3	4	5
0		0.807	0.810	0.810	0.810	0.810
0.25		0.630	0.640	0.650	0.650	0.650
0.5		0.545	0.570	0.580	0.580	0.590
0.75		0.495	0.535	0.545	0.550	0.557
1		0.468	0.510	0.525	0.530	0.540
1.25		0.460	0.495	0.510	0.520	0.530
1.5	0.405	0.455	0.485	0.500	0.510	0.520
2	0.435	0.455	0.470	0.485	0.495	0.505
3	0.445	0.455	0.465	0.480	0.487	0.495
4	0.460	0.470	0.475	0.480	0.480	0.491
5	0.470	0.480	0.480	0.480	0.480	0.490
6	0.470	0.480	0.480	0.480	0.480	0.490
7	0.475	0.480	0.480	0.480	0.480	0.490

Appendix D:

Angle (Degrees)	$\tilde{r}_D$		
	E_a(~2%)	E_a(~5%)	E_a(~10%)
0	6.30	3.70	2.50
15	6.20	3.63	2.42
30	5.78	3.15	2.10
45	4.11	2.47	1.60
65	2.22	1.22	0.86
75	2.52	1.51	1.17
90	3.50	2.10	1.50

Appendix E:

t_D	p_{wD1}	p'_{wD1}	p_{wD2}	p'_{wD2}
1.00E-05	0.1769	0.0289		
1.50E-05	0.1886	0.0289		
2.00E-05	0.1969	0.0289		
2.50E-05	0.2034	0.0289		
3.00E-05	0.2086	0.0289		
3.50E-05	0.2131	0.0289		
4.00E-05	0.2169	0.0289		
4.50E-05	0.2203	0.0289		
5.00E-05	0.2234	0.0289		
6.00E-05	0.2287	0.0289		
7.00E-05	0.2331	0.0289		
8.00E-05	0.2370	0.0289		
9.00E-05	0.2404	0.0289		
1.00E-04	0.2434	0.0289		
1.50E-04	0.2551	0.0289		
2.00E-04	0.2634	0.0289		
2.50E-04	0.2698	0.0289		
3.00E-04	0.2751	0.0289		
3.50E-04	0.2796	0.0289		
4.00E-04	0.2834	0.0289		
4.50E-04	0.2868	0.0289		
5.00E-04	0.2899	0.0289		
6.00E-04	0.2951	0.0289		
7.00E-04	0.2996	0.0289		
8.00E-04	0.3034	0.0289		
9.00E-04	0.3068	0.0290		
1.00E-03	0.3099	0.0292		
1.50E-03	0.3219	0.0309		
2.00E-03	0.3310	0.0332		
2.50E-03	0.3387	0.0360		
3.00E-03	0.3455	0.0389		
3.50E-03	0.3517	0.0416		
4.00E-03	0.3574	0.0443		
4.50E-03	0.3628	0.0468		

5.00E-03	0.3678	0.0492		
6.00E-03	0.3772	0.0535		
7.00E-03	0.3857	0.0575		
8.00E-03	0.3936	0.0612		
9.00E-03	0.4011	0.0646		
1.00E-02	0.4080	0.0679		
1.50E-02	0.4382	0.0818		
2.00E-02	0.4632	0.0928		
2.50E-02	0.4849	0.1022		
3.00E-02	0.5043	0.1105		
3.50E-02	0.5219	0.1179		
4.00E-02	0.5381	0.1246		
4.50E-02	0.5531	0.1308		
5.00E-02	0.5672	0.1364		
6.00E-02	0.5929	0.1466		
7.00E-02	0.6162	0.1556		
8.00E-02	0.6375	0.1637		
9.00E-02	0.6572	0.1709		
0.1	0.6756	0.1774		
0.15	0.7526	0.2034	0.0000	0.0001
0.2	0.8139	0.2223	0.0000	0.0004
0.25	0.8651	0.2367	0.0002	0.0014
0.3	0.9093	0.2481	0.0006	0.0033
0.35	0.9483	0.2575	0.0012	0.0061
0.4	0.9832	0.2653	0.0023	0.0099
0.45	1.0148	0.2719	0.0036	0.0144
0.5	1.0438	0.2774	0.0054	0.0197
0.6	1.0952	0.2866	0.0099	0.0314
0.7	1.1400	0.2939	0.0156	0.0437
0.8	1.1796	0.2998	0.0222	0.0562
0.9	1.2152	0.3046	0.0296	0.0685
1	1.2476	0.3084	0.0374	0.0805
1.5	1.3753	0.3211	0.0799	0.1304
2	1.4689	0.3285	0.1226	0.1664
2.5	1.5428	0.3331	0.1628	0.1930
3	1.6038	0.3362	0.1999	0.2133
3.5	1.6558	0.3384	0.2341	0.2292
4	1.7011	0.3401	0.2656	0.2419

4.5	1.7413	0.3415	0.2947	0.2522
5	1.7773	0.3426	0.3217	0.2607
6	1.8399	0.3443	0.3705	0.2741
7	1.8931	0.3455	0.4136	0.2843
8	1.9393	0.3465	0.4521	0.2922
9	1.9802	0.3472	0.4869	0.2984
10	2.0168	0.3478	0.5187	0.3033
15	2.1582	0.3496	0.6451	0.3188
20	2.2590	0.3506	0.7382	0.3273
25	2.3373	0.3512	0.8119	0.3325
30	2.4013	0.3516	0.8729	0.3359
35	2.4556	0.3519	0.9249	0.3384
40	2.5026	0.3521	0.9702	0.3403
45	2.5441	0.3523	1.0104	0.3417
50	2.5812	0.3524	1.0464	0.3429
60	2.6454	0.3526	1.1091	0.3446
70	2.6998	0.3527	1.1624	0.3459
80	2.7469	0.3528	1.2086	0.3469
90	2.7885	0.3529	1.2495	0.3476
100	2.8257	0.3526	1.2862	0.3482
150	2.9680	0.3524	1.4277	0.3499
200	3.0697	0.3533	1.5286	0.3508
250	3.1485	0.3533	1.6069	0.3514
300	3.2129	0.3534	1.6710	0.3518
350	3.2674	0.3534	1.7253	0.3520
400	3.3146	0.3534	1.7723	0.3522
450	3.3562	0.3534	1.8138	0.3524
500	3.3934	0.3508	1.8509	0.3525
600	3.4566	0.3501	1.9152	0.3526
700	3.5111	0.3535	1.9695	0.3528
800	3.5583	0.3535	2.0167	0.3529
900	3.5999	0.3535	2.0582	0.3530
1000	3.6371	0.3597	2.0954	0.3531